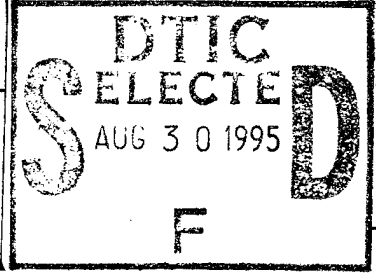


Public reporting burden for this collection of information is estimated to average 1 hour per response, including the time for reviewing instructions, searching existing data sources, gathering and maintaining the data needed, and completing and reviewing the collection of information. Send comments regarding this burden estimate or any other aspect of this collection of information, including suggestions for reducing this burden, to Washington Headquarters Services, Directorate for Information Operations and Reports, 1215 Jefferson Davis Highway, Suite 1204, Arlington, VA 22202-4302, and to the Office of Management and Budget, Paperwork Reduction Project (0704-0188), Washington, DC 20503.

1. AGENCY USE ONLY (Leave blank)		2. REPORT DATE <i>Mar 95</i>		3. REPORT TYPE AND DATES COVERED	
4. TITLE AND SUBTITLE <i>Improvement in Design Oriented Equivalent Water Modeling of Wing Structures</i>				5. FUNDING NUMBERS	
6. AUTHOR(S) <i>Robert Quinn Borchert</i>				7. PERFORMING ORGANIZATION NAME(S) AND ADDRESS(ES) AFIT Students Attending: <i>University of Washington</i>	
9. SPONSORING/MONITORING AGENCY NAME(S) AND ADDRESS(ES) DEPARTMENT OF THE AIR FORCE AFIT/CI 2950 P STREET, BDLG 125 WRIGHT-PATTERSON AFB OH 45433-7765				8. PERFORMING ORGANIZATION REPORT NUMBER AFIT/CI/CIA <i>95-029</i>	
11. SUPPLEMENTARY NOTES				10. SPONSORING/MONITORING AGENCY REPORT NUMBER	
12a. DISTRIBUTION/AVAILABILITY STATEMENT Approved for Public Release IAW AFR 190-1 Distribution Unlimited BRIAN D. GAUTHIER, MSgt, USAF Chief Administration					
13. ABSTRACT (Maximum 200 words)					
14. SUBJECT TERMS				15. NUMBER OF PAGES <i>115</i>	
				16. PRICE CODE	
17. SECURITY CLASSIFICATION OF REPORT		18. SECURITY CLASSIFICATION OF THIS PAGE		19. SECURITY CLASSIFICATION OF ABSTRACT	
				20. LIMITATION OF ABSTRACT	

UNIVERSITY OF WASHINGTON

Abstract

**Improvements in Design Oriented
Equivalent Plate Modeling
of Wing Structures**

by Robert Quinn Borchert

Chairman of Supervisory Committee: Professor Eli Livne
Department of Aeronautics
and Astronautics

Improvements in equivalent plate modeling of aircraft wings are presented. Formulations for wing mass, stiffness, and loads using Classical Plate Theory and First Order Shear Deformation Plate Theory are given in a general manner allowing versatility in the selection of displacement Ritz polynomials. A new technique for approximating the stiffness of an array of spar webs with the stiffness of an equivalent sandwich core is developed. A formulation allowing wing zones modeled with Classical Plate Theory and First Order Shear Deformation Plate Theory to be used together is also presented.

Numerical tests were performed to verify the validity of the new formulations. Tests of a thick, high aspect ratio wing showed that selecting low order Ritz polynomials for the linear in-plane displacements of a symmetric wing can lead to a significant reduction in model order while retaining acceptable accuracy. Additional tests of the thick, high aspect ratio wing and a typical supersonic transport wing showed that an array of spar webs may be accurately replaced by an equivalent core leading to substantial savings in computation time.

Results from this work will allow complex wing configurations to be modeled using equivalent plates with accuracy comparable to finite element analysis, yet with much greater computational efficiency. The results add support for the use of equivalent plate modeling as the primary wing structural analysis tool in multi-disciplinary design optimization of aircraft structures.

Accession For	
NTIS	CRA&I <input checked="" type="checkbox"/>
DTIC	TAB <input type="checkbox"/>
Unannounced <input type="checkbox"/>	
Justification	
By	
Distribution /	
Availability Codes	
Dist	Avail or Special
A-1	

75029

**Improvements in Design Oriented
Equivalent Plate Modeling
of Wing Structures**

by

Robert Quinn Borchert

A thesis submitted in partial fulfillment
of the requirements for the degree of

Master of Science in Aeronautics and Astronautics

University of Washington

1995

Approved by ER. L. J. Le
Chairman of Supervisory Committee

Program Authorized to Offer Degree: Department of Aeronautics and Astronautics

Date: March 17, 1995

Master's Thesis

In presenting this thesis in partial fulfillment of the requirements for a Master's degree at the University of Washington, I agree that the Library shall make its copies freely available for inspection. I further agree that extensive copying of this thesis is allowable only for scholarly purposes, consistent with "fair use" as prescribed in the U.S. Copyright Law. Any other reproduction for any purposes or by any means shall not be allowed without my written permission.

Signature _____

Date _____

Table of Contents

	<i>Page</i>
List of Figures	iv
List of Tables	v
Nomenclature	vi
Introduction	1
Background	1
Motivation	3
Scope of Work	4
Chapter 1: Wing Model	5
1.1 Overview	5
1.2 General Wing Box Configuration	5
1.3 Wing Planform Geometry	6
1.4 Wing Depth and Construction	8
1.5 Material Properties	10
1.6 Ritz Solution Technique	11
1.7 Static Solution for Displacements and Stresses	12
1.8 Eigensolution for Natural Vibration Frequencies and Modes	13
1.9 Output	14
Chapter 2: Equivalent Plate Formulation Using Classical	
Plate Theory	15
2.1 Overview	15
2.2 CPT Displacements and Strains	15
2.3 Skin Contribution to Mass and Stiffness for a CPT Zone	17
2.4 Spar Cap Contribution to Mass and Stiffness for a CPT Zone	19
2.5 Rib Cap Contribution to Mass and Stiffness for a CPT Zone	21
2.6 Concentrated Mass Contribution for a CPT Zone	22
2.7 Load Contributions for a CPT Zone	23
2.8 Displacement and Stress Output	24
Chapter 3: Equivalent Plate Formulation Using First Order Shear	
Deformation Plate Theory	25
3.1 Overview	25
3.2 FSDPT Displacements and Strains	25
3.3 Skin Contribution to Mass and Stiffness for a FSDPT Zone	28
3.4 Spar Cap Contribution to Mass and Stiffness for a FSDPT Zone	30

3.5 Rib Cap Contribution to Mass and Stiffness for a FSDPT Zone	32
3.6 Spar Web Contribution to Mass and Stiffness for a FSDPT Zone	34
3.7 Rib Web Contribution to Mass and Stiffness for a FSDPT Zone	37
3.8 Concentrated Mass Contribution for a FSDPT Zone	40
3.9 Load Contributions for a FSDPT Zone	40
3.10 Displacement and Stress Output	42
Chapter 4: Zone Connections and Boundary Conditions	44
4.1 Overview	44
4.2 Zone Connections in Global Context	44
4.3 Spring Connection of 2 CPT Zones	46
4.4 Spring Connection of 2 FSDPT Zones	50
4.5 Spring Connection of a FSDPT Zone and a CPT Zone	56
4.6 Boundary Conditions	59
Chapter 5: Spar Web Stiffness Approximation	60
5.1 Overview	60
5.2 Spar Web Shear Stiffness	60
5.3 Sandwich Core Shear Stiffness	62
5.4 Spar Web Array - Sandwich Core Stiffness Correlation	64
Chapter 6: Test Case Results	66
6.1 Overview	66
6.2 Swept, Thick, High Aspect Ratio Wing	67
6.3 HSCT Wing	72
Chapter 7: Conclusion	76
7.1 Summary	76
7.2 Future Work	77
References	78
Appendix A: Analytical Foundations of an Equivalent Plate	
Model Using CPT	81
A.1 Overview	81
A.2 Assumptions	81
A.3 Strain-Displacement Relationships	82
A.4 Displacement Function	83
A.5 Mass Matrix Contributions of a Skin Layer	83
A.6 Stiffness Matrix Contributions of a Skin Layer	85
A.7 Mass Matrix Contributions of a Spar	90
A.8 Stiffness Matrix Contributions of a Spar	93
A.9 Mass Matrix Contributions of a Rib	96
A.10 Stiffness Matrix Contributions of a Rib	99
Appendix B: Analytical Foundations of an Equivalent Plate	
Model Using FSDPT	102
B.1 Overview	102
B.2 Assumptions	102

B.3 Strain-Displacement Relationships	103
B.4 Displacement Functions	104
B.5 Mass Matrix Contributions of a Skin Layer	104
B.6 Stiffness Matrix Contributions of a Skin Layer	108
B.7 Mass Matrix Contributions of a Spar	112
B.8 Stiffness Matrix Contributions of a Spar	115
B.9 Mass Matrix Contributions of a Rib	119
B.10 Stiffness Matrix Contributions of a Rib	121
B.11 Mass Matrix Contributions of a Spar Web Layer	124
B.12 Stiffness Matrix Contributions of a Spar Web Layer	130
B.13 Mass Matrix Contributions of a Rib Web Layer	138
B.14 Stiffness Matrix Contributions of a Rib Web Layer	142
Appendix C: Fundamental Integrals and Tables	148
C.1 Introduction	148
C.2 Area Integrals	148
C.3 Spar Line Integrals	150
C.4 Rib Line Integrals	151
Appendix D: Test Case Data	153
D.1 Overview	153
D.2 Turner-Martin-Weikel Wing	153
D.3 HSCT Wing	155
Appendix E: CONNECT Program Information	157
E.1 Overview	157
E.2 Program Subroutines	157
E.3 Program Structure	159

List of Figures

	<i>Page</i>
Figure 1.1: Wing Box Configuration	6
Figure 1.2: Multi-zone Wing Planform	6
Figure 1.3: Skin Panel Shape Design Variables	7
Figure 1.4: Spar and Rib Shape Design Variables	7
Figure 1.5: Spar Web and its Associate Axes	10
Figure 1.6: Complete Polynomials Through 7th Order	12
Figure 1.7: Panel Output Grid	13
Figure 4.1: CPT Attach Line Geometry	46
Figure 4.2: FSDPT Attach Line Geometry	52
Figure 5.1: Composite Sandwich Structure	62
Figure 6.1: Turner-Martin-Weikel Wing	66
Figure 6.2: Vertical Displacement along Rear Spar with Varying Orders of ψ_x and ψ_y Rotation Field Polynomials	67
Figure 6.3: Skin Stress along Root Chord with Varying Orders of ψ_x and ψ_y Rotation Field Polynomials	68
Figure 6.4: Vertical Displacement along Rear Spar Using an Equivalent Shear Core	70
Figure 6.5: Skin Stress along Root Chord Using an Equivalent Shear Core	71
Figure 6.6: HSCT Wing Planform	72
Figure 6.7: HSCT Wing Vertical Displacements	73
Figure 6.8: Normal Stress in Layer Oriented at to Inboard Wing Spar Direction	74
Figure A.1: Positive Rotation of Principal Material Axes from x-y Axes	86
Figure A.2: Skin Layer Thickness and Depth	88
Figure A.3: Spar Geometry	91
Figure A.4: Rib Geometry	97
Figure B.1: Positive Rotation of Principal Material Axes from η -z Axes	132
Figure D.1: FEM Model of the T-M-W Wing	153
Figure D.2: T-M-W Wing Construction	154
Figure D.3: ELFINI Model of HSCT Wing	155

List of Tables

	<i>Page</i>
Table 6.1: Natural Frequencies (in Hz) with Varying Orders of ψ_x and ψ_y Rotation Field Polynomials	69
Table 6.2: Second Natural Frequency (in Hz) for Varying Orders of u_0 and v_0 Displacement Polynomials	69
Table 6.3: Natural Frequencies (in Hz) Using an Equivalent Shear Core	71
Table 6.4: HSCT Natural Frequencies (in Hz)	73
Table 6.5: Stiffness Matrix Assembly Time (CPU seconds)	74
Table A.1: Coefficients and Powers for Curvature Along a Spar Line	95
Table D.1: Root Springs Representing Fuselage Stiffness Along Side of Body Rib	156

Nomenclature

CPT	- Classical Plate Theory
FSDPT	- First Order Shear Deformation Plate Theory
HSCT	- High Speed Civil Transport
x, y, z	- coordinate frame
$y_L, y_R, x_{FL}, x_{FR}, x_{AL}, x_{AR}$	- skin panel shape design variables
sy_L, sy_R, sx_L, sx_R	- spar shape design variables
ry_L, ry_R, y_{RIB}	
$rx_{FL}, rx_{FR}, rx_{AL}, rx_{AR}$	- rib shape design variables
$aty_L, aty_R, atx_L, atx_R$	- attach line design geometry
Λ	- spar sweep angle
η	- spar directional axis
$h_{jl}(x,y)$	- j lth skin layer depth distribution
$t_{jl}(x,y)$	- j lth skin layer thickness
$A_{sp_{js}}(y), A_{rb_{jr}}(x)$	- j sth spar and j rth rib cap areas
$[Q]_{jl}, [\bar{Q}]_{jl}$	- j lth skin layer and j lth web layer constitutive matrices
β	- orientation of composite fiber direction
E_{tot}	- total system energy
U	- potential energy
T	- kinetic energy
Q	- work energy
$[K]$	- stiffness matrix
$[M]$	- mass matrix
$\{P\}$	- generalized load vector
$\{q\}$	- generalized displacement vector
ω	- natural vibrational frequency
$\epsilon_{xx}, \epsilon_{yy}, \epsilon_{zz}$	- normal strains
$\gamma_{xy}, \gamma_{xz}, \gamma_{yz}$	- shear strains
$\sigma_{xx}, \sigma_{yy}, \sigma_{xy}$	- in-plane stresses

u, v, w	- x, y, z direction displacements
$\{a_w\}$	- vector of x - y polynomial terms for CPT w displacement
$\{q_w\}$	- vector of unknown polynomial coefficients for CPT w displacement
ρ	- material density
E	- modulus of elasticity
ν	- Poisson's ratio
$\{\epsilon\}$	- vector of in-plane strains
$\{\kappa\}$	- vector of skin curvatures
$[D]_{jl}$	- j th skin layer's plate bending stiffness matrix
$[W]$	- CPT skin strain matrix
L	- spar length
$S1, S2$	- spar line coefficients
\tilde{M}_{jc}	- j th concentrated mass
$\phi(x, y)$	- polynomial load function
\hat{P}	- concentrated force load
$I_{TR}(m, n)$	- panel integral family
$I_{SP}(m, n)$	- spar integral family
$I_{RB}(m, n)$	- rib integral family
u_0, v_0, w_0	- FSDPT mid-surface displacement fields
Ψ_x, Ψ_y	- FSDPT rotation fields
$\{a_1\} \dots \{a_5\}$	- vectors of x - y polynomial terms for FSDPT deformations
$\{q_1\} \dots \{q_5\}$	- vectors of unknown polynomial coefficients for FSDPT deformations
$[S_0], [S_1]$	- FSDPT displacement matrices
$[R_0], [R_1]$	- FSDPT skin and spar strain matrices
$\{TR\}, [TR_{25}], [TR_{22}]$	- transformation vector and matrices
$[Y_0], [Y_1]$	- FSDPT rib strain matrices
$s\Lambda$	- sine of angle Λ
$c\Lambda$	- cosine of angle Λ
$\epsilon_{\eta\eta}, \gamma_{\eta z}$	- strains in spar web (η - z) plane
$\sigma_{\eta\eta}, \sigma_{\eta z}$	- stresses in spar web plane
$[W_0], [W_1]$	- FSDPT spar web strain matrices

$[F_0], [F_1]$	- FSDPT rib web strain matrices
$K_{r_i s_j}$	- submatrix of the global stiffness matrix
α	- attach line orientation
\bar{t}	- vector defining attach line direction
\bar{r}	- vector defining a direction normal to an attach line
$\bar{\Omega}$	- vector of rotation
$\bar{\chi}$	- vector of in-plane displacement at the mid-surface
θ	- angular displacement
Δ, ζ	- linear displacements
$k_w, k_1, k_2, k_3, k_4, k_5$	- spring stiffness coefficients
$[W_s]$	- equivalent core strain matrix
G, G_{xz}, G_{yz}	- shear moduli
σ_{xz}, σ_{yz}	- transverse shear stresses
$c(x,y)$	- core depth
d	- web density factor
N	- used with added letters to designate the number of terms or components (i.e. Nq_w - # of terms used for $\{q_w\}$ in a CPT zone, or Np - # of panels in a zone)

Acknowledgments

I wish to express my deep appreciation to Professor Eli Livne for his guidance, support, and insight in helping me complete this work.

I also wish to thank my wonderful wife and family for their faithful, loving support throughout my time at the University of Washington.

Introduction

Background

In the early days of mathematical modeling of aircraft wing structures, equivalent beam models were used to suitably represent isotropic high aspect ratio wings. With the growing pursuit of fast subsonic and supersonic flight in the late 1940's, potential wing configurations took on a variety of shapes with low aspect ratio and thin cross section. The new wing configurations, which became subject to chordwise bending, could no longer be accurately modeled using classical beam theory. Attempts in the 1950's to model low aspect ratio wings as wide beams and equivalent plates were essentially abandoned with the development of high speed computing machines and matrix methods of structural analysis (GR61). Finite element (FE) techniques viably emerged from the new computing capability. It made possible the analysis of complex low aspect ratio wing structures giving stress, deflection, and vibration information with acceptable accuracy. The finite element method grew in acceptance as its reliability was tested, and it has now become industry's standard analysis tool for wing design (SCH81).

Difficulties were encountered, however, in the use of the finite element method during the preliminary stages of wing design when structural shape variations are examined. Finite element models lead to large matrix equations that were computationally intensive even with the new computing power. Since the finite element mesh had to change corresponding to shape changes, comparison of many alternative planforms proved to be cumbersome and time consuming. More complexity was added to the modeling problem when fiber composite materials came into use. Thus, interest in the development of alternative, computationally efficient wing models, tailored towards wing shape optimization, was rekindled.

Two different approaches to the problem have emerged: use of expedited finite element modeling and use of equivalent plate modeling. Major advances have been made in improving finite element modeling for use in design oriented structural analysis (HG92). In the area of airframe structures, numerical and analytical methods were used to obtain design sensitivity information with respect to both sizing and shape design variables (HA93, LAN94). Another improvement has been the development of integrated FE / auto-

mated mesh generation, which allows changes in planform and airfoil shapes to be handled efficiently (HA93). Although advances in modeling and improvements in computational power have made practical the shape optimization of finite element models having many design variables, the computational price remains high. In multi-disciplinary design optimization, where the structural analysis is just part of a wider optimization scheme, the cost of using a finite element approach may still be too expensive (LIV90).

The full capability of wing structural modeling based on equivalent plates is still being explored. Equivalent plate models have been found capable of capturing spanwise and chordwise bending of various planforms using a small number of degrees of freedom. An equivalent plate model based on Classical Plate Theory (CPT) was used in the aeroelastic tailoring and structural optimization (TSO) computer program (LRB77,MC83). This simplified capability has been used extensively for preliminary wing design with good results compared to finite element analysis for real wings such as those of the YF16 and F15 fighter aircraft (LRB77,TR80). The high computational efficiency of TSO coupled with its limitation of handling only a single trapezoidal planform motivated the development of an equivalent plate approach capable of handling planforms composed of multiple trapezoidal sections, with and without symmetry about the wing mid-surface (GI86,GI89). Better modeling of the internal wing structure was also included. Results showed that equivalent plate models could accurately predict stresses as well as deflections and mode shapes for wings with complex planforms while offering significant savings in computer time. This capability was extended to include analytically derived design sensitivities with respect to the shape and sizing design variables (LIV90). It was also shown that the planform shape could be modeled such that all integration could be done analytically, thus eliminating the need for coordinate transformations and numerical integration.

A study of equivalent plate modeling applied to a potential High Speed Civil Transport (HSCT) wing revealed some limitations of plate models based on CPT (LSB93). Results from the study showed that a CPT based equivalent plate model does not give good results for a wing with few spars and ribs and low transverse shear stiffness. In light of this finding, a new equivalent plate modeling capability was developed, based on First Order Shear Deformation Plate Theory (FSDPT), which showed much better correlation with finite element results for the HSCT wing (LIV194,LIV294,LSB93).

Motivation

The newly developed equivalent plate structural modeling approach using FSDPT provided more accurate results than a CPT based model for certain wing configurations. Yet in using FSDPT, some of the computational efficiency sought in using a plate modeling approach was lost. The FSDPT capability (in its form presented in LIV194) had limitations that led to increased computational cost. Among the causes for this increased computational effort was the way in which polynomial series were chosen to represent displacement functions in the model. Originally, all displacement functions had to be represented by x-y polynomials of the same order (LIV194). Since five displacement fields are involved with FSDPT modeling compared with one field (w deflection) in CPT, this resulted in a significant increase of the size of the system of equations. Also, a significant computational burden was carried by the original FSDPT approach because of the inclusion of spar webs and rib webs in the model. The computational time required to calculate the mass and stiffness contributions from an array of many webs became very time consuming.

For a low aspect ratio wing, like that of the HSCT, which has a complex planform geometry, low transverse shear stiffness, and multiple control surfaces, equivalent plate models based on CPT alone and FSDPT alone are inadequate. It has already been shown that a CPT based model cannot capture the transverse shear effects of such a wing (LSB93). A FSDPT based model gave good results with added computational cost. However, the computational cost would grow significantly if several control surfaces also modeled using FSDPT were included.

Facing these limitations of the current equivalent plate capabilities, it is important to make improvements in plate modeling to retain the accuracy of the FSDPT approach while bolstering computational efficiency. Specifically, it is sought to generalize the current FSDPT capability to handle multiple "zones" (LSB93) and allow the order of each displacement polynomial to be independently assigned. To further reduce computation time it is desired to approximate the stiffness contribution of an array of spar and rib webs with the stiffness of an equivalent sandwich core (LIV194). Thus, instead of calculating stiffness and mass contributions of spar and rib webs one by one, a single equivalent core is evaluated once per new wing shape. Finally sought is a new capability allowing zones based on FSDPT to be used in conjunction with zones based on CPT, thus allowing wings such as that of the HSCT with control surfaces to be accurately and efficiently modeled using equivalent plates.

Scope of Work

Following this introduction, Chapter 1 discusses the conventions and Ritz solution method used in the wing modeling problem. Chapters 2 and 3 present the equivalent plate formulations for wing structural mass, structural stiffness, and loading conditions using Classical Plate Theory and First Order Shear Deformation Plate Theory respectively. Both formulations are derived for numerical analysis such that they allow the order of each displacement polynomial to be independently chosen. Chapter 4 discusses zone connections and boundary conditions, including a new capability for combining CPT and FSDPT zones. Chapter 5 presents a method used to approximate the stiffness of a spar web array by the stiffness of a sandwich core. Chapter 6 compares the results from use of the new plate modeling capabilities with available data for two different test wings. Chapter 7 concludes with a summary and discussion of possible extensions of this work.

Detailed derivations of the equivalent plate formulations in Chapters 2 and 3 may be found in Appendices A and B. Appendix C contains analytical expressions for all integrals encountered in the wing math model. Appendix D contains data and figures from the test wings. Appendix E contains information concerning the use of the program CONNECT and supporting subroutines developed during this research effort.

Chapter 1: Wing Model

1.1 Overview

In this chapter the parameters for a mathematical wing model based on equivalent plate theory are established, and the solution technique is discussed. The chapter begins by discussing the configuration of a general wing box structure and defining the convention used for the model's shape design variables based on planform geometry and wing depth distribution. Next discussed is the convention used to express wing construction parameters as polynomial series, where the coefficients are the model's sizing design variables. Wing material properties are discussed, and constitutive relationships are given for the wing structural components. Following this is a presentation of the Ritz solution technique as applied to the wing model. Here the stiffness matrix $[K]$, mass matrix $[M]$, generalized displacements vector $\{q\}$, and generalized load vector $\{P\}$ are defined. Briefly discussed are details of the static solution and eigensolution. The chapter concludes with a discussion of output grid specification.

1.2 General Wing Box Configuration

The general wing box configuration considered in this work consists of skins, spar caps, rib caps, spar webs, and rib webs as shown in Figure 1.1. Skins may be constructed of multiple unidirectional fiber composite laminae. The thickness and distance from the wing mid-plane of each skin lamina may vary over the area of wing. Stiffening spars and ribs are attached to the upper and lower skins generally in some systematic array. Along the length of a spar or rib the cap distance from the wing mid-plane may vary. The cap areas of both spars and ribs also may vary linearly along their lengths. Spar webs and rib webs, like skins, may also be constructed of multiple composite layers and are intended primarily to provide shear stiffness. Spar webs connect spar caps on the upper surface with their parallels on the lower surface. Rib caps do the same for parallel rib caps.

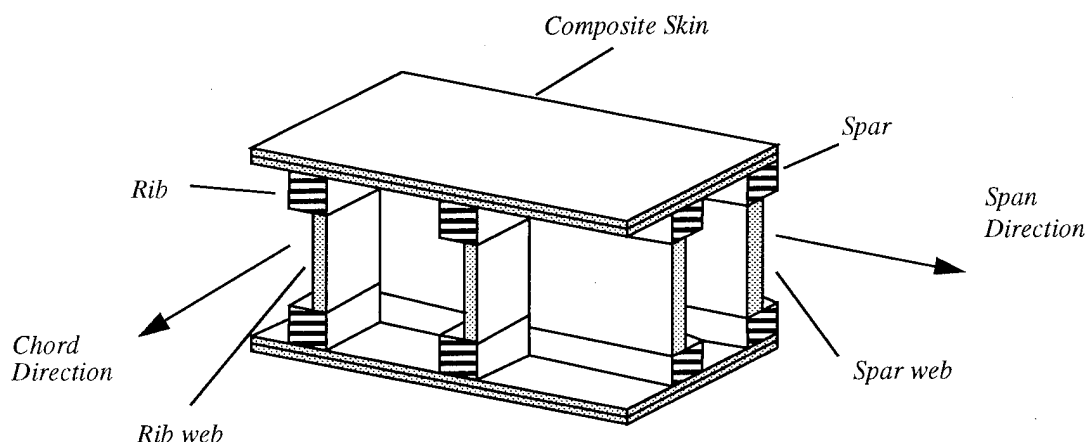


Figure 1.1: Wing Box Configuration

1.3 Wing Planform Geometry

The geometry of a general wing planform is defined in a global x - y - z coordinate system. The x - y plane ($z=0$) corresponds to the reference surface of the wing. A typical wing planform is shown in Figure 1.2. The whole planform may be divided into several “zones”. Each zone may have its geometry defined in its own zonal coordinate system and may use unique Ritz polynomial functions to represent its structural displacements. All zones, however, share a common z axis.

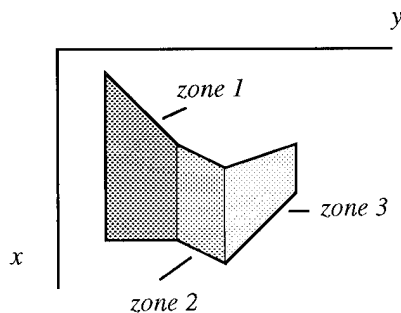


Figure 1.2: Multi-zone Wing Planform

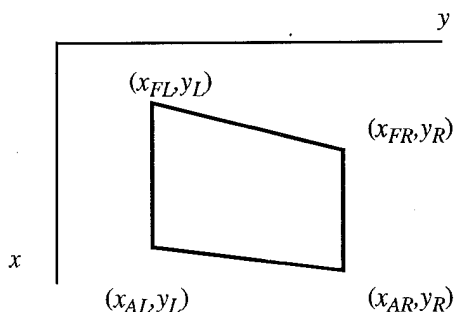


Figure 1.3: Skin Panel Shape Design Variables

Each zone is composed of one or more upper and lower trapezoidal panels. Each panel is defined by 6 shape design variables y_L , y_R , x_{FL} , x_{FR} , x_{AL} , and x_{AR} as shown in Figure 1.3. The variables y_L and y_R define respectively the left and right y coordinates of the sides of the panel which are parallel to the x -axis. The variables x_{FL} and x_{FR} define respectively the front left and front right x coordinates of the panel. Likewise, the variables x_{AL} and x_{AR} define respectively the aft left and aft right x coordinates of the panel. A zone generally will also have associated spars, ribs, and webs. Each spar is defined by the endpoints of a line segment. The 4 shape design variables sy_L , sy_R , sx_L , and sx_R define a spar line's geometry as shown in Figure 1.4. A spar is generally at some angle Λ to the y -axis. Ribs are

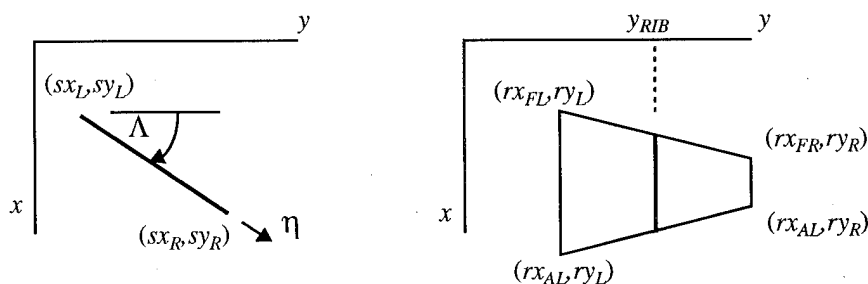


Figure 1.4: Spar and Rib Shape Design Variables

parallel to the x -axis and are defined by 7 shape design variables ry_L , ry_R , rx_{FL} , rx_{FR} , ry_{AL} , ry_{AR} , and y_{RIB} . The first 6 of these variables define a trapezoid in the same manner as the panel trapezoids are defined. The variable y_{RIB} then uniquely defines a rib line of constant y value, whose ends lie on the front and aft lines of the trapezoid as shown in Figure 1.4. Spar and rib web lines match the lines of the spar and rib caps they connect.

Zones may also have associated "attach lines", "attach points", and "free moving points". An attach line identifies the common surface between two adjoining zones. In a particular zone's coordinate system, an attach line is defined by the 4 variables aty_L , aty_R , atx_L , and atx_R which give the left and right x and y coordinates of the line's endpoints. An attach point lying on an attach line is defined simply by its x - y coordinates. At attach points concentrated computational springs may be used to impose boundary conditions or to represent the local stiffness of an attachment between zone boundaries (LIV90, LIV194). Free moving points are also defined by their x - y coordinates and are used to represent points on the wing where mass is lumped or where concentrated force loads are applied (LIV90).

1.4 Wing Depth and Construction

The depth distribution of a wing component is defined as its distance from the $z=0$ reference plane. A depth distribution, expressed as a simple polynomial series, may be defined across an entire zone for each skin layer and each array of spars and ribs. For example, the depth distribution across a single zone for the jl th skin layer is given by

$$h_{jl}(x, y) = \sum_{k=1}^{Nh_{jl}} H_{jl_k} \cdot x^{mh_k} y^{nh_k} \quad (1.1)$$

where the coefficients H_{jl_k} are shape design variables, and the powers mh_k and nh_k may be chosen to specify a polynomial in x and y containing Nh_{jl} terms (Actually, the powers associated with the k th term of the jl th layer should be denoted mh_{jl_k} , nh_{jl_k}). For a wing whose skin thickness is small compared to its depth it is justifiable to use only 2 depth distributions per zone. In such a case, all skins, spars, and ribs on the upper surface may be assigned one distribution $h_u(x, y)$ while those on the lower surface may have a second distribution $h_l(x, y)$ (LIV194).

Upper and lower wing skins may be composed of several layers of fiber composite material. Each layer may have its principal fiber direction oriented at some angle β to the x axis. For each trapezoidal panel the thickness of the jl th layer may be defined by a sim-

ple polynomial series composed of $N_{t_{jl}}$ terms and having the form

$$t_{jl}(x, y) = \sum_{k=1}^{N_{t_{jl}}} \hat{T}_{jl_k} \cdot x^{mt_k} y^{nt_k} \quad (1.2)$$

where the coefficients \hat{T}_{jl_k} are sizing design variables, and the powers mt_k and nt_k are pre-assigned. Again it should be mentioned that the powers associated with term k in layer jl should be denoted mt_{jl_k} , nt_{jl_k} . However, the simpler notation in Eq. 1.2 is adequate at this point for illustrative purposes.

Spar and rib cap areas may vary linearly along their respective longitudinal axes. The cap area of the j sth spar may be expressed as a linear function of y by

$$A_{sp_{js}}(y) = A_{sp0_{js}} + A_{sp1_{js}}y \quad (1.3)$$

where the coefficients $A_{sp0_{js}}$ and $A_{sp1_{js}}$ are sizing design variables. The cap area of the j rth rib varies linearly with x and may be expressed as

$$A_{rb_{jr}}(x) = A_{rb0_{jr}} + A_{rb1_{jr}}x \quad (1.4)$$

where the coefficients $A_{rb0_{jr}}$ and $A_{rb1_{jr}}$ are sizing design variables.

Spar and rib webs are constructed similarly to the wings skins in that each composite layer of a web may have a varying thickness and independently oriented fiber direction. Equation 1.2 may be used to express the thickness of a single web layer. However, for purposes of this work it is desirable to treat the thickness of each layer as varying linearly like the cap areas and having just 2 polynomial coefficients. The spar web thickness then varies linearly in y while the rib web thickness varies linearly in x .

Other sizing design variables include concentrated masses and the stiffness coefficients of concentrated springs. A concentrated mass represents a lumped mass applied at a free moving point or an attach point as discussed in the previous section. Concentrated springs may be used to represented local stiffness at an attach point. Large spring stiffness coefficients may be used in a penalty method to impose a zero displacement and zero rotation boundary condition or to enforce continuity at a point common to 2 zones. Rotational springs may be used to represent hinge and actuator stiffness. Carefully selected spring stiffness coefficients may be used to compensate for differences between numerical testing and experiment by representing the actual flexibility of an experimental support setup (LIV194,LRB77,LSF88,KA92,GR61).

1.5 Material Properties

The material density ρ of each wing component is used in determining the wing's theoretical mass. Material stiffness properties are used in constitutive laws for each wing component to determine the wing's stiffness.

The constitutive relationship between in-plane stresses σ and strains ϵ for the j th skin layer is expressed as

$$\begin{Bmatrix} \sigma_{xx} \\ \sigma_{yy} \\ \sigma_{xy} \end{Bmatrix} = [Q]_{jl} \begin{Bmatrix} \epsilon_{xx} \\ \epsilon_{yy} \\ \gamma_{xy} \end{Bmatrix} \quad (1.5)$$

where the material matrix $[Q]_{jl}$ contains the stiffness properties of the composite layer appropriately transformed into the x - y axes system based on the orientation of the layer's principle material axes. Each spar cap and rib cap is treated as having uniaxial stiffness based the cap's equivalent Young's modulus E .

A spar web lies in the η - z plane where η is the coordinate of the web's associated spar line as seen in Figure 1.5. As discussed in Chapter 3, it is assumed that $\epsilon_{zz}=0$. Therefore, the constitutive relationship for the j th web layer is expressed as

$$\begin{Bmatrix} \sigma_{\eta\eta} \\ \sigma_{\eta z} \end{Bmatrix} = [\bar{Q}]_{jl} \begin{Bmatrix} \epsilon_{\eta\eta} \\ \epsilon_{\eta z} \end{Bmatrix} \quad (1.6)$$

where the material matrix $[\bar{Q}]_{jl}$ contains the stiffness properties of the composite layer

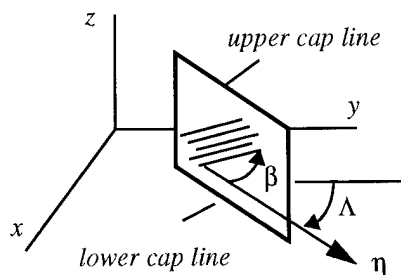


Figure 1.5: Spar Web and its Associate Axes

appropriately transformed into the η - z coordinate system based on the orientation of the layer's principle fiber direction (LIV194). A rib web is treated in a similar manner except that it lies in an x - z plane. The constitutive relationship for the j th layer of a rib web is given by

$$\begin{Bmatrix} \sigma_{xx} \\ \sigma_{xz} \end{Bmatrix} = [Q]_{jl} \begin{Bmatrix} \epsilon_{xx} \\ \epsilon_{xz} \end{Bmatrix} \quad (1.7)$$

The σ_{zz} stress in a web can be retrieved once the deformation and strains are determined.

1.6 Ritz Solution Technique

The Ritz method is used to obtain an approximate solution for the generalized displacements that minimize the total energy of the wing box structure. The total energy E_{tot} associated with the wing model is

$$E_{tot} = U + Q - T \quad (1.8)$$

where U is the potential energy stored in the structure through deformation, Q is the work of the applied loads moving through the corresponding structural deflections, and T is the kinetic energy associated with the mass of the structure (GI86). These energy terms are expressed as functions of the displacements of the structure. All structural displacements can be individually expressed as a polynomial series of the general form

$$f(x, y, t) = \sum_{i=1}^{Nc} c(t)_i \cdot x^{mc_i} y^{nc_i} \quad (1.9)$$

where the coefficients $c(t)_i$ are unknown and vary with time, and the powers mc_i and nc_i are predetermined from possible polynomial combinations of increasing order as shown in Figure 1.5. Since the displacement polynomials are used in determining the energy of the structure, the energy terms U , Q , T , and E_{tot} thus become functions of the unknown $c(t)_i$. The Ritz solution requires

$$\frac{\partial E_{tot}}{\partial c_i} = 0 \quad (1.10)$$

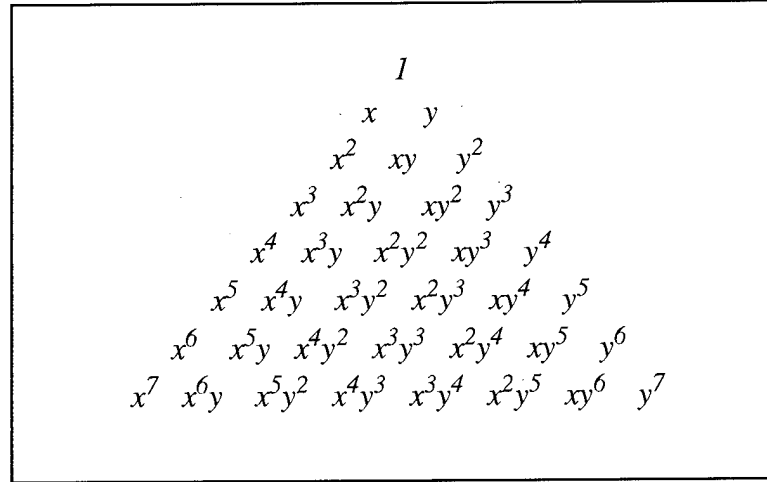


Figure 1.6: Complete Polynomials Through 7th Order

Application of Eq. 1.10 to a vibrating wing under harmonic excitation results in a system of simultaneous equations expressed in matrix form as

$$[K] \{c\} - \omega^2 [M] \{c\} - \{P\} = 0 \quad (1.11)$$

where $[K]$ is the symmetric stiffness matrix derived from the potential energy, $[M]$ is the symmetric mass matrix derived from the kinetic energy, ω is the structure's natural vibrational frequency, $\{P\}$ is the generalized load vector derived from the applied load conditions, and $\{c\}$ is the vector of unknown generalized displacements (GI86). Chapters 2 and 3 discuss how the stiffness matrix, mass matrix, and load vector are derived for a particular wing using different plate theories.

1.7 Static Solution for Displacements and Stresses

For a single static loading condition, Eq. 1.11 becomes

$$[K] \{q\} = \{P\} \quad (1.12)$$

where $\{q\}$ is now the vector of unknown generalized displacements. This equation holds for linear structural systems. The solution subroutines employed in this work make use of

the symmetry and inherent sparsity of the stiffness matrix $[K]$ (FE75). The solution method is based on a modified Cholesky decomposition technique which factorizes $[K]$ as

$$[K] = [L] [D] [L]^T \quad (1.13)$$

where $[L]$ is a lower triangular matrix, and $[D]$ is a nonsingular diagonal matrix. The solution vector $\{q\}$ is then obtained through a series of forward and backward substitutions using the factored matrices (FE75, LIV90).

1.8 Eigensolution for Natural Vibration Frequencies and Modes

For a freely oscillating undamped linear structure, Eq. 1.11 becomes

$$[K - \omega^2 M] \{q\} = [0] \quad (1.14)$$

where $\{q\}$ is now the vector of unknown generalized displacements defining the vibration mode shape which corresponds to the natural frequency ω . The QZ algorithm (GVL89) is used here to find eigenvalues and eigenvectors of the linear generalized eigenvalue problem in Eq. 1.14.

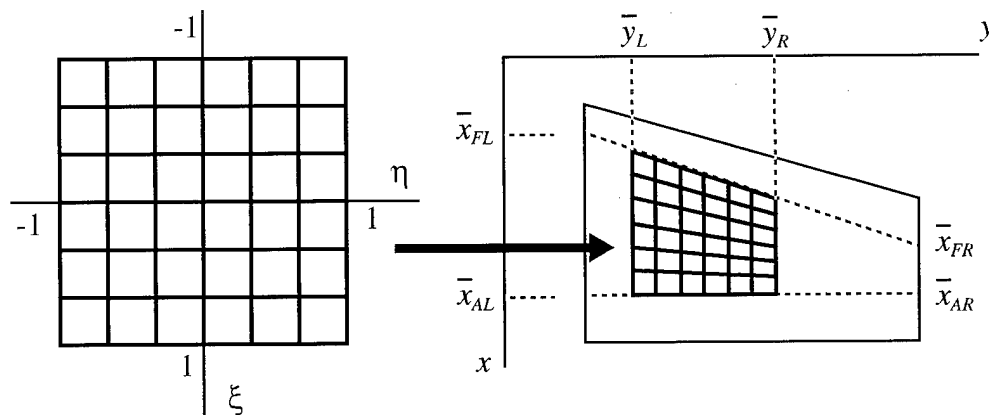


Figure 1.7: Panel Output Grid

1.9 Output

From the static and dynamic solutions, it is possible to give the static deflection, static stress, and modal deflection at any point on the wing model. It is advantageous to be able to establish a grid of output points on panels, spars, and ribs as desired. As shown in Figure 1.6 a panel output grid may be specified over a square where $-1 < \xi < 1$ and $-1 < \eta < 1$ by choosing the number of points desired in the x and y directions. This grid of points is then mapped onto a selected trapezoidal output panel yielding a grid of output points in the x - y axis system. The same thing may be done in one dimension for spars and ribs.

Chapter 2: Equivalent Plate Formulation Using Classical Plate Theory

2.1 Overview

This chapter contains the Classical Plate Theory based formulation of the mass, stiffness, and load contributions needed to solve for the generalized displacements in Eq. 1.11. The chapter begins with a discussion of the assumptions of Classical Plate Theory and the ensuing displacement and strain relationships. Following this foundation is the derivation of the wing skin contribution to the mass and stiffness of the system. Next discussed is the derivation of the spar cap contribution to mass and stiffness. The derivation of the rib cap contribution to mass and stiffness is given as well. Also included is a discussion of the contribution of concentrated masses to the mass of the system. Following this is the formulation of the load vector including concentrated force load and distributed pressure load conditions. Finally presented is the method used to calculate displacement and stress output from the generalized displacement solution. Appendix A includes detailed derivation of mass and stiffness contributions from the wing structural components.

2.2 CPT Displacements and Strains

Classical Plate Theory (CPT) is the name given to the small-deflection theory of bending of elastic thin plates (RE84). The central assumption of CPT, known as the Kirchhoff-Love assumption, is that planes normal to a plate's mid-surface will remain plane and normal to the plate's mid-surface after the plate is deformed in bending (RE84,JO75). This assumption is equivalent to ignoring the shear strains γ_{xz} and γ_{zx} for a plate in the x - y plane. Because the plate is thin, the transverse normal strain ϵ_{zz} is also negligible making this in essence a plane stress problem. Because wing symmetry about the x - y plane is assumed here, there are no in-plane displacements at points on the plate's mid-surface.

According to the above assumptions, the transverse displacement w is a function of x and y only. The Kirchhoff-Love assumption allows the displacement u in the x direction and the displacement v in the y direction to be given in terms of w by

$$u = -z \frac{\partial w}{\partial x} = -zw_{,x} \quad (2.1)$$

$$v = -z \frac{\partial w}{\partial y} = -zw_{,y} \quad (2.2)$$

The in-plane strains ϵ_{xx} , ϵ_{yy} , and γ_{xy} are given by

$$\epsilon_{xx} = \frac{\partial u}{\partial x} = -zw_{,xx} \quad (2.3)$$

$$\epsilon_{yy} = \frac{\partial v}{\partial y} = -zw_{,yy} \quad (2.4)$$

$$\gamma_{xy} = \frac{\partial u}{\partial y} + \frac{\partial v}{\partial x} = -2zw_{,xy} \quad (2.5)$$

(LIV90,RE84). It is evident that all the displacements and strains are functions of the independent transverse displacement w .

In the polynomial Ritz solution method described in Chapter 1, it is necessary to define the displacement function $w(x,y,t)$ as a polynomial series of the form shown in Eq. 1.9 and having Nq_w terms. This polynomial function may be expressed in vector form by

$$w(x, y, t) = \{a_w(x, y)\}^T \{q_w(t)\} \quad (2.6)$$

where

$$\{a_w(x, y)\}^T = \{\dots, x^{mq_i} y^{nq_i}, \dots\} \quad (2.7)$$

and $\{q_w(t)\}$ is a column vector containing the time dependent coefficients that ultimately become the unknown generalized displacements. Both vectors contain Nq_w terms. This vector form for $w(x,y,t)$ will be used in the mass and stiffness matrix formulations.

2.3 Skin Contribution to Mass and Stiffness for a CPT Zone

The contribution to the kinetic energy T of an infinitesimal skin element dx by dy of the j th skin layer of a single trapezoidal panel is

$$dT_{jl} = \frac{1}{2} \rho_{jl} t_{jl}(x, y) \dot{w}^2(x, y, t) dx dy \quad (2.8)$$

where ρ_{jl} is the constant material density of the skin layer, and $t_{jl}(x, y)$ is the thickness of the skin layer. Using Eq. 2.6 for $w(x, y, t)$ and integrating over the whole trapezoidal panel area gives

$$T_{jl} = \frac{1}{2} \rho_{jl} \iint_{yx} t_{jl}(x, y) \{\dot{q}_w\}^T \{a_w\} \{a_w\}^T \{\dot{q}_w\} dx dy \quad (2.9)$$

Summing the kinetic energy contributions of the Nl_U layers of the panel's upper skin, multiplying by 2 because of wing symmetry, and summing over the Np trapezoidal panels in a zone leads to the total skin mass matrix, $Nq_w \times Nq_w$ in dimension, given by

$$[M_{sk}]_{tot} = 2 \sum_{ip=1}^{Np} \sum_{jl=1}^{Nl_U} \rho_{jl} \iint_{yx} t_{jl}(x, y) \{a_w\} \{a_w\}^T dx dy \quad (2.10)$$

where $t_{jl}(x, y)$ is a polynomial function of x and y as given in Eq. 1.2. Each element of $[M_{sk}]_{tot}$ is, thus, a linear combination of trapezoidal area integrals of the form

$$I_{TR}(m, n) = \iint_{yx} x^m y^n dx dy \quad (2.11)$$

Appendix C discusses how an integral table for different m and n combinations may be analytically constructed for each trapezoidal panel.

The contribution to the potential or strain energy U of an infinitesimal skin element dx by dy of the j th skin layer of a single trapezoidal panel is

$$dU_{jl} = \frac{1}{2} \{\kappa\}^T [D]_{jl} \{\kappa\} dx dy \quad (2.12)$$

where

$$\{\kappa\} = - \begin{Bmatrix} w_{,xx} \\ w_{,yy} \\ 2w_{,xy} \end{Bmatrix} \quad (2.13)$$

using Eqs. 2.3, 2.4, and 2.5; and $[D]_{jl}$ is the plate bending stiffness matrix for layer jl defined by

$$[D]_{jl} = \int_z [Q]_{jl} z^2 dz \quad (2.14)$$

(JO75, LIV90). The matrix $[Q]_{jl}$, 3×3 in dimension, is the jl th layer's constitutive matrix referenced to the x - y axes as discussed in Section 1.5. Since CPT zones assume wing symmetry, the depth distribution h will be treated here as the distance between the upper and lower skins. Referring to Figure A.2, the jl th skin layer lies between the coordinates $z=h/2-t_{jl}/2$ and $z=h/2+t_{jl}/2$ such that the z integral from Eq. 2.14 is given by

$$\int_{(h-t_{jl})/2}^{(h+t_{jl})/2} z^2 dz = \frac{h^2}{4} t_{jl} \left[1 + \frac{1}{3} \left(\frac{t_{jl}}{h} \right)^2 \right] \quad (2.15)$$

Since it is assumed that the wing thickness is much smaller than the wing depth ($t_{jl}/h \ll 1$), the right hand side of Eq. 2.15 can be simplified to $h^2 t_{jl}/4$ (LIV90). Substituting Eqs. 2.13 and 2.15 into Eq. 2.12 and integrating over the panel area gives

$$U_{jl} = \frac{1}{2} \iint_{yx} \left(\frac{h(x,y)^2}{4} \right) t_{jl}(x,y) \{q_w\}^T [W]^T [Q]_{jl} [W] \{q_w\} dx dy \quad (2.16)$$

where

$$[W] = \begin{bmatrix} \{a_{w,xx}\}^T \\ \{a_{w,yy}\}^T \\ 2\{a_{w,xy}\}^T \end{bmatrix} = \begin{bmatrix} \dots, m q_i (m q_i - 1) x^{m q_i - 2} y^{n q_i}, \dots \\ \dots, n q_i (n q_i - 1) x^{m q_i} y^{n q_i - 2}, \dots \\ \dots, 2 m q_i n q_i x^{m q_i - 1} y^{n q_i - 1}, \dots \end{bmatrix} \quad (2.17)$$

(LIV90). $[W]$ is $3 \times Nq_w$ in dimension. Summing the potential energy contributions of the Nl_u layers of the panel's upper skin, multiplying by 2 because of wing symmetry, and summing over the Np panels in the zone leads to the total skin stiffness matrix, $Nq_w \times Nq_w$ in dimension, given by

$$[K_{sk}]_{tot} = \frac{1}{2} \sum_{ip=1}^{Np} \sum_{jl=1}^{Nl_U} \iint h^2(x, y) t_{jl}(x, y) [W]^T [Q]_{jl} [W] dx dy \quad (2.18)$$

where $h(x, y)$ and $t_{jl}(x, y)$ are polynomial functions of x and y as defined in Eqs. 1.1 and 1.2. Each element of $[K_{sk}]_{tot}$ is a linear combination of area integrals of the form $I_{TR}(m, n)$ as defined in Eq. 2.11.

2.4 Spar Cap Contribution to Mass and Stiffness for a CPT Zone

The contribution to the kinetic energy T of an element of length $d\eta$ of the j st spar is

$$dT_{js} = \frac{1}{2} \rho_{js} A(\eta)_{sp_{js}} \dot{w}^2 d\eta \quad (2.19)$$

where η is the coordinate along the spar axis rotated from the y axis by an angle Λ , ρ_{js} is the constant material density of the spar, and the cap area $A_{sp_{js}}$ is expressed as a function of η (LIV90). Referring to Figure A.3, all η dependence in this equation may be changed to y dependence using

$$d\eta = dy \cdot \frac{L}{sy_R - sy_L} = \frac{dy}{\cos \Lambda} \quad (2.20)$$

The spar cap area may be expressed as a linear function of y , and the variable x may also be expressed in terms of y using the spar line equation

$$x(y) = S1y + S2 \quad (2.21)$$

Substituting Eqs. 2.6 and 2.20 into Eq. 2.19 and integrating over the length of the spar gives

$$T_{js} = \frac{1}{2} \frac{\rho_{js}}{\cos \Lambda} \int_{y=sy_L}^{y=sy_R} A(y)_{sp_{js}} \{ \dot{q}_w \}^T \{ a_w \} \{ a_w \}^T \{ \dot{q}_w \} dy \quad (2.22)$$

Summing the kinetic energy contributions of the Ns_U spars on the upper wing surface and multiplying by 2 because of wing symmetry leads to the total spar mass matrix, $Nq_w \times Nq_w$ in dimension, given by

$$[M_{sp}]_{tot} = 2 \sum_{js=1}^{Ns_U} \frac{\rho_{js}}{\cos \Lambda} \int_{y=sy_L}^{y=sy_R} A(y)_{sp_{js}} \{a_w\} \{a_w\}^T dy \quad (2.23)$$

where the spar cap area is given by Eq. 1.3. Using Eq. 2.21 for x , each element of $[M_{sp}]_{tot}$ becomes a linear combination of line integrals of the form

$$I_{SP}(m, n) = \frac{1}{\cos \Lambda} \int_{y=sy_L}^{y=sy_R} (S1y + S2)^m y^n dy \quad (2.24)$$

Appendix C discusses how an integral table for different m and n combinations may be analytically constructed for each spar line integral.

The contribution to the potential or strain energy U of an element of length $d\eta$ of the j sth spar is

$$dU_{js} = \frac{1}{2} E_{js} A(\eta)_{sp_{js}} \frac{h(\eta)^2}{4} w_{,\eta\eta}^2 d\eta \quad (2.25)$$

where E_{js} is the longitudinal modulus of elasticity, the cap area $A_{sp_{js}}$ is a function of η , and $h(\eta)$ is the wing depth distribution along the spar line (LIV90). It is necessary to replace η dependence with y dependence in this expression. Referring to Figure A.3 and Eq. 2.20 the transformation for the bending strain is given by

$$w_{,\eta\eta} = \cos^2 \Lambda \cdot w_{,yy} = \left(\frac{sy_R - sy_L}{L} \right)^2 w_{,yy} \quad (2.26)$$

The cap area may be expressed as a linear function of y as shown in Eq. 1.3, and the depth distribution may be expressed as a function of y as shown in Eq. A.74 using the spar line equation of Eq. 2.21. Substituting Eqs. 2.20 and 2.26 into Eq. 2.25 gives

$$dU_{js} = \frac{1}{2} (\cos \Lambda)^3 E_{js} A(y)_{sp_{js}} \frac{h(y)^2}{4} w_{,yy}^2 dy \quad (2.27)$$

Using Eq. 2.6 for $w(x,y,t)$ and integrating over the length of the spar gives

$$U_{js} = \frac{1}{2} (\cos \Lambda)^3 E_{js} \int_{y=sy_L}^{y=sy_R} A(y)_{sp_{js}} \frac{h(y)^2}{4} \cdot \{q_w\}^T \{a_{w,yy}\} \{a_{w,yy}\}^T \{q_w\} dy \quad (2.28)$$

where in $\{a_w\}$ all x terms are replaced by Eq. 2.21 before differentiation with respect to y . Summing the potential energy contributions of the Ns_U spars on the upper wing surface and multiplying by 2 because of wing symmetry leads to the total spar stiffness matrix, $Nq_w \times Nq_w$ in dimension, given by

$$[K_{sp}]_{tot} = \frac{1}{2} \sum_{js=1}^{Ns_U} E_{js} (\cos \Lambda)^4 \frac{1}{\cos \Lambda} \int_{y=sy_L}^{y=sy_R} A(y)_{sp_{js}} h(y)^2 \{a_{w,yy}\} \{a_{w,yy}\}^T dy \quad (2.29)$$

Each element of $[K_{sk}]_{tot}$ becomes a linear combination of line integrals of the form $I_{SP}(m,n)$ as defined in Eq. 2.24.

2.5 Rib Cap Contribution to Mass and Stiffness for a CPT Zone

The contribution to the kinetic energy T of an element of length dx of the j th rib is

$$dT_{jr} = \frac{1}{2} \rho_{jr} A(x)_{rb_{jr}} \dot{w}^2 dx \quad (2.30)$$

where ρ_{jr} is the constant material density of the rib, and the cap area $A_{rb_{jr}}$ is a linear function of x (LIV90). Using Eq. 2.6 for $w(x,y,t)$ and integrating over the length of the rib gives

$$T_{jr} = \frac{1}{2} \rho_{jr} \int_{x=rx_F}^{x=rx_A} A(x)_{rb_{jr}} \{\dot{q}_w\}^T \{a_w\} \{a_w\}^T \{\dot{q}_w\} dx \quad (2.31)$$

where the limits of integration rx_F and rx_A are shown in Figure A.4. Summing the kinetic energy contributions of the Nr_U ribs on the upper wing surface and multiplying by 2 because of wing symmetry leads to the total rib mass matrix, $Nq_w \times Nq_w$ in dimension, given by

$$[M_{rb}]_{tot} = 2 \sum_{jr=1}^{Nr_U} \rho_{jr} \int_{x=rx_F}^{x=rx_A} A(x)_{rb_{jr}} \{a_w\} \{a_w\}^T dx \quad (2.32)$$

where the rib cap area is given by Eq. 1.4. With y equal to a constant y_{RIB} along the length of the rib, each term of $[M_{rb}]_{tot}$ becomes a linear combination of line integrals of the form

$$I_{RB}(m, n) = y_{RIB}^n \int_{x=r_{x_F}}^{x=r_{x_A}} x^m dx \quad (2.33)$$

Appendix C discusses how an integral table for different m and n combinations may be analytically constructed for each rib line integral.

The contribution to the potential or strain energy U of an element of length dx of the j th rib is

$$dU_{jr} = \frac{1}{2} E_{jr} A(x)_{rb_{jr}} \frac{h(x)^2}{4} w_{,xx}^2 dx \quad (2.34)$$

where E_{jr} is the longitudinal modulus of elasticity, the cap area $A_{rb_{jr}}$ is a linear function of x , and $h(x)$ is the wing depth distribution along the rib line (LIV90). Using Eq. 2.6 for $w(x, y, t)$ and integrating along the length of the rib gives

$$U_{jr} = \frac{1}{2} E_{jr} \int_{x=r_{x_F}}^{x=r_{x_A}} A(x)_{rb_{jr}} \frac{h(x)^2}{4} \{q_w\}^T \{a_{w,xx}\} \{a_{w,xx}\}^T \{q_w\} dx \quad (2.35)$$

Summing the stiffness contribution of the Nr_U ribs on the upper wing surface and multiplying by 2 because of wing symmetry leads to the total rib stiffness matrix, $Nq_w \times Nq_w$ in dimension, given by

$$[K_{rb}]_{tot} = \frac{1}{2} \sum_{jr=1}^{Nr_U} E_{jr} \int_{x=r_{x_F}}^{x=r_{x_A}} A(x)_{rb_{jr}} h(x)^2 \{a_{w,xx}\} \{a_{w,xx}\}^T dx \quad (2.36)$$

where $h(x)$ is given by Eq. 1.1 holding y constant, and the rib cap area is given in Eq. 1.4. With y equal to a constant y_{RIB} along the length of the spar, each element of $[K_{rb}]_{tot}$ becomes a linear combination of line integrals of the form $I_{RB}(m, n)$ as defined in Eq. 2.33.

2.6 Concentrated Mass Contribution for a CPT Zone

Concentrated masses having a magnitude of \tilde{M}_{jc} may be designated at any point (x_{jc}, y_{jc}) on the wing structure. The contribution to the kinetic energy T of the j th concentrated mass is

$$T_{jc} = \frac{1}{2} \tilde{M}_{jc} \dot{w}^2(x_{jc}, y_{jc}, t) \quad (2.37)$$

(LIV90). Using Eq. 2.6 for $w(x_{jc}, y_{jc}, t)$ and summing over the N_c masses of a zone leads to the total concentrated mass matrix, $N_{q_w} \times N_{q_w}$ in dimension, given by

$$[M_{cm}]_{tot} = \sum_{jc=1}^{N_c} \tilde{M}_{jc} \{a_w(x_{jc}, y_{jc})\} \{a_w(x_{jc}, y_{jc})\}^T \quad (2.38)$$

2.7 Load Contributions for a CPT Zone

The generalized load vector $\{P\}$ defined in Chapter 1 may contain contributions from distributed pressure loads and concentrated force loads both acting in the vertical direction. A distributed pressure load over a trapezoidal panel area may be defined by a polynomial load function with N_ϕ terms given by

$$\phi(x, y) = \sum_{j=1}^{N_\phi} \Phi_j \cdot x^{m\phi_j} y^{n\phi_j} \quad (2.39)$$

The contribution to the work Q of a load distributed over an area dx by dy and working through the wing deflection is given by

$$dQ = \phi(x, y) w(x, y, t) dx dy \quad (2.40)$$

Using Eq. 2.6 for $w(x, y, t)$ and integrating over the panel area leads to the generalized load vector contribution of the distributed load given by

$$\{P_\phi\} = \sum_{j=1}^{N_\phi} \Phi_j \iint_{yx} x^{m\phi_j} y^{n\phi_j} \{a_w\} dx dy \quad (2.41)$$

The vector $\{P_\phi\}$ contains N_{q_w} terms, and its i th term may be expressed as a linear combination of area integrals of the form $I_{TR}(m, n)$ as defined in Eq. 2.11, where

$$m = m\phi_j + mq_i \quad (2.42)$$

$$n = n\phi_j + nq_i \quad (2.43)$$

For a concentrated force load of magnitude \hat{P} acting at the point (x_{jc}, y_{jc}) , the load vector contribution is simply

$$\{P_c\} = \hat{P} \{a_w\} \quad (2.44)$$

where $\{a_w\}$ is evaluated at (x_{jc}, y_{jc}) . For a single zone, the total generalized load vector $\{P\}_{tot}$ is obtained by adding the load contributions from all distributed and concentrated loads acting on the zone.

2.8 Displacement and Stress Output

The CPT zone generalized displacements resulting from the solution of Eq. 1.12 may be used to calculate the static displacement and stress at any point on the zone. Choosing a point (x_{out}, y_{out}) from an output grid, the vertical deflection w at that point may be determined simply by using Eq. 2.6 where $\{a_w\}$ is evaluated at the point. Using Eqs. 1.5, 2.3-2.5, and 2.17, stresses at a point (x_{out}, y_{out}) on the jl th skin layer may be determined from

$$\begin{Bmatrix} \sigma_{xx} \\ \sigma_{yy} \\ \sigma_{xy} \end{Bmatrix}_{jl} = [Q]_{jl} \begin{Bmatrix} \epsilon_{xx} \\ \epsilon_{yy} \\ \gamma_{xy} \end{Bmatrix} = -z [Q]_{jl} [W] \{q_w\} \quad (2.45)$$

where $[W]$ is evaluated at the point. Using Eqs. 2.6 and 2.26, the uniaxial stress at a point (x_{out}, y_{out}) on the js th spar may be determined from

$$\sigma_{js} = -z E_{js} w_{,\eta\eta} = -z E_{js} \cos^2 \Lambda \{a_{w,yy}\}^T \{q_w\} \quad (2.46)$$

where $\{a_{w,yy}\}$ is evaluated at the point (again, the x powers of $\{a_w\}$ are replaced by Eq. 2.21 before the differentiation with respect to y). Similarly, the uniaxial stress at a point (x_{out}, y_{out}) on the jr th rib may be determined from

$$\sigma_{jr} = -z E_{jr} w_{,xx} = -z E_{jr} \{a_{w,xx}\}^T \{q_w\} \quad (2.47)$$

where $\{a_{w,xx}\}$ is evaluated at the point.

The generalized displacements for a particular natural frequency resulting from the solution of Eq. 1.14 may be used to calculate the mode shape displacement at any point on the zone. As with static deflection, the modal deflection w at a point (x_{out}, y_{out}) may be determined by using Eq. 2.6 where $\{a_w\}$ is evaluated at the point.

Chapter 3: **Equivalent Plate Formulation Using** **First Order Shear Deformation Plate Theory**

3.1 Overview

This chapter contains the First Order Shear Deformation Plate Theory based formulation of the mass, stiffness, and generalized load contributions needed to solve for the generalized displacements in Eq. 1.11. The chapter begins with a discussion of the displacement and strain representations used in this approach. Following this is the derivation of the wing skin contributions to the mass and stiffness of the system. Next discussed are the derivations of the spar cap and rib cap contributions to mass and stiffness. This is followed by the derivations of the spar web and rib web contributions to mass and stiffness. Also included is a discussion of the contribution of concentrated masses to the mass of the system. Following this is the formulation of the load vector from concentrated force load and distributed pressure load conditions. Finally presented are the methods used to calculate displacement and stress output from the generalized displacement solution. Appendix B contains a more detailed derivation of mass and stiffness contributions from wing structural components.

3.2 FSDPT Displacements and Strains

First Order Shear Deformation Plate Theory (FSDPT) differs from Classical Plate Theory in that the Kirchhoff-Love assumption is not employed. Rather, it is assumed that plane sections normal to the plate's mid-surface remain plane but not necessarily normal to that surface after deformation. Hence, the shear strains γ_{xz} and γ_{yz} may not be ignored as they are in CPT (RE84,LIV194). It is assumed that the out of plane displacements are small, and there may be in-plane displacement of points at the plate's mid-surface since the wing is not assumed to be symmetric with respect to the x - y plane. As with CPT, the transverse normal strain ϵ_{zz} is negligible since the transverse deflection does not vary through the thickness of the plate, thus resulting in the transverse normal displacement w being a function of x and y only.

Using FSDPT the displacements in the x , y , and z directions respectively are approximated by

$$u(x, y, z) = u_0(x, y) + z\psi_x(x, y) \quad (3.1)$$

$$v(x, y, z) = v_0(x, y) + z\psi_y(x, y) \quad (3.2)$$

$$w(x, y, z) = w_0(x, y) \quad (3.3)$$

where u_0 , v_0 , w_0 are the x, y, z displacement components, respectively, of a point along the reference mid-surface, and ψ_x and ψ_y are rotations of a line element, originally perpendicular to the mid-surface plane, about the y and x axes respectively (RE84, LIV194). The associated strains are given by

$$\epsilon_{xx} = \frac{\partial u}{\partial x} = \frac{\partial u_0}{\partial x} + z \frac{\partial \psi_x}{\partial x} \quad (3.4)$$

$$\epsilon_{yy} = \frac{\partial v}{\partial y} = \frac{\partial v_0}{\partial y} + z \frac{\partial \psi_y}{\partial y} \quad (3.5)$$

$$\gamma_{xy} = \frac{\partial u}{\partial y} + \frac{\partial v}{\partial x} = \frac{\partial u_0}{\partial y} + \frac{\partial v_0}{\partial x} + z \left(\frac{\partial \psi_x}{\partial y} + \frac{\partial \psi_y}{\partial x} \right) \quad (3.6)$$

$$\gamma_{xz} = \psi_x + \frac{\partial w_0}{\partial x} \quad (3.7)$$

$$\gamma_{yz} = \psi_y + \frac{\partial w_0}{\partial y} \quad (3.8)$$

(LIV194, RE84). These displacement and strain relationships form the basis for the mass and stiffness matrix formulations.

To use the Ritz method described in Chapter 1, it is necessary to approximate each of the five x, y, t dependent deformation fields by polynomial series given in vector form as

$$u_0(x, y, t) = \{a_1(x, y)\}^T \{q_1(t)\} \quad (3.9)$$

$$v_0(x, y, t) = \{a_2(x, y)\}^T \{q_2(t)\} \quad (3.10)$$

$$\psi_x(x, y, t) = \{a_3(x, y)\}^T \{q_3(t)\} \quad (3.11)$$

$$\psi_y(x, y, t) = \{a_4(x, y)\}^T \{q_4(t)\} \quad (3.12)$$

$$w_0(x, y, t) = \{a_5(x, y)\}^T \{q_5(t)\} \quad (3.13)$$

where

$$\{a_1(x, y)\}^T = \{\dots, x^{mq_1}, y^{nq_1}, \dots\} \quad (3.14)$$

and similar expressions are used for $\{a_2\}^T$, $\{a_3\}^T$, $\{a_4\}^T$, and $\{a_5\}^T$ (LIV194). The column vectors $\{q_1\}$, $\{q_2\}$, $\{q_3\}$, $\{q_4\}$, and $\{q_5\}$ contain the polynomial coefficients which are the generalized displacements in the Ritz formulation. These polynomials have Nq_1 , Nq_2 , Nq_3 , Nq_4 , and Nq_5 terms respectively, and the x and y powers are predetermined.

When the vectors $\{q_1\}$, $\{q_2\}$, $\{q_3\}$, $\{q_4\}$, and $\{q_5\}$ are combined into one column vector of the form

$$\{q\}^T = \{q_1^T, q_2^T, q_3^T, q_4^T, q_5^T\} \quad (3.15)$$

the u, v, w components of deformation may be written as

$$\begin{Bmatrix} u \\ v \\ w \end{Bmatrix} = \{[S_0(x, y)] + z[S_1(x, y)]\} \{q(t)\} \quad (3.16)$$

where S_0 and S_1 are matrices containing polynomial terms of the form $x^{mS_0(r, i)} y^{nS_0(r, i)}$ and $x^{mS_1(r, i)} y^{nS_1(r, i)}$ respectively. Partitioned into subvectors of dimension $1 \times Nq_n$ ($n=1,2,\dots,5$), the matrices are given as

$$[S_0(x, y)] = \begin{bmatrix} a_1^T & 0 & 0 & 0 & 0 \\ 0 & a_2^T & 0 & 0 & 0 \\ 0 & 0 & 0 & 0 & a_5^T \end{bmatrix} \quad (3.17)$$

$$[S_1(x, y)] = \begin{bmatrix} 0 & 0 & a_3^T & 0 & 0 \\ 0 & 0 & 0 & a_4^T & 0 \\ 0 & 0 & 0 & 0 & 0 \end{bmatrix} \quad (3.18)$$

where both are $3 \times Nq_{tot}$ in dimension with

$$Nq_{tot} = Nq_1 + Nq_2 + Nq_3 + Nq_4 + Nq_5 \quad (3.19)$$

based on the length of the subvectors. Note that different orders of approximation polynomials are allowed for different displacement fields.

3.3 Skin Contribution to Mass and Stiffness for a FSDPT Zone

The contribution to the kinetic energy T of an infinitesimal skin element dx by dy of the j th skin layer of a single trapezoidal panel is

$$dT_{jl} = \frac{1}{2} \rho_{jl} t_{jl}(x, y) \left\{ \begin{matrix} \dot{u} \\ \bar{v} \\ \bar{w} \end{matrix} \right\}^T \left\{ \begin{matrix} \dot{u} \\ \bar{v} \\ \bar{w} \end{matrix} \right\} dx dy \quad (3.20)$$

where ρ_{jl} is the constant material density of the skin layer, and $t_{jl}(x, y)$ is the thickness of the skin layer (LIV194). Using Eq. 3.16 for the displacements and integrating over the whole trapezoidal panel area (placed at a distance z from the reference plane) gives

$$T_{jl} = \frac{1}{2} \rho_{jl} \iint_{yx} t_{jl}(x, y) \{ \dot{q} \}^T \left[S_0^T S_0 + z \left(S_0^T S_1 \right) + z \left(S_1^T S_0 \right) + z^2 \left(S_1^T S_1 \right) \right] \{ \dot{q} \} dx dy \quad (3.21)$$

Summing the kinetic energy contributions of the Nl_{TOT} skin layers in the panel and summing over the Np panels in the zone leads to the total skin mass matrix, $Nq_{tot} \times Nq_{tot}$ in dimension, given by

$$[M_{sk}]_{tot} = \sum_{ip=1}^{Np} \sum_{jl=1}^{Nl_{TOT}} \rho_{jl} \iint_{yx} t_{jl}(x, y) \left[S_0^T S_0 + h_{jl}(x, y) \left(S_0^T S_1 \right) + h_{jl}(x, y) \left(S_1^T S_0 \right) + h_{jl}^2(x, y) \left(S_1^T S_1 \right) \right] dx dy \quad (3.22)$$

where $h_{jl}(x,y)$, the layer depth distribution substituted for z , and $t_{jl}(x,y)$ are polynomial functions of x and y as given in Eqs. 1.1 and 1.2 (LIV194). Thus, each element of $[M_{sk}]_{tot}$ is a linear combination of area integrals of the form $I_{TR}(m,n)$ as defined in Eq. 2.11.

In assessing the strain energy of the skin, each skin layer is treated as a plane stress panel for which the only strains of concern are ϵ_{xx} , ϵ_{yy} , and γ_{xy} . Substituting Eqs. 3.9-3.13 into Eqs. 3.4-3.6 allows these strains to be written as

$$\begin{Bmatrix} \epsilon_{xx} \\ \epsilon_{yy} \\ \gamma_{xy} \end{Bmatrix} = \{ [R_0(x,y)] + z [R_1(x,y)] \} \{ q(t) \} \quad (3.23)$$

where

$$[R_0(x,y)] = \begin{bmatrix} a_{1,x}^T & 0 & 0 & 0 & 0 \\ 0 & a_{2,y}^T & 0 & 0 & 0 \\ a_{1,y}^T & a_{2,x}^T & 0 & 0 & 0 \end{bmatrix} \quad (3.24)$$

$$[R_1(x,y)] = \begin{bmatrix} 0 & 0 & a_{3,x}^T & 0 & 0 \\ 0 & 0 & 0 & a_{4,y}^T & 0 \\ 0 & 0 & a_{3,y}^T & a_{4,x}^T & 0 \end{bmatrix} \quad (3.25)$$

Partitioned into subvectors of dimension $1 \times Nq_n$ ($n=1,2,\dots,5$), these matrices are $3 \times Nq_{tot}$ in dimension. Now the contribution to the potential or strain energy U of an infinitesimal skin element dx by dy of the j th skin layer of a single trapezoidal panel is

$$dU_{jl} = \frac{1}{2} t_{jl}(x,y) \begin{Bmatrix} \epsilon_{xx} \\ \epsilon_{yy} \\ \gamma_{xy} \end{Bmatrix}^T [Q]_{jl} \begin{Bmatrix} \epsilon_{xx} \\ \epsilon_{yy} \\ \gamma_{xy} \end{Bmatrix} dx dy \quad (3.26)$$

where the matrix $[Q]_{jl}$, 3×3 in dimension, is the j th layer's constitutive matrix referenced to the x - y axes, and $t_{jl}(x,y)$ is the thickness of the skin layer (LIV194). Using Eq. 3.23 for the strains and integrating over the trapezoidal panel area gives

$$U_{jl} = \frac{1}{2} \iint_{yx} t_{jl}(x, y) \{q\}^T \left[R_0^T [Q]_{jl} R_0 + z \left(R_0^T [Q]_{jl} R_1 \right) + z \left(R_1^T [Q]_{jl} R_0 \right) + z^2 \left(R_1^T [Q]_{jl} R_1 \right) \right] \{q\} dx dy \quad (3.27)$$

Summing the potential energy contributions of the Nl_{TOT} skin layers in the panel and summing over the Np panels in the zone leads to the total skin stiffness matrix, $Nq_{tot} \times Nq_{tot}$ in dimension, given by

$$[K_{sk}]_{tot} = \sum_{ip=1}^{Np} \sum_{jl=1}^{Nl_{TOT}} \iint_{yx} t_{jl}(x, y) \left[R_0^T [Q]_{jl} R_0 + h_{jl}(x, y) \left(R_0^T [Q]_{jl} R_1 \right) + h_{jl}(x, y) \left(R_1^T [Q]_{jl} R_0 \right) + h_{jl}^2(x, y) \left(R_1^T [Q]_{jl} R_1 \right) \right] dx dy \quad (3.28)$$

where the depth distribution $h_{jl}(x, y)$ in Eq. 1.1 has been substituted for z , and $t_{jl}(x, y)$ is given in Eq. 1.2. Each element of $[K_{sk}]_{tot}$ is a linear combination of area integrals of the form $I_{TR}(m, n)$.

3.4 Spar Cap Contribution to Mass and Stiffness for a FSDPT Zone

The contribution to the kinetic energy T of an element of length $d\eta$ of the j st spar is

$$dT_{js} = \frac{1}{2} \rho_{js} A(\eta)_{sp_{js}} \left\{ \begin{matrix} \dot{u} \\ \dot{v} \\ \dot{w} \end{matrix} \right\}^T \left\{ \begin{matrix} \dot{u} \\ \dot{v} \\ \dot{w} \end{matrix} \right\} d\eta \quad (3.29)$$

where η is the coordinate along the spar axis rotated from the y axis by an angle Λ , ρ_{js} is the constant material density of the spar, and the cap area $A_{sp_{js}}$ is expressed as a function of η (LIV194). Referring to Figure A.3, all η dependence of this equation may be changed to y dependence using Eq. 2.20. The spar cap area may be expressed as a linear function of y , and the variable x may be expressed in terms of y using the spar line equation from Eq. 2.21. Using Eqs. 2.20 and 3.16 and integrating over the length of the spar gives

$$T_{js} = \frac{1}{2} \frac{\rho_{js}}{\cos \Lambda} \int_{y=sy_L}^{y=sy_R} A(y)_{sp_{js}} \{ \dot{q} \}^T \left[S_0^T S_0 + z \left(S_0^T S_1 \right) + z \left(S_1^T S_0 \right) + z^2 \left(S_1^T S_1 \right) \right] \{ \dot{q} \} dy \quad (3.30)$$

Summing the kinetic energy contributions of the N_{sTOT} spars in a zone leads to the total spar mass matrix, $Nq_{tot} \times Nq_{tot}$ in dimension, given by

$$[M_{sp}]_{tot} = \sum_{js=1}^{N_{sTOT}} \frac{\rho_{js}}{\cos \Lambda} \int_{y=sy_L}^{y=sy_R} A(y) {}_{sp_{js}} \left[S_0^T S_0 + h_{js}(x, y) \begin{pmatrix} S_0^T S_1 \\ S_1^T S_0 \end{pmatrix} + h_{js}(x, y) \begin{pmatrix} S_1^T S_0 \\ S_0^T S_1 \end{pmatrix} + h_{js}^2(x, y) \begin{pmatrix} S_1^T S_1 \end{pmatrix} \right] dy \quad (3.31)$$

where the spar depth distribution $h_{js}(x, y)$ has been substituted for z using Eq. 1.1, and the spar cap area is given in Eq. 1.3 (LIV194). When Eq. 2.21 is used for x , each element of $[M_{sp}]_{tot}$ becomes a linear combination of spar line integrals of the form $I_{sp}(m, n)$ as defined in Eq. 2.24.

The contribution to the potential or strain energy U of an element of length $d\eta$ of the j stth spar is

$$dU_{js} = \frac{1}{2} E_{js} A(\eta) {}_{sp_{js}} \epsilon_{\eta\eta}^2 d\eta \quad (3.32)$$

where E_{js} is the longitudinal modulus of elasticity, the cap area $A_{sp_{js}}$ is a function of the spar line coordinate η , and $\epsilon_{\eta\eta}$ is the normal strain along the spar axis (LIV194). The spar cap area may be expressed as a linear function of y . Referring to Figure A.3 and using standard tensor transformation rules, the normal strain in the η direction may be written in terms of strains in the x and y directions by

$$\epsilon_{\eta\eta} = \{TR\}^T \begin{Bmatrix} \epsilon_{xx} \\ \epsilon_{yy} \\ \gamma_{xy} \end{Bmatrix} \quad (3.33)$$

where

$$\{TR\}^T = \{\sin^2 \Lambda, \cos^2 \Lambda, \sin \Lambda \cos \Lambda\} = \{s^2 \Lambda, c^2 \Lambda, s \Lambda c \Lambda\} \quad (3.34)$$

Let us define

$$[Q_{sp}] = \{TR\} \{TR\}^T \quad (3.35)$$

Substituting Eq. 2.20 for $d\eta$, using Eqs. 3.23 and 3.33 for the strain, and integrating over

the length of the spar gives

$$U_{js} = \frac{1}{2} \frac{E_{js}}{\cos \Lambda} \int_{y=sy_L}^{y=sy_R} A(y)_{sp_{js}} \{q\}^T \left[R_0^T [Q_{sp}] R_0 + z \left(R_0^T [Q_{sp}] R_1 \right) \right. \\ \left. + z \left(R_1^T [Q_{sp}] R_0 \right) + z^2 \left(R_1^T [Q_{sp}] R_1 \right) \right] \{q\} dy \quad (3.36)$$

Summing the potential energy contributions of the N_{sTOT} spars in the zone leads to the total spar stiffness matrix, $N_{q_{tot}} \times N_{q_{tot}}$ in dimension, given by

$$[K_{sp}]_{tot} = \sum_{js=1}^{N_{sTOT}} \frac{E_{js}}{\cos \Lambda} \int_{y=sy_L}^{y=sy_R} A(y)_{sp_{js}} \left[R_0^T [Q_{sp}] R_0 + h_{js}(x, y) \left(R_0^T [Q_{sp}] R_1 \right) \right. \\ \left. + h_{js}(x, y) \left(R_1^T [Q_{sp}] R_0 \right) + h_{js}^2(x, y) \left(R_1^T [Q_{sp}] R_1 \right) \right] dy \quad (3.37)$$

where the spar depth distribution $h_{js}(x, y)$ has been substituted for z using Eq. 1.1, and the spar cap area is given in Eq. 1.3 (LIV194). When Eq. 2.21 is used for x , each element of $[K_{sp}]_{tot}$ becomes a linear combination of spar line integrals of the form $I_{sp}(m, n)$.

3.5 Rib Cap Contribution to Mass and Stiffness for a FSDPT Zone

The contribution to the kinetic energy T of an element of length dx of the j th rib is

$$dT_{jr} = \frac{1}{2} \rho_{jr} A(x)_{rb_{jr}} \left\{ \begin{array}{c} \dot{u} \\ \dot{\bar{v}} \\ \dot{\bar{w}} \end{array} \right\}^T \left\{ \begin{array}{c} \dot{u} \\ \dot{\bar{v}} \\ \dot{\bar{w}} \end{array} \right\} dx \quad (3.38)$$

where ρ_{jr} is the constant material density of the rib, and the cap area $A_{rb_{jr}}$ is a linear function of x . Using Eq. 3.16 for the displacements and integrating over the length of the rib gives

$$T_{jr} = \frac{1}{2} \rho_{jr} \int_{x=rx_F}^{x=rx_A} A(x)_{rb_{jr}} \{ \dot{q} \}^T \left[S_0^T S_0 + z \left(S_0^T S_1 \right) + z \left(S_1^T S_0 \right) + z^2 \left(S_1^T S_1 \right) \right] \{ \dot{q} \} dx \quad (3.39)$$

where the limits of integration rx_F and rx_A are shown in Figure A.4. Summing the kinetic energy contributions of the N_{rTOT} ribs in the zone leads to the total rib mass matrix, $N_{q_{tot}} \times$

Nq_{tot} in dimension, given by

$$[M_{rb}]_{tot} = \sum_{jr=1}^{Nr_{TOT}} \rho_{jr} \int_{x=r x_F}^{x=r x_A} A(x)_{rb_{jr}} \left[S_0^T S_0 + h_{jr}(x, y) \left(S_0^T S_1 \right) \right. \\ \left. + h_{jr}(x, y) \left(S_1^T S_0 \right) + h_{jr}^2(x, y) \left(S_1^T S_1 \right) \right] dx \quad (3.40)$$

where the rib depth distribution $h_{jr}(x, y)$ has been substituted for z , and the rib cap area is given by Eq. 1.4. With y equal to a constant y_{RIB} along the length of the spar, each element of $[M_{rb}]_{tot}$ becomes a linear combination of line integrals of the form $I_{RB}(m, n)$ as defined in Eq. 2.33.

The contribution to the potential or strain energy U of an element of length dx of the jr th rib is

$$dU_{jr} = \frac{1}{2} E_{jr} A(x)_{rb_{jr}} \epsilon_{xx}^2 dx \quad (3.41)$$

where E_{jr} is the longitudinal modulus of elasticity, and the cap area $A_{rb_{jr}}$ is a linear function of x . Focusing on a subset of the displacement fields (using Eqs. B.4, B.9, and B.11) the uniaxial strain along a rib cap is expressed by

$$\epsilon_{xx} = \{ [Y_0(x, y)] + z [Y_1(x, y)] \} \{ \hat{q}(t) \} \quad (3.42)$$

where

$$\{ \hat{q} \}^T = \{ q_1^T, q_3^T \} \quad (3.43)$$

$$[Y_0(x, y)] = \begin{bmatrix} \{ a_{1,x}^T \} & \{ 0 \} \end{bmatrix} \quad (3.44)$$

$$[Y_1(x, y)] = \begin{bmatrix} \{ 0 \} & \{ a_{3,x}^T \} \end{bmatrix} \quad (3.45)$$

Both matrices, $1 \times (Nq_1 + Nq_3)$ in dimension, are partitioned into 2 subvectors having Nq_1 and Nq_3 terms respectively. Using Eq. 3.42 for the strain and integrating over the length of the rib gives

$$U_{jr} = \frac{1}{2} E_{jr} \int_{x=r x_F}^{x=r x_A} A(x) {}_{rb_{jr}} \{\hat{q}\}^T \left[Y_0^T Y_0 + z \left(Y_0^T Y_1 \right) + z \left(Y_1^T Y_0 \right) + z^2 \left(Y_1^T Y_1 \right) \right] \{\hat{q}\} dx \quad (3.46)$$

Summing the potential energy contributions of the Nr_{TOT} ribs in the zone leads to the total rib mass matrix, $(Nq_1+Nq_3) \times (Nq_1+Nq_3)$ in dimension (and submatrix entries corresponding to $\{q_1\}$ and $\{q_3\}$), given by

$$[K_{rb}]_{tot} = \sum_{jr=1}^{Nr_{TOT}} E_{jr} \int_{x=r x_F}^{x=r x_A} A(x) {}_{rb_{jr}} \left[Y_0^T Y_0 + h_{jr}(x, y) \left(Y_0^T Y_1 \right) + h_{jr}(x, y) \left(Y_1^T Y_0 \right) + h_{jr}^2(x, y) \left(Y_1^T Y_1 \right) \right] dx \quad (3.47)$$

where the rib depth distribution $h_{jr}(x, y)$ has been substituted for z , and the rib cap area is given by Eq. 1.4. With y equal to a constant y_{RIB} along the length of the spar, each element of $[K_{rb}]_{tot}$ becomes a linear combination of line integrals of the form $I_{RB}(m, n)$.

3.6 Spar Web Contribution to Mass and Stiffness for a FSDPT Zone

A spar web is positioned in the vertical plane between parallel spar caps on the upper and lower wing surfaces. This plane is defined to be the η - z plane where η is the coordinate along the corresponding parallel upper and lower spar axes rotated from the y axis by an angle Λ . See Figure A.3 for spar line geometry. The contribution to the kinetic energy T of an infinitesimal element $d\eta$ by dz of the jl th spar web layer is

$$dT_{jl} = \frac{1}{2} \rho_{jl} t_{jl}(\eta, z) \left\{ \begin{array}{c} \dot{u} \\ \dot{\bar{v}} \\ \dot{\bar{w}} \end{array} \right\}^T \left\{ \begin{array}{c} \dot{u} \\ \dot{\bar{v}} \\ \dot{\bar{w}} \end{array} \right\} d\eta dz \quad (3.48)$$

where ρ_{jl} is the constant material density of the web layer, and $t_{jl}(\eta, z)$ is the thickness of the layer (LIV194). The layer thickness may be expressed as a linear function of y only, and the variable x may be expressed in terms of y using the spar line equation from Eq. 2.21. All η dependence may be changed to y dependence using Eq. 2.20. Substituting Eq. 2.20 for $d\eta$, using Eq. 3.16 for the displacements, and integrating over the area of the web gives

$$T_{jl} = \frac{1}{2} \frac{\rho_{jl}}{\cos \Lambda} \int_{y=sy_L}^{y=sy_R} \int_{h_L(y)}^{h_U(y)} t_{jl}(y) \{ \dot{q} \}^T \left[S_0^T S_0 + z \left(S_0^T S_1 \right) \right. \\ \left. + z \left(S_1^T S_0 \right) + z^2 \left(S_1^T S_1 \right) \right] \{ \dot{q} \} dz dy \quad (3.49)$$

where the limits of z integration are the depth distributions of the lower and upper spar caps given by Eqs. B.133 and B.134. Summing the kinetic energy contributions of the Nl_{swb} spar web layers of each of the Nsw spar webs in the zone leads to the total spar web mass matrix, $Nq_{tot} \times Nq_{tot}$ in dimension, given by

$$[M_{swb}]_{tot} = \sum_{is=1}^{Nsw} \sum_{jl=1}^{Nl_{swb}} \frac{\rho_{jl}}{\cos \Lambda} \int_{y=sy_L}^{y=sy_R} \int_{h_L(y)}^{h_U(y)} t_{jl}(y) \left[S_0^T S_0 + z \left(S_0^T S_1 \right) \right. \\ \left. + z \left(S_1^T S_0 \right) + z^2 \left(S_1^T S_1 \right) \right] dz dy \quad (3.50)$$

where $t_{jl}(y)$ is given in Eq. B.130. The z integration may be performed analytically using Eq. B.137 thus leaving only a spar line integral to be evaluated. Therefore, when Eq. 2.21 is used for x , each element of $[M_{swb}]_{tot}$ becomes a linear combination of line integrals of the form $I_{sp}(m,n)$ as defined in Eq. 2.24.

In assessing the strain energy of a spar web, each layer is treated as a plane stress panel where the only strains of importance are $\epsilon_{\eta\eta}$, ϵ_{zz} , and $\gamma_{\eta z}$. From the assumptions of FSDPT, ϵ_{zz} may be neglected. In Eq. 3.33, the normal strain $\epsilon_{\eta\eta}$ has been defined in terms of strains in the x - y plane. Using standard tensor transformation rules, the shear strain $\gamma_{\eta z}$ may also be defined in terms of strains in the x - y plane by

$$\gamma_{\eta z} = \{ \sin \Lambda, \cos \Lambda \} \begin{Bmatrix} \gamma_{xz} \\ \gamma_{yz} \end{Bmatrix} = \{ s\Lambda, c\Lambda \} \begin{Bmatrix} \gamma_{xz} \\ \gamma_{yz} \end{Bmatrix} \quad (3.51)$$

where Λ is the angle of rotation of the η axis from the y axis (LIV194). Combining Eqs. 3.33 and 3.51 let us define

$$\begin{Bmatrix} \epsilon_{\eta\eta} \\ \gamma_{\eta z} \end{Bmatrix} = [TR_{25}] \{ \epsilon \} \quad (3.52)$$

where

$$\{ \epsilon \}^T = \{ \epsilon_{xx}, \epsilon_{yy}, \gamma_{xy}, \gamma_{xz}, \gamma_{yz} \} \quad (3.53)$$

$$[TR_{25}] = \begin{bmatrix} (s^2\Lambda) & (c^2\Lambda) & (s\Lambda c\Lambda) & 0 & 0 \\ 0 & 0 & 0 & (s\Lambda) & (c\Lambda) \end{bmatrix} \quad (3.54)$$

Using Eqs. 3.4-3.15 to expand Eq. 3.53 gives

$$\{\epsilon\}^T = \{ [W_0(x, y)] + z [W_1(x, y)] \} \{q(t)\} \quad (3.55)$$

where

$$[W_0(x, y)] = \begin{bmatrix} a_{1,x}^T & 0 & 0 & 0 & 0 \\ 0 & a_{2,y}^T & 0 & 0 & 0 \\ a_{1,y}^T & a_{2,x}^T & 0 & 0 & 0 \\ 0 & 0 & a_3^T & 0 & a_{5,x}^T \\ 0 & 0 & 0 & a_4^T & a_{5,y}^T \end{bmatrix} \quad (3.56)$$

$$[W_1(x, y)] = \begin{bmatrix} 0 & 0 & a_{3,x}^T & 0 & 0 \\ 0 & 0 & 0 & a_{4,y}^T & 0 \\ 0 & 0 & a_{3,y}^T & a_{4,x}^T & 0 \\ 0 & 0 & 0 & 0 & 0 \\ 0 & 0 & 0 & 0 & 0 \end{bmatrix} \quad (3.57)$$

Partitioned into subvectors of dimension $1 \times Nq_n$ ($n=1,2,\dots,5$), both matrices are $5 \times Nq_{tot}$ in dimension. Now the contribution to the potential or strain energy U of an infinitesimal element $d\eta$ by dz of the j th spar web layer is

$$dU_{jl} = \frac{1}{2} t_{jl}(\eta, z) \left\{ \begin{matrix} \epsilon_{\eta\eta} \\ \gamma_{\eta z} \end{matrix} \right\}^T [\bar{Q}]_{jl} \left\{ \begin{matrix} \epsilon_{\eta\eta} \\ \gamma_{\eta z} \end{matrix} \right\} d\eta dz \quad (3.58)$$

where $[\bar{Q}]_{jl}$ is the j th layer's constitutive matrix referenced to the η - z axes as discussed in Section 1.5, and $t_{jl}(\eta, z)$ is the thickness of the layer (LIV194). The layer thickness may be expressed as a linear function of y only, and the variable x may be expressed in terms of y using the spar line equation from Eq. 2.21. Let us now define

$$[Q_s] = [TR_{25}]^T [\bar{Q}]_{jl} [TR_{25}] \quad (3.59)$$

Substituting Eq. 2.20 for $d\eta$, combining Eqs. 3.52, 3.55, and 3.59 for the strains, and integrating over the area of the web gives

$$U_{jl} = \frac{1}{2} \frac{1}{\cos \Lambda} \int_{y=sy_L}^{y=sy_R} \int_{h_L(y)}^{h_U(y)} t_{jl}(y) \{q\}^T \left[W_0^T [Q_s] W_0 + z \left(W_0^T [Q_s] W_1 \right) \right. \\ \left. + z \left(W_1^T [Q_s] W_0 \right) + z^2 \left(W_1^T [Q_s] W_1 \right) \right] \{q\} dz dy \quad (3.60)$$

where the limits of z integration are the depth distributions of the lower and upper spar caps given in Eqs. B.133 and B.134. Summing the potential energy contributions of the Nl_{swb} spar web layers of each of the Nsw spar webs in the zone leads to the total spar web stiffness matrix, $Nq_{tot} \times Nq_{tot}$ in dimension, given by

$$[K_{swb}]_{tot} = \sum_{is=1}^{Nsw} \sum_{jl=1}^{Nl_{swb}} \frac{1}{\cos \Lambda} \int_{y=sy_L}^{y=sy_R} \int_{h_L(y)}^{h_U(y)} t_{jl}(y) \left[W_0^T [Q_s] W_0 + z \left(W_0^T [Q_s] W_1 \right) \right. \\ \left. + z \left(W_1^T [Q_s] W_0 \right) + z^2 \left(W_1^T [Q_s] W_1 \right) \right] dz dy \quad (3.61)$$

where $t_{jl}(y)$ is given in Eq. B.130. The z integration may be performed analytically using Eq. B.137 thus leaving only a spar line integral to be evaluated. Therefore, each element of $[K_{swb}]_{tot}$ becomes a linear combination of line integrals of the form $I_{sp}(m,n)$.

3.7 Rib Web Contribution to Mass and Stiffness for a FSDPT Zone

A rib web is positioned in the vertical plane between parallel rib caps on the upper and lower wing surfaces. This plane is the x - z plane located at $y=y_{RIB}$. The contribution to the kinetic energy T of an infinitesimal element dx by dz of the jl th rib web layer is

$$dT_{jl} = \frac{1}{2} \rho_{jl} t_{jl}(x, z) \left\{ \begin{array}{c} \dot{u} \\ \dot{\bar{v}} \\ \dot{\bar{w}} \end{array} \right\}^T \left\{ \begin{array}{c} \dot{u} \\ \dot{\bar{v}} \\ \dot{\bar{w}} \end{array} \right\} dx dz \quad (3.62)$$

where ρ_{jl} is the constant material density of the web layer, and $t_{jl}(x,z)$ is the thickness of the layer. The layer thickness may be expressed as a linear function of x only. Using Eq. 3.16

for the displacements and integrating over the area of the web gives

$$T_{jl} = \frac{1}{2} \rho_{jl} \int_{x=r_{x_F}}^{x=r_{x_A}} \int_{h_L(x,y)}^{h_U(x,y)} t_{jl}(x) \{ \dot{q} \}^T \left[S_0^T S_0 + z \left(S_0^T S_1 \right) \right. \\ \left. + z \left(S_1^T S_0 \right) + z^2 \left(S_1^T S_1 \right) \right] \{ \dot{q} \} dz dx \quad (3.63)$$

where the limits of z integration are the depth distributions of the upper and lower rib caps given respectively by Eqs. B.133 and B.134. Summing the kinetic energy contributions of the of Nl_{rwb} rib web layers of each of the Nrw rib webs in the zone leads to the total rib web mass matrix, $Nq_{tot} \times Nq_{tot}$ in dimension, given by

$$[M_{rwb}]_{tot} = \sum_{ir=1}^{Nrw} \sum_{jl=1}^{Nl_{rwb}} \rho_{jl} \int_{x=r_{x_F}}^{x=r_{x_A}} \int_{h_L(y)}^{h_U(y)} t_{jl}(x) \left[S_0^T S_0 + z \left(S_0^T S_1 \right) \right. \\ \left. + z \left(S_1^T S_0 \right) + z^2 \left(S_1^T S_1 \right) \right] dz dx \quad (3.64)$$

where $t_{jl}(x)$ is given in Eq. B.199. The z integration may be performed analytically using Eq. B.137 thus leaving only a rib line integral to be evaluated. Therefore, with y equal to a constant y_{RIB} along the rib line, each element of $[M_{rwb}]_{tot}$ becomes a linear combination of line integrals of the form $I_{RB}(m,n)$ as defined in Eq.2.33.

In assessing the strain energy of a rib web, each layer is treated as a plane stress panel where the only strains of importance are ϵ_{xx} , ϵ_{zz} , and γ_{xz} . From the assumptions of FSDPT, ϵ_{zz} may be neglected. Using Eqs. 3.4, 3.7, 3.9, 3.11, and 3.13 let us define

$$\begin{Bmatrix} \epsilon_{xx} \\ \gamma_{xz} \end{Bmatrix} = \{ [F_0(x,y)] + z [F_1(x,y)] \} \{ \tilde{q}(t) \} \quad (3.65)$$

where

$$\{ \tilde{q} \}^T = \{ q_1^T, q_3^T, q_5^T \} \quad (3.66)$$

$$[F_0(x,y)] = \begin{bmatrix} a_{1,x}^T & 0 & 0 \\ 0 & a_3^T & a_{5,x}^T \end{bmatrix} \quad (3.67)$$

$$[F_1(x, y)] = \begin{bmatrix} 0 & a_{3,x}^T & 0 \\ 0 & 0 & 0 \end{bmatrix} \quad (3.68)$$

Partitioned into subvectors of dimension $1 \times Nq_n$ ($n=1,3,5$), both matrices F_0 and F_1 are $2 \times (Nq_1+Nq_3+Nq_5)$ in dimension. Now the contribution to the potential or strain energy U of an infinitesimal element dx by dz of the j lth rib web layer is

$$dU_{jl} = \frac{1}{2} t_{jl}(x, z) \left\{ \begin{matrix} \epsilon_{xx} \\ \gamma_{xz} \end{matrix} \right\}^T [\bar{Q}]_{jl} \left\{ \begin{matrix} \epsilon_{xx} \\ \gamma_{xz} \end{matrix} \right\} dx dz \quad (3.69)$$

where $[\bar{Q}]_{jl}$ is the j lth layer's constitutive matrix referenced to the x - z axes as discussed in Section 1.5, and $t_{jl}(x, z)$ is the thickness of the layer. The layer thickness may be expressed as a linear function of x only. Using Eq. 3.65 for the strains and integrating over the area of the web gives

$$U_{jl} = \frac{1}{2} \int_{x=r_{x_F}}^{x=r_{x_A}} \int_{h_L(y)}^{h_U(y)} t_{jl}(x) \{ \tilde{q} \}^T \left[F_0^T [\bar{Q}]_{jl} F_0 + z \left(F_0^T [\bar{Q}]_{jl} F_1 \right) \right. \\ \left. + z \left(F_1^T [\bar{Q}]_{jl} F_0 \right) + z^2 \left(F_1^T [\bar{Q}]_{jl} F_1 \right) \right] \{ \tilde{q} \} dz dx \quad (3.70)$$

where the limits of z integration are the depth distributions of the upper and lower rib caps given in Eqs. B.133 and B.134. Summing the potential energy contributions of the of Nl_{rwb} rib web layers of each of the Nrw rib webs in the zone leads to the total rib web stiffness matrix, $(Nq_1+Nq_3+Nq_5) \times (Nq_1+Nq_3+Nq_5)$ in dimension, given by

$$[K_{rwb}]_{tot} = \sum_{ir=1}^{Nrw} \sum_{jl=1}^{Nl_{rwb}} \int_{x=r_{x_F}}^{x=r_{x_A}} \int_{h_L(y)}^{h_U(y)} t_{jl}(x) \left[F_0^T [\bar{Q}]_{jl} F_0 + z \left(F_0^T [\bar{Q}]_{jl} F_1 \right) \right. \\ \left. + z \left(F_1^T [\bar{Q}]_{jl} F_0 \right) + z^2 \left(F_1^T [\bar{Q}]_{jl} F_1 \right) \right] dz dx \quad (3.71)$$

where $t_{jl}(x)$ is given in Eq. B.199. The z integration may be performed analytically using Eq. B.137 thus leaving only a rib line integral to be evaluated. Therefore, each element of $[K_{rwb}]_{tot}$ becomes a linear combination of line integrals of the form $I_{RB}(m, n)$.

3.8 Concentrated Mass Contribution for a FSDPT Zone

Concentrated masses having a magnitude of \tilde{M}_{jc} may be designated at free moving points (x_{jc}, y_{jc}) on the wing structure. Each point is also associated with some depth distribution. The contribution to the kinetic energy T of the j th point mass is

$$T_{jc} = \frac{1}{2} \tilde{M}_{jc} \begin{Bmatrix} \dot{u} \\ \dot{v} \\ \dot{w} \end{Bmatrix}^T \begin{Bmatrix} \dot{u} \\ \dot{v} \\ \dot{w} \end{Bmatrix} \quad (3.72)$$

Using Eq. 3.16 for the displacements and summing over the N_c masses of a zone leads to the total point mass matrix, $N_{q_{tot}} \times N_{q_{tot}}$ in dimension, given by

$$[M_{cm}]_{tot} = \sum_{jc=1}^{N_c} \tilde{M}_{jc} \left[\left(S_0^T S_0 \right) + z \left(S_0^T S_1 \right) + z \left(S_1^T S_0 \right) + z^2 \left(S_1^T S_1 \right) \right] \quad (3.73)$$

where S_0 and S_1 are evaluated at (x_{jc}, y_{jc}) . The z coordinate of a point is determined from its depth distribution.

3.9 Load Contributions for a FSDPT Zone

As discussed in Section 2.7, the generalized load vector $\{P\}$ may contain contributions from distributed pressure loads and concentrated force loads. A distributed load over a trapezoidal panel area was defined in Eq. 2.39. For a FSDPT zone the pressure may have components in the x and y directions as well as the z direction. If the component distributions in the x , y , and z directions are ϕ_x , ϕ_y , ϕ_z respectively, then the 3 directional contributions to the potential energy Q of a load distributed over an area dx by dy of a panel and working through the wing deflections are given by

$$dQ_x = \phi_x(x, y) u(x, y, z, t) dx dy = \phi_x(x, y) [u_0(x, y, t) + z \psi_x(x, y, t)] dx dy \quad (3.74)$$

$$dQ_y = \phi_y(x, y) v(x, y, z, t) dx dy = \phi_y(x, y) [v_0(x, y, t) + z \psi_y(x, y, t)] dx dy \quad (3.75)$$

$$dQ_z = \phi_z(x, y) w(x, y, z, t) dx dy = \phi_z(x, y) [w_0(x, y, t)] dx dy \quad (3.76)$$

Using 3.9-3.13 for the deformation fields, we get an expression for the virtual work in the

form

$$\delta Q = \iint_{xy} \left(\phi_x \{a_1\} \{\delta q_1\} + \phi_x z \{a_3\} \{\delta q_3\} + \phi_y \{a_2\} \{\delta q_2\} + \right. \\ \left. \phi_y z \{a_4\} \{\delta q_4\} + \phi_z \{a_5\} \{\delta q_5\} \right) dx dy \quad (3.77)$$

Let the polynomial loads now be defined as

$$\phi_x(x, y) = \sum_{j=1}^{N\phi_x} \Phi_{x_j} x^{m\phi_j} y^{n\phi_j} \quad (3.78)$$

$$\phi_y(x, y) = \sum_{j=1}^{N\phi_y} \Phi_{y_j} x^{m\phi_j} y^{n\phi_j} \quad (3.79)$$

$$\phi_z(x, y) = \sum_{j=1}^{N\phi_z} \Phi_{z_j} x^{m\phi_j} y^{n\phi_j} \quad (3.80)$$

The generalized load vector is now partitioned as

$$\{P\}^T = \{P_1^T, P_2^T, P_3^T, P_4^T, P_5^T\} \quad (3.81)$$

where

$$\{P_1\} = \sum_{j=1}^{N\phi_x} \Phi_{x_j} \iint_{yx} x^{m\phi_j} y^{n\phi_j} \{a_1(x, y)\} dx dy \quad (3.82)$$

$$\{P_2\} = \sum_{j=1}^{N\phi_y} \Phi_{y_j} \iint_{yx} x^{m\phi_j} y^{n\phi_j} \{a_2(x, y)\} dx dy \quad (3.83)$$

$$\{P_3\} = z \sum_{j=1}^{N\phi_x} \Phi_{x_j} \iint_{yx} x^{m\phi_j} y^{n\phi_j} \{a_3(x, y)\} dx dy \quad (3.84)$$

$$\{P_4\} = z \sum_{j=1}^{N\phi_y} \Phi_{y_j} \iint_{yx} x^{m\phi_j} y^{n\phi_j} \{a_4(x, y)\} dx dy \quad (3.85)$$

$$\{P_5\} = \sum_{j=1}^{N\phi_z} \Phi_{z_j} \iint_{yx} x^{m\phi_j} y^{n\phi_j} \{a_5(x, y)\} dx dy \quad (3.86)$$

The depth distribution of the loaded panel is substituted for z in terms where it appears, depending on where the in-plane forces are applied. Each term of the vector may be expressed as a linear combination of area integrals of the form $I_{TR}(m,n)$, as defined in Eq. 2.11. For a concentrated force load with components $\hat{P}_x, \hat{P}_y, \hat{P}_z$ acting at point (x_{jc}, y_{jc}) , the load vector contribution is simply

$$\{P_c\} = \begin{Bmatrix} \hat{P}_x \{a_1\} \\ \hat{P}_y \{a_2\} \\ \hat{P}_{xz} \{a_3\} \\ \hat{P}_{yz} \{a_4\} \\ \hat{P}_z \{a_5\} \end{Bmatrix} \quad (3.87)$$

where all polynomial terms are evaluated at (x_{jc}, y_{jc}) , and z is evaluated from the points depth distribution. For a single zone, the total load vector $\{P\}_{tot}$ is obtained by adding the load contributions from all distributed and concentrated loads acting on the zone.

3.10 Displacement and Stress Output

The FSDPT zone generalized displacements resulting from the solution of Eq. 1.12 may be used to calculate the static displacement and stress at a selected point in the zone. Choosing a point (x_{out}, y_{out}) from an output grid and determining z_{out} from the point's depth distribution, the displacements u , v , and w at that point may be determined by using Eq. 3.16 where S_0 and S_1 are evaluated at the point. Using Eqs. 1.5 and 3.23, stresses at a point (x_{out}, y_{out}) on the jl th skin layer may be determined from

$$\begin{Bmatrix} \sigma_{xx} \\ \sigma_{yy} \\ \sigma_{xy} \end{Bmatrix}_{jl} = [Q]_{jl} \{ [R_0(x, y)] + z_{out} [R_1(x, y)] \} \{q\} \quad (3.88)$$

where R_0 and R_1 are evaluated at the point, and z_{out} is evaluated from the layer's depth distribution at the point. Using Eqs. 3.23 and 3.33, the uniaxial stress at a point (x_{out}, y_{out}) on

the j stth spar may be determined from

$$\sigma_{js} = E_{js} \{TR\}^T \{ [R_0(x, y)] + z_{out} [R_1(x, y)] \} \{q\} \quad (3.89)$$

where R_0 and R_1 are evaluated at the point, and z_{out} is evaluated from the spar's depth distribution at the point. Using Eq. 3.42, the uniaxial stress at a point (x_{out}, y_{out}) on the j rth rib may be determined from

$$\sigma_{jr} = E_{jr} \{ [Y_0(x, y)] + z_{out} [Y_1(x, y)] \} \{\hat{q}\} \quad (3.90)$$

where Y_0 and Y_1 are evaluated at the point, and z_{out} is evaluated from the rib's depth distribution at the point.

The generalized displacements for a particular natural frequency resulting from the solution of Eq. 1.14 may be used to calculate the mode shape displacement at a selected point in the zone. As with static displacements, the modal displacements at a point (x_{out}, y_{out}) may be determined by using Eq. 3.16 where S_0 and S_1 are evaluated at the point, and z_{out} is evaluated from the point's depth distribution.

Chapter 4: Zone Connections and Boundary Conditions

4.1 Overview

This chapter presents the global synthesis of a multi-zone wing model. The chapter begins by discussing how the stiffness, mass, and load contributions from multiple CPT and FSDPT zones are merged into the global math model. Next presented is the derivation of stiffness matrix contributions from the spring connection of two CPT zones. Following this is the derivation of stiffness matrix contributions from the spring connection of two FSDPT zones. These are extended with the derivation of the stiffness matrix contributions from the spring connection of a CPT zone and a FSDPT zone. Finally discussed is the imposition of wing root boundary conditions.

4.2 Zone Connections in Global Context

When multiple zones are used to characterize a wing, compatibility of displacements at the zone interfaces must be enforced. This may be done using a penalty method via computational springs. A spring stiffness coefficient represents local stiffness at an attach point common to two zones. A large stiffness coefficient represents very rigid connection while a smaller coefficient may represent more flexible connection, such as that provided by an actuator. Linear springs may be used to enforce compatibility of linear displacements, and rotational springs may be used to enforce compatibility of slopes or angular displacements.

In a multiple zone configuration, the stiffness matrix, mass matrix, and load vector contributions of each zone must be merged into their global counterparts, $[K_{glob}]$, $[M_{glob}]$, and $\{P\}_{glob}$. These correspond to the vector of global generalized displacements formed from the generalized displacements of each zone. As an example, a wing with 2 FSDPT zones (zones #1 and #2) and 2 CPT zones (zones #3 and #4) will have a vector of global generalized displacements given by

$$\{q\}_{glob}^T = \{q_{1,1}^T, q_{2,1}^T, q_{3,1}^T, q_{4,1}^T, q_{5,1}^T | q_{1,2}^T, q_{2,2}^T, q_{3,2}^T, q_{4,2}^T, q_{5,2}^T | q_{w_3}^T | q_{w_4}^T\} \quad (4.1)$$

(Refer to Chapters 2 and 3 for the notation of generalized displacements for CPT and FSDPT zones). The additional second subscript here denotes the zone number out of a possible Nz zones. The vector in Eq. 4.1 is of length Nq_{glob} where

$$Nq_{glob} = Nq_{tot_1} + Nq_{tot_2} + Nq_{w_3} + Nq_{w_4} \quad (4.2)$$

Thus, the global stiffness and mass matrices will be $Nq_{glob} \times Nq_{glob}$ in dimension, and the global load vector will be of length Nq_{glob} . The global stiffness matrix may be partitioned into submatrices as follows:

$$[K_{glob}] = \begin{bmatrix} K_{1,1,1} & K_{1,1,2} & K_{1,1,3} & K_{1,1,4} & K_{1,1,5} & K_{1,1,2} & K_{1,1,2} & K_{1,1,3} & K_{1,1,4} & K_{1,1,5} & K_{1,1,w_3} & K_{1,1,w_4} \\ K_{2,1,1} & K_{2,1,2} & K_{2,1,3} & K_{2,1,4} & K_{2,1,5} & K_{2,1,2} & K_{2,1,2} & K_{2,1,3} & K_{2,1,4} & K_{2,1,5} & K_{2,1,w_3} & K_{2,1,w_4} \\ K_{3,1,1} & K_{3,1,2} & K_{3,1,3} & K_{3,1,4} & K_{3,1,5} & K_{3,1,2} & K_{3,1,2} & K_{3,1,3} & K_{3,1,4} & K_{3,1,5} & K_{3,1,w_3} & K_{3,1,w_4} \\ K_{4,1,1} & K_{4,1,2} & K_{4,1,3} & K_{4,1,4} & K_{4,1,5} & K_{4,1,2} & K_{4,1,2} & K_{4,1,3} & K_{4,1,4} & K_{4,1,5} & K_{4,1,w_3} & K_{4,1,w_4} \\ K_{5,1,1} & K_{5,1,2} & K_{5,1,3} & K_{5,1,4} & K_{5,1,5} & K_{5,1,2} & K_{5,1,2} & K_{5,1,3} & K_{5,1,4} & K_{5,1,5} & K_{5,1,w_3} & K_{5,1,w_4} \\ \overline{K}_{1,2,1} & \overline{K}_{1,2,2} & \overline{K}_{1,2,3} & \overline{K}_{1,2,4} & \overline{K}_{1,2,5} & \overline{K}_{1,2,2} & \overline{K}_{1,2,2} & \overline{K}_{1,2,3} & \overline{K}_{1,2,4} & \overline{K}_{1,2,5} & \overline{K}_{1,2,w_3} & \overline{K}_{1,2,w_4} \\ K_{2,2,1} & K_{2,2,2} & K_{2,2,3} & K_{2,2,4} & K_{2,2,5} & K_{2,2,2} & K_{2,2,2} & K_{2,2,3} & K_{2,2,4} & K_{2,2,5} & K_{2,2,w_3} & K_{2,2,w_4} \\ K_{3,2,1} & K_{3,2,2} & K_{3,2,3} & K_{3,2,4} & K_{3,2,5} & K_{3,2,2} & K_{3,2,2} & K_{3,2,3} & K_{3,2,4} & K_{3,2,5} & K_{3,2,w_3} & K_{3,2,w_4} \\ K_{4,2,1} & K_{4,2,2} & K_{4,2,3} & K_{4,2,4} & K_{4,2,5} & K_{4,2,2} & K_{4,2,2} & K_{4,2,3} & K_{4,2,4} & K_{4,2,5} & K_{4,2,w_3} & K_{4,2,w_4} \\ K_{5,2,1} & K_{5,2,2} & K_{5,2,3} & K_{5,2,4} & K_{5,2,5} & K_{5,2,2} & K_{5,2,2} & K_{5,2,3} & K_{5,2,4} & K_{5,2,5} & K_{5,2,w_3} & K_{5,2,w_4} \\ \overline{K}_{w_3,1,1} & \overline{K}_{w_3,1,2} & \overline{K}_{w_3,1,3} & \overline{K}_{w_3,1,4} & \overline{K}_{w_3,1,5} & \overline{K}_{w_3,1,2} & \overline{K}_{w_3,1,2} & \overline{K}_{w_3,1,3} & \overline{K}_{w_3,1,4} & \overline{K}_{w_3,1,5} & \overline{K}_{w_3,1,w_3} & \overline{K}_{w_3,1,w_4} \\ \overline{K}_{w_4,1,1} & \overline{K}_{w_4,1,2} & \overline{K}_{w_4,1,3} & \overline{K}_{w_4,1,4} & \overline{K}_{w_4,1,5} & \overline{K}_{w_4,1,2} & \overline{K}_{w_4,1,2} & \overline{K}_{w_4,1,3} & \overline{K}_{w_4,1,4} & \overline{K}_{w_4,1,5} & \overline{K}_{w_4,1,w_3} & \overline{K}_{w_4,1,w_4} \end{bmatrix} \quad (4.3)$$

where each submatrix K_{r,s_j} is of dimension $Nq_{r_i} \times Nq_{s_j}$ ($r,s=w,1,2,3,4,5$ and $i,j=1,2,\dots,Nz$). The global mass matrix will be partitioned like $[K_{glob}]$, and the global load vector will be partitioned like $\{q\}_{glob}$. Contributions to stiffness and mass from each zone's structural components are placed in the corresponding submatrices on the diagonal where, for a submatrix K_{r,s_j} , $i=j=zone \#$. There are no mass contributions in submatrices where $i \neq j$. However, spring connections do provide connectivity between zones and therefore produce contributions to stiffness in submatrices where $i \neq j$.

4.3 Spring Connection of 2 CPT Zones

Let us begin by defining an “attach line” which corresponds to the common surface of 2 CPT zones to be connected. Springs act at selected “attach points” along this line to provide local stiffness. The left and right endpoints of the attach line are given by the coordinates (atx_L, aty_L) and (atx_R, aty_R) . Referring to the attach line in Figure 4.1, let us define the unit vector \hat{i} in the direction of the attach line given by

$$\hat{i} = \cos\alpha\hat{i} + \sin\alpha\hat{j} \quad (4.4)$$

where

$$\cos\alpha = \frac{atx_R - atx_L}{\sqrt{(atx_R - atx_L)^2 + (aty_R - aty_L)^2}} \quad (4.5)$$

$$\sin\alpha = \frac{aty_R - aty_L}{\sqrt{(atx_R - atx_L)^2 + (aty_R - aty_L)^2}} \quad (4.6)$$

A vector of rotation having positive rotational vector components in the x and y directions may be given by

$$\bar{\Omega} = (\Omega_x)\hat{i} + (\Omega_y)\hat{j} \quad (4.7)$$

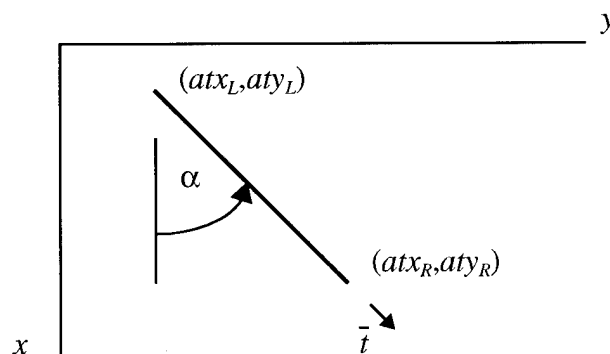


Figure 4.1: CPT Attach Line Geometry

Using the right hand rule for a CPT zone, Ω_x corresponds to the displacement slope $w_{,y}$ while Ω_y corresponds to $-w_{,x}$. Positive rotation about \hat{t} may then be given as

$$\theta = \bar{\Omega} \cdot \hat{t} = w_{,y} \cos \alpha - w_{,x} \sin \alpha \quad (4.8)$$

(LIV190). Recall from Section 1.3 that each zone may have its geometry defined in an independent axis system. Therefore, the attach line common to both zones may be defined with a unique orientation α_1 in zone 1 and α_2 in zone 2. This results in

$$\theta_1 = w_{1,y} \cos \alpha_1 - w_{1,x} \sin \alpha_1 \quad (4.9)$$

$$\theta_2 = w_{2,y} \cos \alpha_2 - w_{2,x} \sin \alpha_2 \quad (4.10)$$

where, from Eq. 2.6, we have

$$w_1 = \{a_{w_1}\}^T \{q_{w_1}\} \quad (4.11)$$

$$w_2 = \{a_{w_2}\}^T \{q_{w_2}\} \quad (4.12)$$

Now let a linear spring with stiffness k_w connect point (x_1, y_1) on zone 1 with point (x_2, y_2) on zone 2 by providing vertical displacement compatibility. The contribution to the potential energy U of the spring resisting vertical displacement is

$$U_{k_w} = \frac{1}{2} k_w \Delta^2 \quad (4.13)$$

where

$$\Delta = w_1 - w_2 \quad (4.14)$$

Substituting Eqs. 4.14, 4.11, and 4.12 into Eq. 4.13 gives

$$U_{k_w} = \frac{1}{2} k_w \left[\{q_{w_1}\}^T \{a_{w_1}\} \{a_{w_1}\}^T \{q_{w_1}\} - \{q_{w_1}\}^T \{a_{w_1}\} \{a_{w_2}\}^T \{q_{w_2}\} \right. \\ \left. - \{q_{w_2}\}^T \{a_{w_2}\} \{a_{w_1}\}^T \{q_{w_1}\} + \{q_{w_2}\}^T \{a_{w_2}\} \{a_{w_2}\}^T \{q_{w_2}\} \right] \quad (4.15)$$

This leads to the stiffness submatrix contributions given by

$$\begin{aligned}
 [K_{w_1 w_1}]_{k_w} &= k_w \{a_{w_1}\} \{a_{w_1}\}^T \\
 [K_{w_1 w_2}]_{k_w} &= -k_w \{a_{w_1}\} \{a_{w_2}\}^T \\
 [K_{w_2 w_1}]_{k_w} &= -k_w \{a_{w_2}\} \{a_{w_1}\}^T \\
 [K_{w_2 w_2}]_{k_w} &= k_w \{a_{w_2}\} \{a_{w_2}\}^T
 \end{aligned} \tag{4.16}$$

where $\{a_{w_1}\}$ and $\{a_{w_2}\}$ are evaluated at (x_1, y_1) and (x_2, y_2) respectively. These submatrices are merged into the global stiffness matrix having the form

$$[K_{glob}] = \begin{bmatrix} K_{w_1 w_1} & K_{w_1 w_2} \\ K_{w_2 w_1} & K_{w_2 w_2} \end{bmatrix} \tag{4.17}$$

for each linear spring connection that is used.

Also let a rotational spring with stiffness k_θ connect point (x_1, y_1) on zone 1 with point (x_2, y_2) on zone 2 by providing slope compatibility. The contribution to the potential energy U of the spring resisting angular displacement is

$$U_{k_\theta} = \frac{1}{2} k_\theta (\theta_1 - \theta_2)^2 \tag{4.18}$$

Substituting Eqs. 4.9-4.12 into Eq. 4.18 gives

$$\begin{aligned}
 U_{k_\theta} = \frac{1}{2} k_\theta & \left[\{q_{w_1}\}^T \left(\cos^2 \alpha_1 \{a_{w_1, y}\} \{a_{w_1, y}\}^T - \cos \alpha_1 \sin \alpha_1 \{a_{w_1, y}\} \{a_{w_1, x}\}^T \right. \right. \\
 & \left. \left. - \cos \alpha_1 \sin \alpha_1 \{a_{w_1, x}\} \{a_{w_1, y}\}^T + \sin^2 \alpha_1 \{a_{w_1, x}\} \{a_{w_1, x}\}^T \right) \{q_{w_1}\} \right. \\
 & \left. - \{q_{w_1}\}^T \left(\cos \alpha_1 \cos \alpha_2 \{a_{w_1, y}\} \{a_{w_2, y}\}^T - \cos \alpha_1 \sin \alpha_2 \{a_{w_1, y}\} \{a_{w_2, x}\}^T \right. \right. \\
 & \left. \left. - \cos \alpha_2 \sin \alpha_1 \{a_{w_1, x}\} \{a_{w_2, y}\}^T + \sin \alpha_1 \sin \alpha_2 \{a_{w_1, x}\} \{a_{w_2, x}\}^T \right) \{q_{w_2}\} \right]
 \end{aligned}$$

$$\begin{aligned}
& -\{q_{w_2}\}^T \left(\cos\alpha_1 \cos\alpha_2 \{a_{w_2,y}\} \{a_{w_1,y}\}^T - \cos\alpha_2 \sin\alpha_1 \{a_{w_2,y}\} \{a_{w_1,x}\}^T \right. \\
& \quad \left. - \cos\alpha_1 \sin\alpha_2 \{a_{w_2,x}\} \{a_{w_1,y}\}^T + \sin\alpha_1 \sin\alpha_2 \{a_{w_2,x}\} \{a_{w_1,x}\}^T \right) \{q_{w_1}\} \\
& + \{q_{w_2}\}^T \left(\cos^2\alpha_2 \{a_{w_2,y}\} \{a_{w_2,y}\}^T - \cos\alpha_2 \sin\alpha_2 \{a_{w_2,y}\} \{a_{w_2,x}\}^T \right. \\
& \quad \left. - \cos\alpha_2 \sin\alpha_2 \{a_{w_2,x}\} \{a_{w_2,y}\}^T + \sin^2\alpha_2 \{a_{w_2,x}\} \{a_{w_2,x}\}^T \right) \{q_{w_2}\} \Big] \quad (4.19)
\end{aligned}$$

This leads to the stiffness submatrix contributions given by

$$\begin{aligned}
[K_{w_1 w_1}]_{k_\theta} &= k_\theta \left[\cos^2\alpha_1 \{a_{w_1,y}\} \{a_{w_1,y}\}^T - \cos\alpha_1 \sin\alpha_1 \{a_{w_1,y}\} \{a_{w_1,x}\}^T \right. \\
& \quad \left. - \cos\alpha_1 \sin\alpha_1 \{a_{w_1,x}\} \{a_{w_1,y}\}^T + \sin^2\alpha_1 \{a_{w_1,x}\} \{a_{w_1,x}\}^T \right] \\
[K_{w_1 w_2}]_{k_\theta} &= -k_\theta \left[\left(\cos\alpha_1 \cos\alpha_2 \{a_{w_1,y}\} \{a_{w_2,y}\}^T - \cos\alpha_1 \sin\alpha_2 \{a_{w_1,y}\} \{a_{w_2,x}\}^T \right. \right. \\
& \quad \left. \left. - \cos\alpha_2 \sin\alpha_1 \{a_{w_1,x}\} \{a_{w_2,y}\}^T + \sin\alpha_1 \sin\alpha_2 \{a_{w_1,x}\} \{a_{w_2,x}\}^T \right) \right] \quad (4.20) \\
[K_{w_2 w_1}]_{k_\theta} &= -k_\theta \left[\cos\alpha_1 \cos\alpha_2 \{a_{w_2,y}\} \{a_{w_1,y}\}^T - \cos\alpha_2 \sin\alpha_1 \{a_{w_2,y}\} \{a_{w_1,x}\}^T \right. \\
& \quad \left. - \cos\alpha_1 \sin\alpha_2 \{a_{w_2,x}\} \{a_{w_1,y}\}^T + \sin\alpha_1 \sin\alpha_2 \{a_{w_2,x}\} \{a_{w_1,x}\}^T \right] \\
[K_{w_2 w_2}]_{k_\theta} &= k_\theta \left[\cos^2\alpha_2 \{a_{w_2,y}\} \{a_{w_2,y}\}^T - \cos\alpha_2 \sin\alpha_2 \{a_{w_2,y}\} \{a_{w_2,x}\}^T \right. \\
& \quad \left. - \cos\alpha_2 \sin\alpha_2 \{a_{w_2,x}\} \{a_{w_2,y}\}^T + \sin^2\alpha_2 \{a_{w_2,x}\} \{a_{w_2,x}\}^T \right]
\end{aligned}$$

where $\{a_{w_1,y}\}$ and $\{a_{w_1,x}\}$ are evaluated at (x_1, y_1) , and $\{a_{w_2,y}\}$ and $\{a_{w_2,x}\}$ are evaluated at (x_2, y_2) (LIV190). These submatrices are merged into the global stiffness matrix having the form shown in Eq. 4.17 for each rotational spring connection that is used.

4.4 Spring Connection of 2 FSDPT Zones

Point compatibility of relative vertical displacements between 2 FSDPT zones may be enforced with a linear spring in the same fashion as it is done for CPT zones. Let a linear spring with stiffness k_5 connect point (x_1, y_1) on FSDPT zone 1 with point (x_2, y_2) on FSDPT zone 2. Using Eqs. 3.3 and 3.13 let us define

$$w_1 = \{a_{5_1}\}^T \{q_{5_1}\} \quad (4.21)$$

$$w_2 = \{a_{5_2}\}^T \{q_{5_2}\} \quad (4.22)$$

These relationships for w_1 and w_2 may be used in Eq. 4.13 to express the contribution to the potential energy of the spring as

$$U_{k_5} = \frac{1}{2}k_5 \left[\{q_{5_1}\}^T \{a_{5_1}\} \{a_{5_1}\}^T \{q_{5_1}\} - \{q_{5_1}\}^T \{a_{5_1}\} \{a_{5_2}\}^T \{q_{5_2}\} \right. \\ \left. - \{q_{5_2}\}^T \{a_{5_2}\} \{a_{5_1}\}^T \{q_{5_1}\} + \{q_{5_2}\}^T \{a_{5_2}\} \{a_{5_2}\}^T \{q_{5_2}\} \right] \quad (4.23)$$

This leads to stiffness submatrix contributions given by

$$\begin{aligned} [K_{5_1 5_1}]_{k_5} &= k_5 \{a_{5_1}\} \{a_{5_1}\}^T \\ [K_{5_1 5_2}]_{k_5} &= -k_5 \{a_{5_1}\} \{a_{5_2}\}^T \\ [K_{5_2 5_1}]_{k_5} &= -k_5 \{a_{5_2}\} \{a_{5_1}\}^T \\ [K_{5_2 5_2}]_{k_5} &= k_5 \{a_{5_2}\} \{a_{5_2}\}^T \end{aligned} \quad (4.24)$$

where $\{a_{5_1}\}$ and $\{a_{5_2}\}$ are evaluated at (x_1, y_1) and (x_2, y_2) respectively. These submatrices are merged into the global stiffness matrix having the form

$$[K_{glob}] = \begin{bmatrix} K_{1,1,1} & K_{1,1,2} & K_{1,1,3} & K_{1,1,4} & K_{1,1,5} & K_{1,1,2} & K_{1,1,2} & K_{1,1,3} & K_{1,1,4} & K_{1,1,5} \\ K_{2,1,1} & K_{2,1,2} & K_{2,1,3} & K_{2,1,4} & K_{2,1,5} & K_{2,1,2} & K_{2,1,2} & K_{2,1,3} & K_{2,1,4} & K_{2,1,5} \\ K_{3,1,1} & K_{3,1,2} & K_{3,1,3} & K_{3,1,4} & K_{3,1,5} & K_{3,1,2} & K_{3,1,2} & K_{3,1,3} & K_{3,1,4} & K_{3,1,5} \\ K_{4,1,1} & K_{4,1,2} & K_{4,1,3} & K_{4,1,4} & K_{4,1,5} & K_{4,1,2} & K_{4,1,2} & K_{4,1,3} & K_{4,1,4} & K_{4,1,5} \\ K_{5,1,1} & K_{5,1,2} & K_{5,1,3} & K_{5,1,4} & K_{5,1,5} & K_{5,1,2} & K_{5,1,2} & K_{5,1,3} & K_{5,1,4} & K_{5,1,5} \\ K_{1,2,1} & K_{1,2,2} & K_{1,2,3} & K_{1,2,4} & K_{1,2,5} & K_{1,2,2} & K_{1,2,2} & K_{1,2,3} & K_{1,2,4} & K_{1,2,5} \\ K_{2,2,1} & K_{2,2,2} & K_{2,2,3} & K_{2,2,4} & K_{2,2,5} & K_{2,2,2} & K_{2,2,2} & K_{2,2,3} & K_{2,2,4} & K_{2,2,5} \\ K_{3,2,1} & K_{3,2,2} & K_{3,2,3} & K_{3,2,4} & K_{3,2,5} & K_{3,2,2} & K_{3,2,2} & K_{3,2,3} & K_{3,2,4} & K_{3,2,5} \\ K_{4,2,1} & K_{4,2,2} & K_{4,2,3} & K_{4,2,4} & K_{4,2,5} & K_{4,2,2} & K_{4,2,2} & K_{4,2,3} & K_{4,2,4} & K_{4,2,5} \\ K_{5,2,1} & K_{5,2,2} & K_{5,2,3} & K_{5,2,4} & K_{5,2,5} & K_{5,2,2} & K_{5,2,2} & K_{5,2,3} & K_{5,2,4} & K_{5,2,5} \end{bmatrix} \quad (4.25)$$

for each vertical spring connection that is used.

Linear in-plane displacement compatibility between 2 FSDPT zones must also be enforced. Referring to Eqs. 3.1-3.2, the in-plane displacements u and v both consist of a linear translation (u_0, v_0) and a rotation (ψ_x, ψ_y). There are 2 ways to enforce point compatibility of these translational and rotational components. A coupled pair of linear springs, both at a distance h from the mid-surface, may be used to enforce compatibility of both components. Alternately, a linear spring may be used at the mid-surface to enforce translational compatibility, and a separate rotational spring may be used to enforce rotational or slope compatibility. Both methods become equivalent when the stiffness coefficient of the rotational spring is chosen to be the stiffness coefficient of the linear springs divided by h^2 . Since the latter method has no complicating depth distribution dependence, it is the one used and presented in this work.

Referring to Figure 4.2, let us define the unit vector \bar{r} , perpendicular to the attach line, given by

$$\bar{r} = \sin\alpha\hat{i} - \cos\alpha\hat{j} \quad (4.26)$$

where Eqs. 4.5 and 4.6 define $\sin\alpha$ and $\cos\alpha$. Let us also define a vector of mid-surface in-plane displacement with components in the positive x and y directions given by

$$\chi = u_0\hat{i} + v_0\hat{j} \quad (4.27)$$

Linear displacement perpendicular to the attach line at the mid-surface is then given by

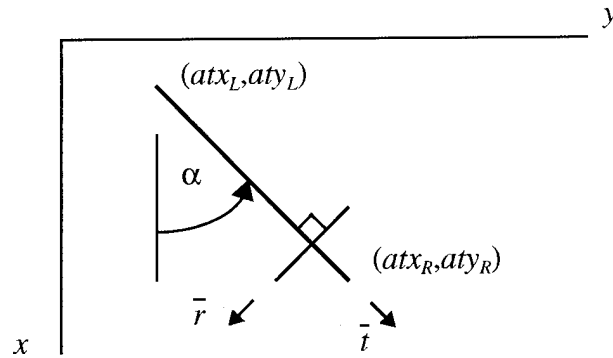


Figure 4.2: FSDPT Attach Line Geometry

$$\zeta = \vec{x} \cdot \vec{r} = u_0 \sin \alpha - v_0 \cos \alpha \quad (4.28)$$

Given that the attach line may be oriented differently in each zone's axis system, Eqs. 3.9 and 3.10 may be used to express linear displacements for zone 1 and zone 2 respectively by

$$\zeta_1 = \sin \alpha_1 \{a_{1_1}\}^T \{q_{1_1}\} - \cos \alpha_1 \{a_{2_1}\}^T \{q_{2_1}\} \quad (4.29)$$

$$\zeta_2 = \sin \alpha_2 \{a_{1_2}\}^T \{q_{1_2}\} - \cos \alpha_2 \{a_{2_2}\}^T \{q_{2_2}\} \quad (4.30)$$

Now let a linear spring with stiffness k_1 act perpendicular to the attach line and connect point (x_1, y_1) on zone 1 with point (x_2, y_2) on zone 2. The contribution to the potential energy U of the spring resisting in-plane displacement is

$$U_{k_1} = \frac{1}{2} k_1 (\zeta_1 - \zeta_2)^2 \quad (4.31)$$

Substituting Eqs. 4.29 and 4.30 into Eq. 4.31 gives

$$U_{k_1} = \frac{1}{2} k_1$$

$$\begin{aligned}
& \left[\sin^2 \alpha_1 \{q_{1_1}\}^T \{a_{1_1}\} \{a_{1_1}\}^T \{q_{1_1}\} - \cos \alpha_1 \sin \alpha_1 \{q_{1_1}\}^T \{a_{1_1}\} \{a_{2_1}\}^T \{q_{2_1}\} \right. \\
& - \cos \alpha_1 \sin \alpha_1 \{q_{2_1}\}^T \{a_{2_1}\} \{a_{1_1}\}^T \{q_{1_1}\} + \cos^2 \alpha_1 \{q_{2_1}\}^T \{a_{2_1}\} \{a_{2_1}\}^T \{q_{2_1}\} \\
& - \sin \alpha_1 \sin \alpha_2 \{q_{1_1}\}^T \{a_{1_1}\} \{a_{1_2}\}^T \{q_{1_2}\} + \cos \alpha_2 \sin \alpha_1 \{q_{1_1}\}^T \{a_{1_1}\} \{a_{2_2}\}^T \{q_{2_2}\} \\
& + \cos \alpha_1 \sin \alpha_2 \{q_{2_1}\}^T \{a_{2_1}\} \{a_{1_2}\}^T \{q_{1_2}\} - \cos \alpha_1 \cos \alpha_2 \{q_{2_1}\}^T \{a_{2_1}\} \{a_{2_2}\}^T \{q_{2_2}\} \\
& - \sin \alpha_1 \sin \alpha_2 \{q_{1_2}\}^T \{a_{1_2}\} \{a_{1_1}\}^T \{q_{1_1}\} + \cos \alpha_1 \sin \alpha_2 \{q_{1_2}\}^T \{a_{1_2}\} \{a_{2_1}\}^T \{q_{2_1}\} \\
& + \cos \alpha_2 \sin \alpha_1 \{q_{2_2}\}^T \{a_{2_2}\} \{a_{1_1}\}^T \{q_{1_1}\} - \cos \alpha_1 \cos \alpha_2 \{q_{2_2}\}^T \{a_{2_2}\} \{a_{2_1}\}^T \{q_{2_1}\} \\
& \sin^2 \alpha_2 \{q_{1_2}\}^T \{a_{1_2}\} \{a_{1_2}\}^T \{q_{1_2}\} - \cos \alpha_2 \sin \alpha_2 \{q_{1_2}\}^T \{a_{1_2}\} \{a_{2_2}\}^T \{q_{2_2}\} \\
& \left. - \cos \alpha_2 \sin \alpha_2 \{q_{2_2}\}^T \{a_{2_2}\} \{a_{1_2}\}^T \{q_{1_2}\} + \cos^2 \alpha_2 \{q_{2_2}\}^T \{a_{2_2}\} \{a_{2_2}\}^T \{q_{2_2}\} \right] \quad (4.32)
\end{aligned}$$

This leads to stiffness submatrix contributions given by

$$\begin{aligned}
\begin{bmatrix} K_{1_1 1_1} & K_{1_1 2_1} \\ K_{2_1 1_1} & K_{2_1 2_1} \end{bmatrix} &= k_1 \begin{bmatrix} \begin{bmatrix} \sin^2 \alpha_1 \{a_{1_1}\} \{a_{1_1}\}^T \\ -\cos \alpha_1 \sin \alpha_1 \{a_{2_1}\} \{a_{1_1}\}^T \end{bmatrix} & \begin{bmatrix} -\cos \alpha_1 \sin \alpha_1 \{a_{1_1}\} \{a_{2_1}\}^T \\ \cos^2 \alpha_1 \{a_{2_1}\} \{a_{2_1}\}^T \end{bmatrix} \\ \begin{bmatrix} -\cos \alpha_1 \sin \alpha_1 \{a_{2_1}\} \{a_{1_1}\}^T \\ \cos^2 \alpha_1 \{a_{2_1}\} \{a_{2_1}\}^T \end{bmatrix} & \begin{bmatrix} -\cos \alpha_1 \sin \alpha_1 \{a_{1_1}\} \{a_{2_1}\}^T \\ \cos^2 \alpha_1 \{a_{2_1}\} \{a_{2_1}\}^T \end{bmatrix} \end{bmatrix} \\
\begin{bmatrix} K_{1_1 1_2} & K_{1_1 2_2} \\ K_{2_1 1_2} & K_{2_1 2_2} \end{bmatrix} &= k_1 \begin{bmatrix} \begin{bmatrix} -\sin \alpha_1 \sin \alpha_2 \{a_{1_1}\} \{a_{1_2}\}^T \\ \cos \alpha_1 \sin \alpha_2 \{a_{2_1}\} \{a_{1_2}\}^T \end{bmatrix} & \begin{bmatrix} \cos \alpha_2 \sin \alpha_1 \{a_{1_1}\} \{a_{2_2}\}^T \\ -\cos \alpha_1 \cos \alpha_2 \{a_{2_1}\} \{a_{2_2}\}^T \end{bmatrix} \\ \begin{bmatrix} -\sin \alpha_1 \sin \alpha_2 \{a_{1_2}\} \{a_{1_1}\}^T \\ \cos \alpha_2 \sin \alpha_1 \{a_{2_2}\} \{a_{1_1}\}^T \end{bmatrix} & \begin{bmatrix} \cos \alpha_1 \sin \alpha_2 \{a_{1_2}\} \{a_{2_1}\}^T \\ -\cos \alpha_1 \cos \alpha_2 \{a_{2_2}\} \{a_{2_1}\}^T \end{bmatrix} \end{bmatrix} \quad (4.33) \\
\begin{bmatrix} K_{1_2 1_1} & K_{1_2 2_1} \\ K_{2_2 1_1} & K_{2_2 2_1} \end{bmatrix} &= k_1 \begin{bmatrix} \begin{bmatrix} -\sin \alpha_1 \sin \alpha_2 \{a_{1_2}\} \{a_{1_1}\}^T \\ \cos \alpha_2 \sin \alpha_1 \{a_{2_2}\} \{a_{1_1}\}^T \end{bmatrix} & \begin{bmatrix} \cos \alpha_1 \sin \alpha_2 \{a_{1_2}\} \{a_{2_1}\}^T \\ -\cos \alpha_1 \cos \alpha_2 \{a_{2_2}\} \{a_{2_1}\}^T \end{bmatrix} \\ \begin{bmatrix} -\sin \alpha_1 \sin \alpha_2 \{a_{1_2}\} \{a_{1_1}\}^T \\ \cos \alpha_2 \sin \alpha_1 \{a_{2_2}\} \{a_{1_1}\}^T \end{bmatrix} & \begin{bmatrix} \cos \alpha_1 \sin \alpha_2 \{a_{1_2}\} \{a_{2_1}\}^T \\ -\cos \alpha_1 \cos \alpha_2 \{a_{2_2}\} \{a_{2_1}\}^T \end{bmatrix} \end{bmatrix}
\end{aligned}$$

$$\begin{bmatrix} K_{1_2 1_2} & K_{1_2 2_2} \\ K_{2_2 1_2} & K_{2_2 2_2} \end{bmatrix} = k_1 \begin{bmatrix} \begin{bmatrix} \sin^2 \alpha_2 \{a_{1_2}\} \{a_{1_2}\}^T \\ -\cos \alpha_2 \sin \alpha_2 \{a_{2_2}\} \{a_{1_2}\}^T \end{bmatrix} & \begin{bmatrix} -\cos \alpha_2 \sin \alpha_2 \{a_{1_2}\} \{a_{2_2}\}^T \\ \cos^2 \alpha_2 \{a_{2_2}\} \{a_{2_2}\}^T \end{bmatrix} \end{bmatrix}$$

where $\{a_{1_1}\}$ and $\{a_{2_1}\}$ are evaluated at (x_1, y_1) , and $\{a_{1_2}\}$ and $\{a_{2_2}\}$ are evaluated at (x_2, y_2) . These submatrices are merged into the global stiffness matrix having the form shown in Eq. 4.25 for each translational spring connection that is used. Note that if a linear spring of stiffness k_2 is used to resist translation parallel to the attach line, Eq. 4.33 may be used to find the stiffness contributions with $\sin \alpha$ replaced by $\cos \alpha$, $\cos \alpha$ replaced by $-\sin \alpha$, and k_1 replaced by k_2 .

Enforcement of rotational or slope compatibility is done in a manner similar to that for translational compatibility. Recall that a vector of rotations was defined in Eq. 4.7. Using the right hand rule for a FSDPT zone, Ω_x corresponds to $-\psi_y$, and Ω_y correspond to ψ_x . Using Eqs. 4.4 and 4.7, positive rotation about the attach line may be given as

$$\theta = \bar{\Omega} \cdot \bar{i} = \psi_x \sin \alpha - \psi_y \cos \alpha \quad (4.34)$$

Given that the attach line may be oriented differently in each zone's axis system, Eqs. 3.11 and 3.12 may be used to write rotational displacements for zone 1 and zone 2 respectively given by

$$\theta_1 = \sin \alpha_1 \{a_{3_1}\}^T \{q_{3_1}\} - \cos \alpha_1 \{a_{4_1}\}^T \{q_{4_1}\} \quad (4.35)$$

$$\theta_2 = \sin \alpha_2 \{a_{3_2}\}^T \{q_{3_2}\} - \cos \alpha_2 \{a_{4_2}\}^T \{q_{4_2}\} \quad (4.36)$$

Now let a rotational spring with stiffness k_3 act in resistance to rotation about the attach line and connect point (x_1, y_1) on zone 1 with point (x_2, y_2) on zone 2. The contribution to the potential energy U of the spring is

$$U_{k_3} = \frac{1}{2} k_3 (\theta_1 - \theta_2)^2 \quad (4.37)$$

Substituting Eqs. 4.35 and 4.36 into Eq. 4.37 gives

$$U_{k_3} = \frac{1}{2}k_3$$

$$\begin{aligned} & \left[\sin^2 \alpha_1 \{q_{3_1}\}^T \{a_{3_1}\} \{a_{3_1}\}^T \{q_{3_1}\} - \cos \alpha_1 \sin \alpha_1 \{q_{3_1}\}^T \{a_{3_1}\} \{a_{4_1}\}^T \{q_{4_1}\} \right. \\ & - \cos \alpha_1 \sin \alpha_1 \{q_{4_1}\}^T \{a_{4_1}\} \{a_{3_1}\}^T \{q_{3_1}\} + \cos^2 \alpha_1 \{q_{4_1}\}^T \{a_{4_1}\} \{a_{4_1}\}^T \{q_{4_1}\} \\ & - \sin \alpha_1 \sin \alpha_2 \{q_{3_1}\}^T \{a_{3_1}\} \{a_{3_2}\}^T \{q_{3_2}\} + \cos \alpha_2 \sin \alpha_1 \{q_{3_1}\}^T \{a_{3_1}\} \{a_{4_2}\}^T \{q_{4_2}\} \\ & + \cos \alpha_1 \sin \alpha_2 \{q_{4_1}\}^T \{a_{4_1}\} \{a_{3_2}\}^T \{q_{3_2}\} - \cos \alpha_1 \cos \alpha_2 \{q_{4_1}\}^T \{a_{4_1}\} \{a_{4_2}\}^T \{q_{4_2}\} \\ & \left. - \sin \alpha_1 \sin \alpha_2 \{q_{3_2}\}^T \{a_{3_2}\} \{a_{3_1}\}^T \{q_{3_1}\} + \cos \alpha_1 \sin \alpha_2 \{q_{3_2}\}^T \{a_{3_2}\} \{a_{4_1}\}^T \{q_{4_1}\} \right. \\ & + \cos \alpha_2 \sin \alpha_1 \{q_{4_2}\}^T \{a_{4_2}\} \{a_{3_1}\}^T \{q_{3_1}\} - \cos \alpha_1 \cos \alpha_2 \{q_{4_2}\}^T \{a_{4_2}\} \{a_{4_1}\}^T \{q_{4_1}\} \\ & \sin^2 \alpha_2 \{q_{3_2}\}^T \{a_{3_2}\} \{a_{3_2}\}^T \{q_{3_2}\} - \cos \alpha_2 \sin \alpha_2 \{q_{3_2}\}^T \{a_{3_2}\} \{a_{4_2}\}^T \{q_{4_2}\} \\ & \left. - \cos \alpha_2 \sin \alpha_2 \{q_{4_2}\}^T \{a_{4_2}\} \{a_{3_2}\}^T \{q_{3_2}\} + \cos^2 \alpha_2 \{q_{4_2}\}^T \{a_{4_2}\} \{a_{4_2}\}^T \{q_{4_2}\} \right] \end{aligned} \quad (4.38)$$

This leads to stiffness submatrix contributions given by

$$\begin{bmatrix} K_{3_1 3_1} & K_{3_1 4_1} \\ K_{4_1 3_1} & K_{4_1 4_1} \end{bmatrix} = k_3 \begin{bmatrix} \left[\sin^2 \alpha_1 \{a_{3_1}\} \{a_{3_1}\}^T \right] & \left[-\cos \alpha_1 \sin \alpha_1 \{a_{3_1}\} \{a_{4_1}\}^T \right] \\ \left[-\cos \alpha_1 \sin \alpha_1 \{a_{4_1}\} \{a_{3_1}\}^T \right] & \left[\cos^2 \alpha_1 \{a_{4_1}\} \{a_{4_1}\}^T \right] \end{bmatrix}$$

$$\begin{bmatrix} K_{3_1 3_2} & K_{3_1 4_2} \\ K_{4_1 3_2} & K_{4_1 4_2} \end{bmatrix} = k_3 \begin{bmatrix} \left[-\sin \alpha_1 \sin \alpha_2 \{a_{3_1}\} \{a_{3_2}\}^T \right] & \left[\cos \alpha_2 \sin \alpha_1 \{a_{3_1}\} \{a_{4_2}\}^T \right] \\ \left[\cos \alpha_1 \sin \alpha_2 \{a_{4_1}\} \{a_{3_2}\}^T \right] & \left[-\cos \alpha_1 \cos \alpha_2 \{a_{4_1}\} \{a_{4_2}\}^T \right] \end{bmatrix}$$

$$\begin{aligned}
 & \begin{bmatrix} K_{3_2 3_1} & K_{3_2 4_1} \\ K_{4_2 3_1} & K_{4_2 4_1} \end{bmatrix} = k_3 \begin{bmatrix} \begin{bmatrix} -\sin \alpha_1 \sin \alpha_2 \{a_{3_2}\} \{a_{3_1}\}^T \\ \cos \alpha_2 \sin \alpha_1 \{a_{4_1}\} \{a_{3_2}\}^T \end{bmatrix} & \begin{bmatrix} \cos \alpha_1 \sin \alpha_2 \{a_{3_2}\} \{a_{4_1}\}^T \\ -\cos \alpha_1 \cos \alpha_2 \{a_{4_2}\} \{a_{4_1}\}^T \end{bmatrix} \\ \begin{bmatrix} \sin^2 \alpha_2 \{a_{3_2}\} \{a_{3_2}\}^T \\ -\cos \alpha_2 \sin \alpha_2 \{a_{4_2}\} \{a_{3_2}\}^T \end{bmatrix} & \begin{bmatrix} -\cos \alpha_2 \sin \alpha_2 \{a_{3_2}\} \{a_{4_2}\}^T \\ \cos^2 \alpha_2 \{a_{4_2}\} \{a_{4_2}\}^T \end{bmatrix} \end{bmatrix} \quad (4.39) \\
 & \begin{bmatrix} K_{3_2 3_2} & K_{3_2 4_2} \\ K_{4_2 3_2} & K_{4_2 4_2} \end{bmatrix} = k_3 \begin{bmatrix} \begin{bmatrix} \sin^2 \alpha_2 \{a_{3_2}\} \{a_{3_2}\}^T \\ -\cos \alpha_2 \sin \alpha_2 \{a_{4_2}\} \{a_{3_2}\}^T \end{bmatrix} & \begin{bmatrix} -\cos \alpha_2 \sin \alpha_2 \{a_{3_2}\} \{a_{4_2}\}^T \\ \cos^2 \alpha_2 \{a_{4_2}\} \{a_{4_2}\}^T \end{bmatrix} \\ \begin{bmatrix} \sin^2 \alpha_2 \{a_{3_2}\} \{a_{3_2}\}^T \\ -\cos \alpha_2 \sin \alpha_2 \{a_{4_2}\} \{a_{3_2}\}^T \end{bmatrix} & \begin{bmatrix} -\cos \alpha_2 \sin \alpha_2 \{a_{3_2}\} \{a_{4_2}\}^T \\ \cos^2 \alpha_2 \{a_{4_2}\} \{a_{4_2}\}^T \end{bmatrix} \end{bmatrix}
 \end{aligned}$$

where $\{a_{3_1}\}$ and $\{a_{4_1}\}$ are evaluated at (x_1, y_1) , and $\{a_{3_2}\}$ and $\{a_{4_2}\}$ are evaluated at (x_2, y_2) . These submatrices are merged into the global stiffness matrix having the form shown in Eq. 4.25 for each rotational spring connection that is used. Note that if a rotational spring of stiffness k_4 is used to resist rotation about an axis perpendicular to the attach line, Eq. 4.39 may be used to find the stiffness contributions with $\sin \alpha$ replaced by $-\cos \alpha$, $\cos \alpha$ replaced by $\sin \alpha$, and k_3 replaced by k_4 .

4.5 Spring Connection of a FSDPT Zone and a CPT Zone

Let us define zone 1 to be a FSDPT zone and zone 2 to be a CPT zone. Point compatibility of relative vertical displacements between the two zones may be enforced as follows. Let a linear spring of stiffness k_5 connect point (x_1, y_1) on zone 1 with point (x_2, y_2) on zone 2 by resisting linear vertical displacement. The displacement w_1 for the FSDPT zone is defined in Eq. 4.21, and the displacement w_2 for the CPT zone is defined in Eq. 4.12. These relationships may be used along with Eq. 4.13 to express the contribution to the potential energy U of the spring as

$$\begin{aligned}
 U_{k_5} = \frac{1}{2} k_5 & \left[\{q_{5_1}\}^T \{a_{5_1}\} \{a_{5_1}\}^T \{q_{5_1}\} - \{q_{5_1}\}^T \{a_{5_1}\} \{a_{w_2}\}^T \{q_{w_2}\} \right. \\
 & \left. - \{q_{w_2}\}^T \{a_{w_2}\} \{a_{5_1}\}^T \{q_{5_1}\} + \{q_{w_2}\}^T \{a_{w_2}\} \{a_{w_2}\}^T \{q_{w_2}\} \right] \quad (4.40)
 \end{aligned}$$

This leads to stiffness submatrix contributions given by

$$\begin{aligned}
 [K_{5_1 5_1}]_{k_5} &= k_5 \{a_{5_1}\} \{a_{5_1}\}^T \\
 [K_{5_1 w_2}]_{k_5} &= -k_5 \{a_{5_1}\} \{a_{w_2}\}^T \\
 [K_{w_2 5_1}]_{k_5} &= -k_5 \{a_{w_2}\} \{a_{5_1}\}^T \\
 [K_{w_2 w_2}]_{k_5} &= k_5 \{a_{w_2}\} \{a_{w_2}\}^T
 \end{aligned} \tag{4.41}$$

where $\{a_{5_1}\}$ and $\{a_{w_2}\}$ are evaluated at (x_1, y_1) and (x_2, y_2) respectively. These submatrices are merged into the global stiffness matrix having the form

$$[K_{glob}] = \begin{bmatrix} K_{1,1,1} & K_{1,1,2} & K_{1,1,3} & K_{1,1,4} & K_{1,1,5} & K_{1,w_2} \\ K_{2,1,1} & K_{2,1,2} & K_{2,1,3} & K_{2,1,4} & K_{2,1,5} & K_{2,w_2} \\ K_{3,1,1} & K_{3,1,2} & K_{3,1,3} & K_{3,1,4} & K_{3,1,5} & K_{3,w_2} \\ K_{4,1,1} & K_{4,1,2} & K_{4,1,3} & K_{4,1,4} & K_{4,1,5} & K_{4,w_2} \\ K_{5,1,1} & K_{5,1,2} & K_{5,1,3} & K_{5,1,4} & K_{5,1,5} & K_{5,w_2} \\ \overline{K_{w_2,1}} & \overline{K_{w_2,2}} & \overline{K_{w_2,3}} & \overline{K_{w_2,4}} & \overline{K_{w_2,5}} & \overline{K_{w_2,w_2}} \end{bmatrix} \tag{4.42}$$

for each vertical spring connection that is used

Since a CPT zone with a symmetric cross section (as used here) does not have any in-plane displacement at its mid-surface, there is no necessity to enforce in-plane translational compatibility with the FSDPT zone. This leaves only rotational or slope compatibility to be enforced. The rotation θ_1 about the attach line for the FSDPT zone is defined in Eq. 4.35, and the rotation θ_2 about the attach line for the CPT zone is defined by Eq. 4.10. Let a rotational spring with stiffness k_3 act in resistance to rotation about the attach line and connect point (x_1, y_1) on zone 1 with point (x_2, y_2) on zone 2. Substitution of Eqs. 4.35 and 4.10 into Eq. 4.37 results in the potential energy contribution of the spring given in Eq. 4.38 where $\{q_{3_2}\}$ and $\{q_{4_2}\}$ are replaced with $\{q_{w_2}\}$, $\{a_{3_2}\}$ is replaced with $-\{a_{w_2,x}\}$, and $\{a_{4_2}\}$ is replaced with $-\{a_{w_2,y}\}$. The resulting stiffness submatrix contributions are given by

$$\begin{bmatrix} K_{3_1 3_1} & K_{3_1 4_1} \\ K_{4_1 3_1} & K_{4_1 4_1} \end{bmatrix} = k_3 \begin{bmatrix} \begin{bmatrix} \sin^2 \alpha_1 \{a_{3_1}\} \{a_{3_1}\}^T \\ -\cos \alpha_1 \sin \alpha_1 \{a_{4_1}\} \{a_{3_1}\}^T \end{bmatrix} & \begin{bmatrix} -\cos \alpha_1 \sin \alpha_1 \{a_{3_1}\} \{a_{4_1}\}^T \\ \cos^2 \alpha_1 \{a_{4_1}\} \{a_{4_1}\}^T \end{bmatrix} \\ \begin{bmatrix} -\cos \alpha_1 \sin \alpha_1 \{a_{4_1}\} \{a_{3_1}\}^T \\ \cos^2 \alpha_1 \{a_{4_1}\} \{a_{4_1}\}^T \end{bmatrix} & \end{bmatrix}$$

$$\begin{bmatrix} K_{3_1 w_2} \\ K_{4_1 w_2} \end{bmatrix} = k_3 \begin{bmatrix} \begin{bmatrix} \sin \alpha_1 \sin \alpha_2 \{a_{3_1}\} \{a_{w_2, x}\}^T - \cos \alpha_2 \sin \alpha_1 \{a_{3_1}\} \{a_{w_2, y}\}^T \\ -\cos \alpha_1 \sin \alpha_2 \{a_{4_1}\} \{a_{w_2, x}\}^T + \cos \alpha_1 \cos \alpha_2 \{a_{4_1}\} \{a_{w_2, y}\}^T \end{bmatrix} \\ \begin{bmatrix} -\cos \alpha_1 \sin \alpha_2 \{a_{4_1}\} \{a_{w_2, x}\}^T + \cos \alpha_1 \cos \alpha_2 \{a_{4_1}\} \{a_{w_2, y}\}^T \end{bmatrix} \end{bmatrix}$$

(4.43)

$$\begin{bmatrix} K_{w_2 3_1}^T & K_{w_2 4_1}^T \end{bmatrix} = k_3 \begin{bmatrix} \begin{bmatrix} \sin \alpha_1 \sin \alpha_2 \{a_{w_2, x}\} \{a_{3_1}\}^T - \cos \alpha_2 \sin \alpha_1 \{a_{w_2, y}\} \{a_{3_1}\}^T \\ -\cos \alpha_1 \sin \alpha_2 \{a_{w_2, x}\} \{a_{4_1}\}^T + \cos \alpha_1 \cos \alpha_2 \{a_{w_2, y}\} \{a_{4_1}\}^T \end{bmatrix} \\ \begin{bmatrix} -\cos \alpha_1 \sin \alpha_2 \{a_{w_2, x}\} \{a_{4_1}\}^T + \cos \alpha_1 \cos \alpha_2 \{a_{w_2, y}\} \{a_{4_1}\}^T \end{bmatrix} \end{bmatrix}$$

$$\begin{bmatrix} K_{w_2 w_2} \end{bmatrix} = k_3 \begin{bmatrix} \sin^2 \alpha_2 \{a_{w_2, x}\} \{a_{w_2, x}\}^T - \cos \alpha_2 \sin \alpha_2 \{a_{w_2, x}\} \{a_{w_2, y}\}^T \\ -\cos \alpha_2 \sin \alpha_2 \{a_{w_2, y}\} \{a_{w_2, x}\}^T + \cos^2 \alpha_2 \{a_{w_2, y}\} \{a_{w_2, y}\}^T \end{bmatrix}$$

where $\{a_{3_1}\}$ and $\{a_{4_1}\}$ are evaluated at (x_1, y_1) , and $\{a_{w_2, x}\}$ and $\{a_{w_2, y}\}$ are evaluated at (x_2, y_2) . These submatrices are merged into the global stiffness matrix having the form shown in Eq. 4.42 for each rotational spring connection that is used. Note that if a rotational spring of stiffness k_4 is used to resist rotation about an axis perpendicular to the attach line, Eq. 4.43 may be used to find the stiffness contributions with $\sin \alpha$ replaced by $-\cos \alpha$, $\cos \alpha$ replaced by $\sin \alpha$, and k_3 replaced by k_4 .

4.6 Boundary Conditions

Boundary conditions along the wing root may be imposed exactly through specific selection of displacement polynomials, or approximately through the use of computational springs. For a CPT zone, exact zero displacement along the root line $y=0$ may be achieved by using displacement polynomials that exclude all terms containing y^0 . A cantilevered condition along the same line may be achieved exactly by using polynomials that exclude all terms containing y^0 and y^1 . For a FSDPT zone, a cantilevered condition may be achieved by using displacement polynomials that exclude all terms containing y^0 .

In using springs, a zone is constrained at points along the root line which becomes the attach line. At a particular attach point on a FSDPT zone, five different springs may be used to constrain vertical, in-plane translational, and rotational displacements. Assuming the FSDPT zone to be zone #1, the stiffness contribution of a linear spring with stiffness k_5 resisting vertical displacement is given by the first submatrix expression in Eq. 4.24. The stiffness contribution of a linear spring with stiffness k_1 resisting in-plane translation perpendicular to the attach line is given by the first submatrix expression in Eq. 4.33. Likewise, the contribution of a rotational spring with stiffness k_3 resisting angular displacement about the attach line is given by the first submatrix expression in Eq. 4.39. As mentioned in Section 4.4, springs with stiffness coefficients k_2 and k_4 may also be used respectively to constrain in-plane translations parallel to the attach line and angular displacements about an axis perpendicular to the attach line in a similar manner. All of these stiffness contributions are merged into the global stiffness matrix. Note that a very large spring stiffness coefficient will force displacement to approximately zero. However, ill-conditioning of the stiffness matrix results from using coefficients that are too large.

Chapter 5: Spar Web Stiffness Approximation

5.1 Overview

This chapter discusses the use of an equivalent sandwich core to approximate the stiffness contributions of an array of spar webs. Discussed first is the case where spar webs provide only transverse shear stiffness to the wing. Presented next is the derivation of the stiffness contribution of a sandwich core structure. Finally discussed are the correlation factors allowing the stiffness matrix contribution of an array of webs to be approximated by a sandwich core over an associated panel area.

5.2 Spar Web Shear Stiffness

Recall from Chapter 3 that for a FSDPT zone the potential energy contribution due to an infinitesimal element of the j th spar web layer is given by

$$dU_{jl} = \frac{1}{2} t_{jl}(\eta, z) \begin{Bmatrix} \epsilon_{\eta\eta} \\ \gamma_{\eta z} \end{Bmatrix}^T [\mathcal{Q}]_{jl} \begin{Bmatrix} \epsilon_{\eta\eta} \\ \gamma_{\eta z} \end{Bmatrix} d\eta dz \quad (5.1)$$

The composition of the web layer constitutive matrix $[\mathcal{Q}]_{jl}$ is given by (Eq. B.166)

$$[\mathcal{Q}]_{jl} = \begin{bmatrix} \mathcal{Q}_{11} & \mathcal{Q}_{16} \\ \mathcal{Q}_{16} & \mathcal{Q}_{66} \end{bmatrix} \quad (5.2)$$

Now it is reasonable to allow the non-shear terms of $[\mathcal{Q}]_{jl}$ to be approximately zero since spar webs may contribute very little to in-plane stiffness. Using this assumption, the web is turned into a shear web, and the only nonzero constitutive term is \mathcal{Q}_{66} . Thus, the potential energy expression in Eq. 5.1 may be reduced to

$$dU_{jl} = \frac{1}{2} t_{jl}(\eta, z) \mathcal{Q}_{66} \gamma_{\eta z}^2 d\eta dz \quad (5.3)$$

Using Eq. 2.20 for $d\eta$, using Eq. 3.51 for $\gamma_{\eta z}$, and letting the layer thickness be a linear function of y gives

$$dU_{jl} = \frac{1}{2\cos\Lambda} t_{jl}(y) \bar{Q}_{66} \left\{ \begin{matrix} \gamma_{xz} \\ \gamma_{yz} \end{matrix} \right\}^T [TR_{22}] \left\{ \begin{matrix} \gamma_{xz} \\ \gamma_{yz} \end{matrix} \right\} dydz \quad (5.4)$$

where

$$[TR_{22}] = \begin{bmatrix} (s^2\Lambda) & (s\Lambda c\Lambda) \\ (s\Lambda c\Lambda) & (c^2\Lambda) \end{bmatrix} \quad (5.5)$$

Using Eqs. 3.7, 3.9, and 3.11-3.13 let us define

$$\left\{ \begin{matrix} \gamma_{xz} \\ \gamma_{yz} \end{matrix} \right\} = [W_s] \{q'\} \quad (5.6)$$

where

$$[W_s] = \begin{bmatrix} a_3^T & 0 & a_{5,x}^T \\ 0 & a_4^T & a_{5,y}^T \end{bmatrix} \quad (5.7)$$

$$\{q'\}^T = \{q_3^T, q_4^T, q_5^T\} \quad (5.8)$$

The matrix $[W_s]$, $2 \times (Nq_3 + Nq_4 + Nq_5)$ in dimension, is partitioned into subvectors of dimension $1 \times Nq_n$ ($n=3,4,5$). Substituting Eq. 5.6 into Eq. 5.4 gives

$$dU_{jl} = \frac{1}{2\cos\Lambda} t_{jl}(y) \bar{Q}_{66} \{q'\}^T [W_s]^T [TR_{22}] [W_s] \{q'\} dydz \quad (5.9)$$

Integrating over the area of the web, first with respect to z and then with respect to y , gives

$$U_{jl} = \frac{1}{2\cos\Lambda} \bar{Q}_{66} \int_{y=sy_L}^{y=sy_R} \int_{h_L(y)}^{h_U(y)} t_{jl}(y) \{q'\}^T [W_s]^T [TR_{22}] [W_s] \{q'\} dzdy \quad (5.10)$$

where the limits of z integration are the depth distributions of the lower and upper spar caps (see Eqs. B.133 and B.144). The z integration may be performed analytically (Eq. B.137) leading to stiffness matrix contribution of the jl th spar web layer in terms of a spar

line integral given by

$$[K_{swb}]_{jl} = \frac{1}{\cos \Lambda} Q_{66} \int_{y=sy_L}^{y=sy_R} [h_U(x, y) - h_L(x, y)] t_{jl}(y) [W_s]^T [TR_{22}] [W_s] dy \quad (5.11)$$

where x along the spar line is a function of y according to Eq. 2.21. This leads to linear combinations of spar line integrals defined in Eq. 2.24. If a wing contains many spars, the evaluation of web contributions to the stiffness matrix can be quite time consuming when done web by web using Eq. 5.11.

5.3 Sandwich Core Shear Stiffness

Let us examine the case where a sandwich core is used to model the internal structure of the wing between the composite skins as shown in Figure 5.1. The motivation here is to replace an array of many spars and ribs by a single equivalent core, whose stiffness can be evaluated once. Typical honeycomb core structures theoretically provide only transverse shear stiffness in bending. The elastic moduli and in-plane shear stiffness of the core are assumed to be zero (AL69). Only the shear moduli G_{xz} and G_{yz} are non-zero. The core constitutive relationship may be expressed by

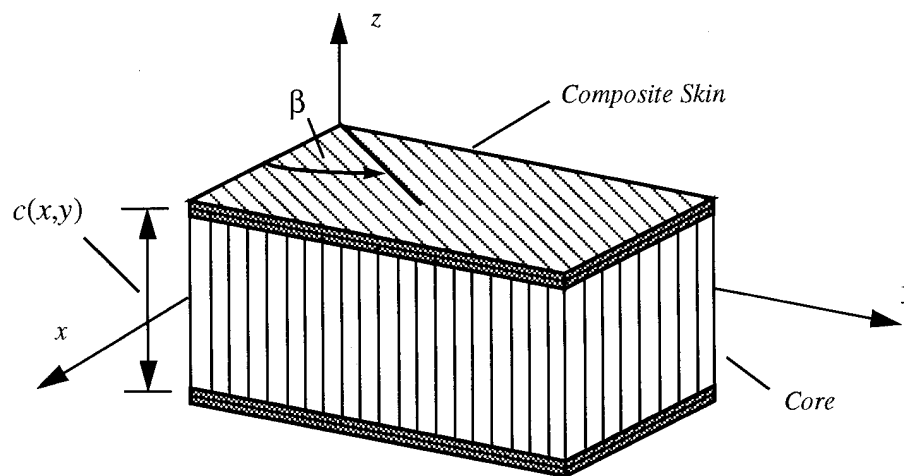


Figure 5.1: Composite Sandwich Structure

$$\begin{Bmatrix} \sigma_{xz} \\ \sigma_{yz} \end{Bmatrix} = \begin{bmatrix} G_{xz} & 0 \\ 0 & G_{yz} \end{bmatrix} \begin{Bmatrix} \gamma_{xz} \\ \gamma_{yz} \end{Bmatrix} \quad (5.12)$$

When the core is rotated by an angle β from the x - y reference axes as shown in Figure 5.1, this relationship may be restated by

$$\begin{Bmatrix} \sigma_{xz} \\ \sigma_{yz} \end{Bmatrix} = \begin{bmatrix} Q_{44} & Q_{45} \\ Q_{45} & Q_{55} \end{bmatrix} \begin{Bmatrix} \gamma_{xz} \\ \gamma_{yz} \end{Bmatrix} \quad (5.13)$$

where

$$Q_{44} = G_{xz} \sin^2 \beta + G_{yz} \cos^2 \beta \quad (5.14)$$

$$Q_{45} = (G_{xz} - G_{yz}) \sin \beta \cos \beta \quad (5.15)$$

$$Q_{55} = G_{xz} \cos^2 \beta + G_{yz} \sin^2 \beta \quad (5.16)$$

(JH92). If the core is assumed to be isotropic such that $G_{xz} = G_{yz} = G$, then Eq. 5.13 becomes

$$\begin{Bmatrix} \sigma_{xz} \\ \sigma_{yz} \end{Bmatrix} = \begin{bmatrix} G & 0 \\ 0 & G \end{bmatrix} \begin{Bmatrix} \gamma_{xz} \\ \gamma_{yz} \end{Bmatrix} \quad (5.17)$$

The constitutive relationship for a core with shear stiffness along the direction of spar lines, η , at an angle Λ from the y axis may be given by

$$\sigma_{\eta z} = G \gamma_{\eta z} \quad (5.18)$$

The contribution to the potential energy U of such a rotated core is given by

$$U_c = \frac{1}{2} \iiint G \gamma_{\eta z}^2 dV \quad (5.19)$$

(AL69,JH92). Using Eqs. 3.51 and 5.5 this may be rewritten as

$$U_c = \frac{G}{2} \iiint_{z,y,x} \begin{Bmatrix} \gamma_{xz} \\ \gamma_{yz} \end{Bmatrix}^T [TR_{22}] \begin{Bmatrix} \gamma_{xz} \\ \gamma_{yz} \end{Bmatrix} dx dy dz \quad (5.20)$$

The z integration may be replaced by the core depth $c(x,y)$ shown in Figure 5.1. Substituting this and Eq. 5.6 into Eq. 5.20 gives

$$U_c = \frac{G}{2} \iint_{y,x} c(x,y) \{q'\}^T [W_s]^T [TR_{22}] [W_s] \{q'\} dx dy \quad (5.21)$$

Finally, the resulting stiffness matrix contribution in terms of an area integral is given by

$$[K]_c = G \iint_{y,x} c(x,y) [W_s]^T [TR_{22}] [W_s] dx dy \quad (5.22)$$

5.4 Spar Web Array - Sandwich Core Stiffness Correlation

Now let us consider an array of spar webs where all Nwb webs are equally spaced and oriented at the same angle Λ to the y axis. Referring to Eqs. 5.11 and 5.22, it seems reasonable to assume there must be a way to correlate the stiffness matrix contributions of such an array with the stiffness matrix contributions of a sandwich core structure in an approximate manner. Doing so would effectively reduce the computationally intensive stiffness calculations of several spar webs composed of multiple layers to relatively simple calculations over a small number of single-layered panels.

Using Eq. 5.11, an averaged spar web stiffness matrix can be determined for an array of spar webs corresponding to a particular trapezoidal panel area. The web "density factor" d may be determined from the number of webs per chord dimension of the panel. Referring to Figure 1.3, this is given by

$$d = \frac{Nwb}{x_{AL} - x_{FL}} \quad (5.23)$$

We assume that all spar webs have Nl_{wb} layers each with the same thickness. Therefore, an average web thickness $t_{wb}(y)$ can be determined by summing over the layer thicknesses of one web. We allow for each composite layer to have a different shear stiffness due to principal material axis orientation. An average shear stiffness for the whole web can be determined at any y coordinate along one web using

$$Q_{wb} = \frac{1}{t_{wb}(y)} \sum_{jl=1}^{Nl_{wb}} t_{jl}(y) [Q_{66}]_{jl} \quad (5.24)$$

Using these averaged values, the averaged spar web stiffness matrix is given by

$$[K]_{wb} = \frac{d}{\cos \Lambda} Q_{wb} \int_{y=sy_L}^{y=sy_R} t_{wb}(y) [h_U(x, y) - h_L(x, y)] [W_s]^T [TR_{22}] [W_s] dy \quad (5.25)$$

Thus, Eq. 5.22 becomes approximately equivalent to Eq. 5.25 when $G = Q_{wb}$ and

$$c(x, y) = \frac{d}{\cos \Lambda} t_{wb}(y) [h_U(x, y) - h_L(x, y)] \quad (5.26)$$

Therefore, the stiffness matrix contribution of an approximately equivalent core over the panel area associated with the web array is given by

$$[K]_c = \frac{d}{\cos \Lambda} Q_{wb} \iint_{yx} t_{wb}(y) [h_U(x, y) - h_L(x, y)] [W_s]^T [TR_{22}] [W_s] dx dy \quad (5.27)$$

A whole array of evenly distributed spar webs having the same web construction can now be replaced by a single layer of equivalent core material. Evaluation of the core stiffness contribution is done using the same integral tables used to evaluate contributions of cover skins, thus leading to substantial saving of computational resources. A similar simplification may be made for an array of rib webs.

Chapter 6: Test Case Results

6.1 Overview

This chapter presents numerical results obtained with the new equivalent plate modeling capabilities focusing on two different test cases. The first test case involves a swept, thick, high aspect ratio wing of the type used for subsonic transports. This case was used to study the effects of using Ritz polynomials of different orders for different displacement fields and to study the accuracy of replacing detailed spar web modeling by an equivalent core are studied. A Boeing HSCT candidate wing represents a configuration made of a low aspect ratio inner section and a high aspect ratio outer wing, densely packed with supporting internal spars. Effectiveness and accuracy of equivalent core modeling are tested with this wing.

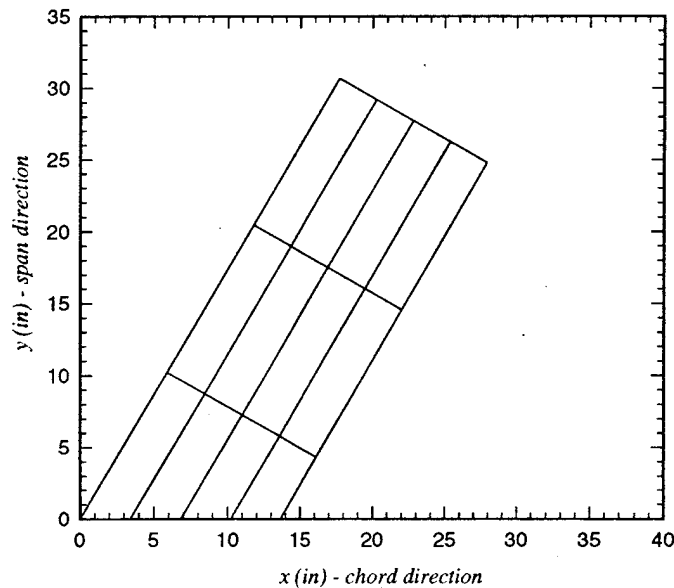


Figure 6.1: Turner-Martin-Weikel Wing

6.2 Swept, Thick, High Aspect Ratio Wing

A all aluminum subsonic transport type wing, for which experimental and numerical results are available, is discussed in TMW64 and LIV194 . Shown in Figure 6.1 is the geometry of this wing which has a symmetric airfoil (see Appendix D for more detail). This wing is used here first to test the effect of varying the order of polynomials used for different displacement and rotation fields in the FSDPT model. Recall from Chapter 3 that there are 3 independent linear mid-plane displacements u_0 , v_0 , w_0 and 2 independent rotational displacements ψ_x , ψ_y in the model. Obviously, the vertical deflection, stress, and natural frequency predictions of the model will deteriorate if polynomials of low order are used. However, the question is whether it is possible to use lower order polynomials for the shear rotation fields or any other deformation field without severely degrading the overall accuracy. If this is so, the overall order of wing models may be reduced leading to computational savings in storage and CPU time.

The numerical tests involved first varying the powers of the polynomials used for ψ_x and ψ_y alone. Then the powers of the polynomials used for u_0 and v_0 alone were varied.

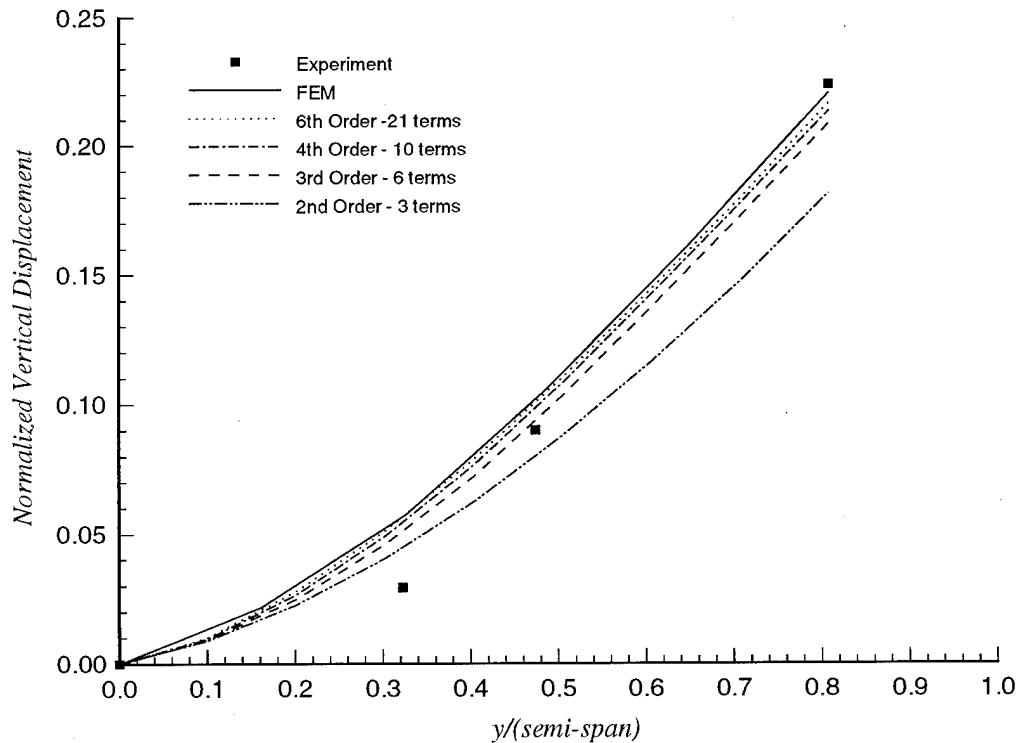


Figure 6.2: Vertical Displacement along Rear Spar with Varying Orders of ψ_x and ψ_y Rotation Field Polynomials

The reference case was based on using complete 6th order polynomials for all 5 displacement fields. Root cantilever boundary conditions along $y=0$ were enforced by omitting terms containing y^0 from the displacement polynomials, thus leaving 21 terms for each displacement for a total of 105 degrees of freedom. A 1 lb. vertical load was applied at the outboard point on the trailing edge.

Available experimental test data and finite element results are used here for comparison. Figure 6.2 shows the vertical deflections along the rear spar with rotation ψ_x and ψ_y polynomials varying in order from second to sixth order. Shown in Figure 6.3 is the normal stress in the primary spar direction ($\sigma_{\eta\eta}$) along the root chord from front to rear. Note that the finite element stress results do not correlate well in the region of higher stress gradient due to choice of mesh size. Natural frequency results are given in Table 6.1. The results show that although deflection and natural frequency correlation is still good for polynomials of 4th order (10 terms) stress correlation deteriorates quickly in the area of high stress gradients at the inboard trailing edge. Still, with 4th order rotation field polynomials, overall stress accuracy is comparable to the finite element results.

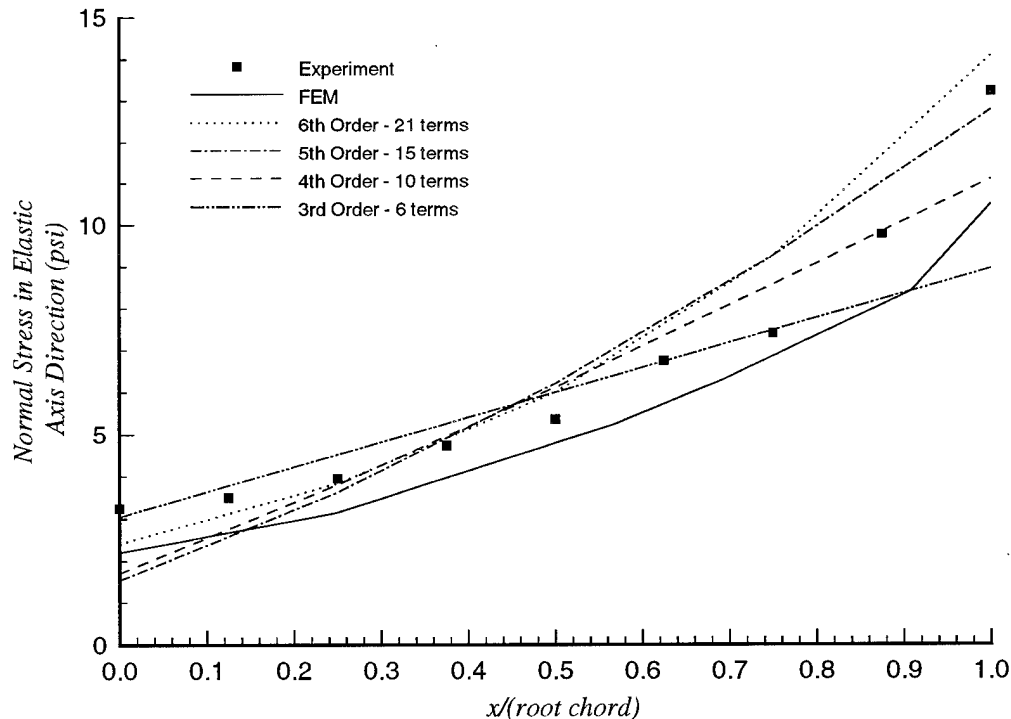


Figure 6.3: Skin Stress $\sigma_{\eta\eta}$ along Root Chord with Varying Orders of ψ_x and ψ_y Rotation Field Polynomials

Table 6.1: Natural Frequencies (in Hz) with Varying Orders of ψ_x and ψ_y Rotation Field Polynomials

Frequency # (Shape)	FEM	6th Order	5th Order	4th Order	3rd Order	2nd Order
#1 (1st Bending)	115.6	114.7	115.1	115.8	118.1	125.7
#2 (Fore/ aft)	317.6	312.4	312.4	312.4	312.4	312.4
#3 (1st Torsion)	418.4	428.9	430.3	431.9	441.6	484.8
#4 (2nd Bending)	576.4	575.3	576.9	582.8	591.9	715.0
#5 (2nd Torsion)	1086	1125	1136	1157	1251	1251

When the order of polynomials used for u_0 and v_0 was changed, no change from the reference case was observed in vertical deflections or stresses using polynomials down to 1st order (1 term). The 2nd natural frequency, corresponding to fore/aft motion, was the only value that changed at all throughout the comparison. This data is shown in Table 6.2. Such results could be expected because of the symmetry of airfoil cross section. If inaccurate prediction of the fore/aft vibration frequency can be tolerated (which is indeed the case when classical flutter is involved), then only 53 degrees of freedom (21 for w_0 , 15 for ψ_x and ψ_y , and 1 for u_0 and v_0) are needed for the wing. This is approximately a 50% reduction in model size (compared with the $5 \times 21 = 105$ dof model) leading to just a small reduction in accuracy.

Table 6.2: Second Natural Frequency (in Hz) for Varying Orders of u_0 and v_0 Displacement Polynomials

6th Order	5th Order	4th Order	3rd Order	2nd Order	1st Order
312.4	316.3	329.7	364.1	428.9	428.9

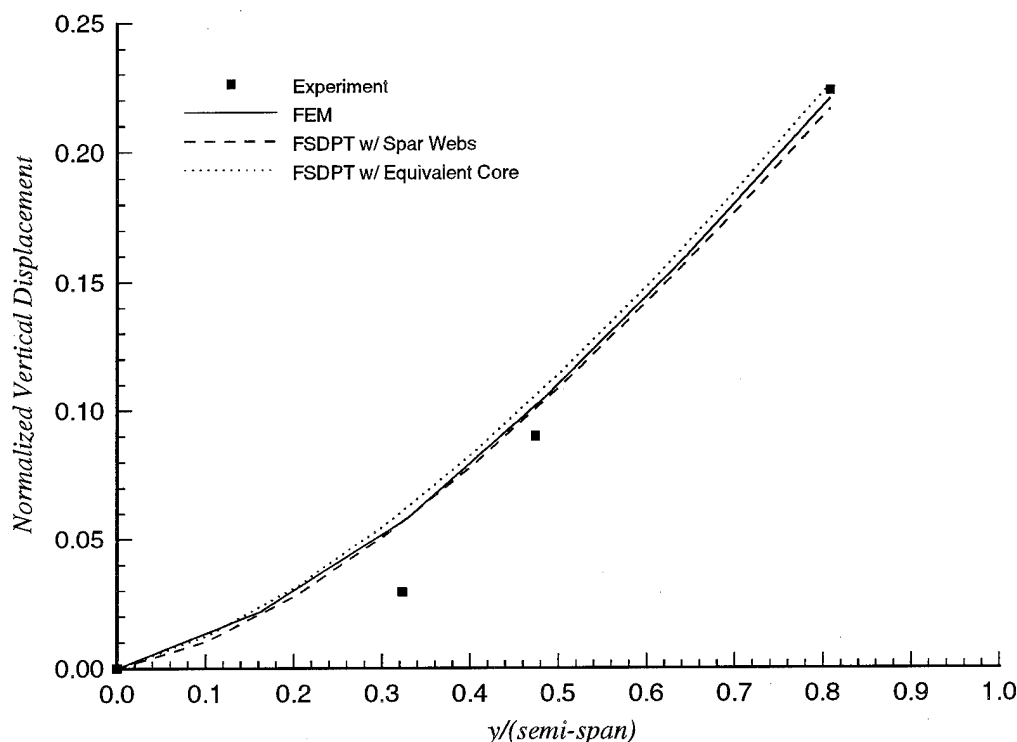


*Figure 6.4: Vertical Displacement along Rear Spar
Using an Equivalent Shear Core*

The Turner-Martin-Weikel wing is also used here as a test case to assess the accuracy of an equivalent core representation for shear web stiffness. Stiffness of the array of 5 spar webs parallel to the leading edge is approximated by a single shear core using Eq. 5.27. The same loading condition and displacement polynomials from the reference case above are used here. Vertical deflections along the rear spar are shown in Figure 6.4. Correlation with the reference case is reasonable with an error of 4.4% at the outboard point. Stress results along the root chord are shown in Figure 6.5. Correlation is reasonable here as well with an error of 6.1% at the inboard point on the trailing edge. Natural frequency results are reported in Table 6.3. The most serious discrepancies with respect to the reference case occur in the 3rd frequency (9.4% error) and the 5th frequency (6.4% error), both of which correspond to torsion modes. However, notice that these results have an error of only 7.1% and 3.0% respectively when compared to the finite element standard. Results from the test indicate that the equivalent core approximation works well for this thick, high aspect ratio wing.

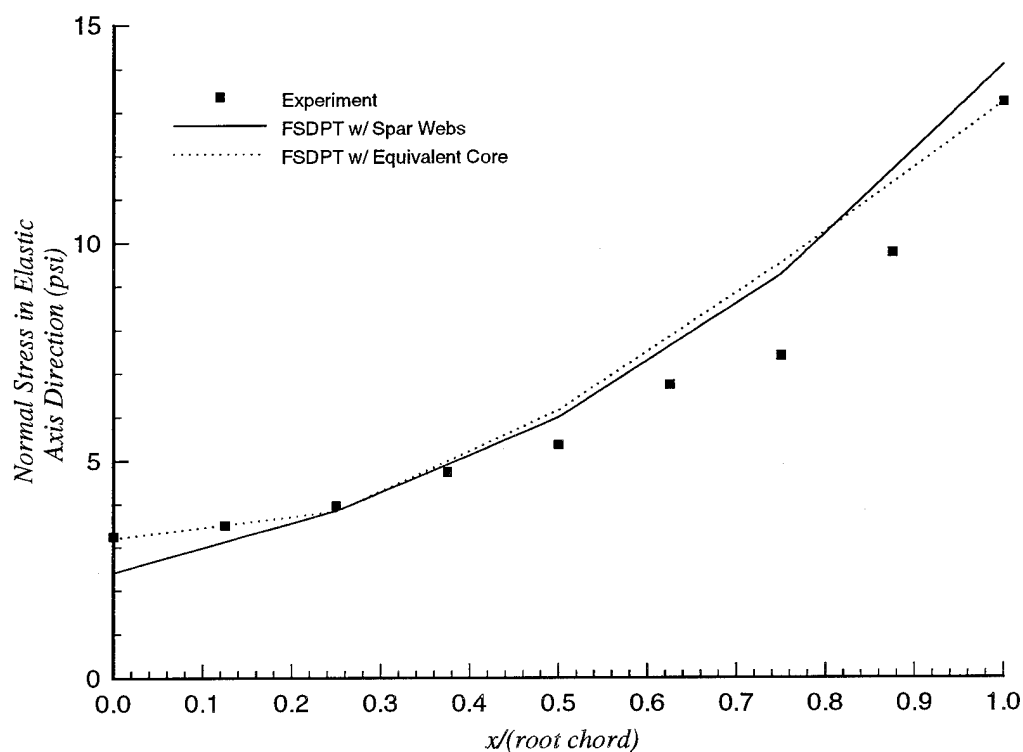


Figure 6.5: Skin Stress $\sigma_{\eta\eta}$ along Root Chord
Using an Equivalent Shear Core

Table 6.3: Natural Frequencies (in Hz) Using
an Equivalent Shear Core

Frequency # (Shape)	FEM	FSDPT Reference	FSDPT Equiv. Core
#1 (1st Bending)	115.6	114.7	114.4
#2 (Fore/ aft)	317.6	312.4	312.4
#3 (1st Torsion)	418.4	428.9	388.7
#4 (2nd Bending)	576.4	575.3	568.9
#5 (2nd Torsion)	1086	1125	1053

6.3 HSCT Wing

A simplified model of a representative HSCT wing was used to assess the accuracy of CPT based modeling of wings (LSB93). The simplified wing is symmetric about the mid-plane and has a linearly varying depth from root to tip. Its planform layout is shown in Figure 6.6 (see Appendix D). Previous HSCT numerical tests included finite element results obtained using the airframe structural optimization code ELFINI (LSB93,LP87). With 42 spar webs, this wing provides a challenging test case for the equivalent core approximation. If the preparation of stiffness contributions due to 42 webs, done one by one as in LSB93, can be replaced by the evaluation of stiffness contribution of one core, then CPU time savings can be significant.

Figure 6.7 shows vertical displacements for the HSCT wing along lines of constant y . The results show that use of the equivalent core gives good correlation with displacements based on individual spar webs. Using the equivalent core leads to a discrepancy of only 2.9% at the outer wing tip. Stress results are given in Figure 6.8 for the skin layer oriented at 0° to the inboard wing spar direction. Use of the equivalent core gives good correlation here as well.

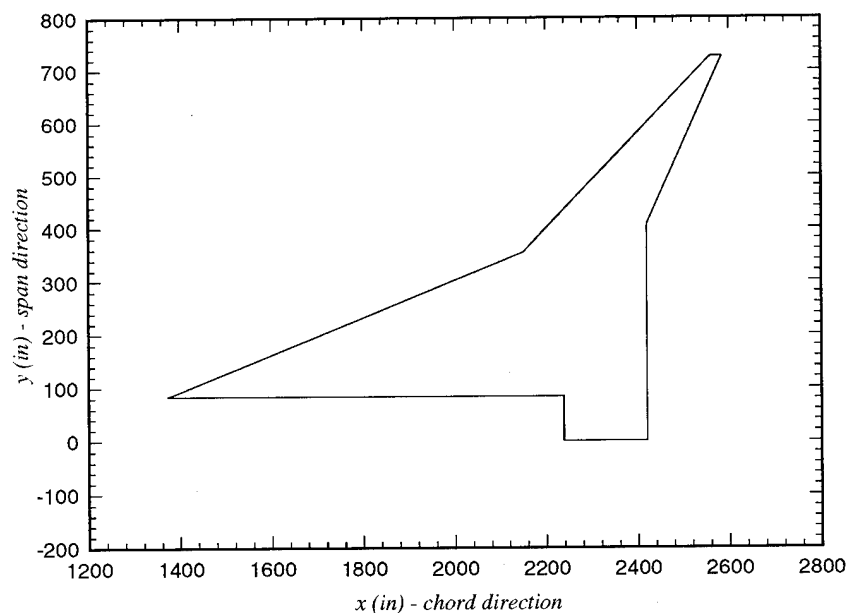


Figure 6.6: HSCT Wing Planform

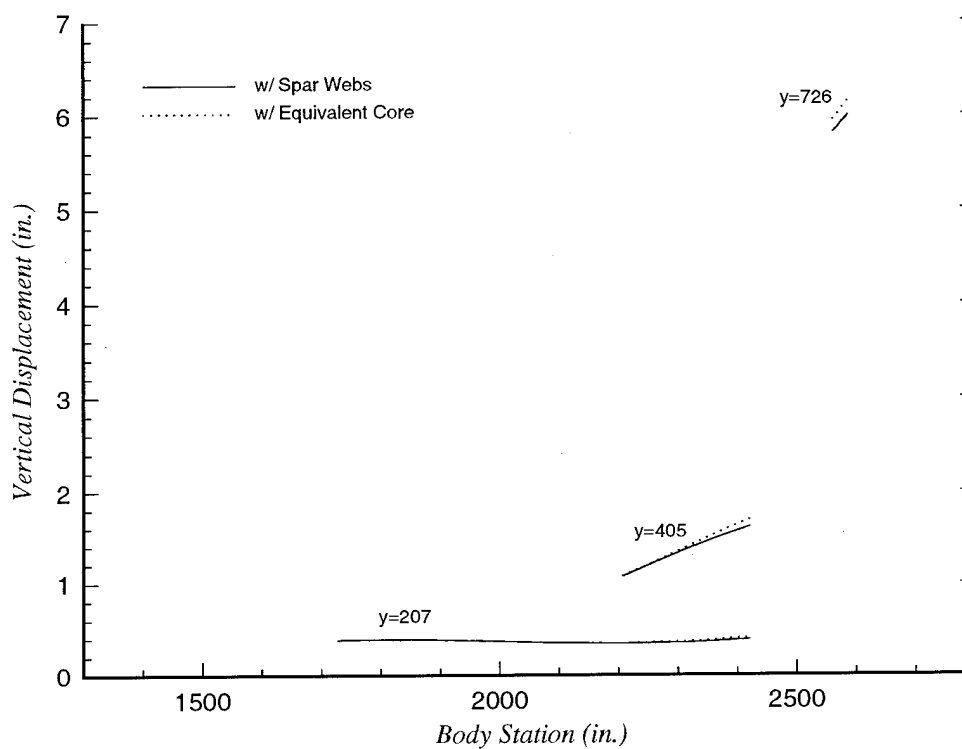
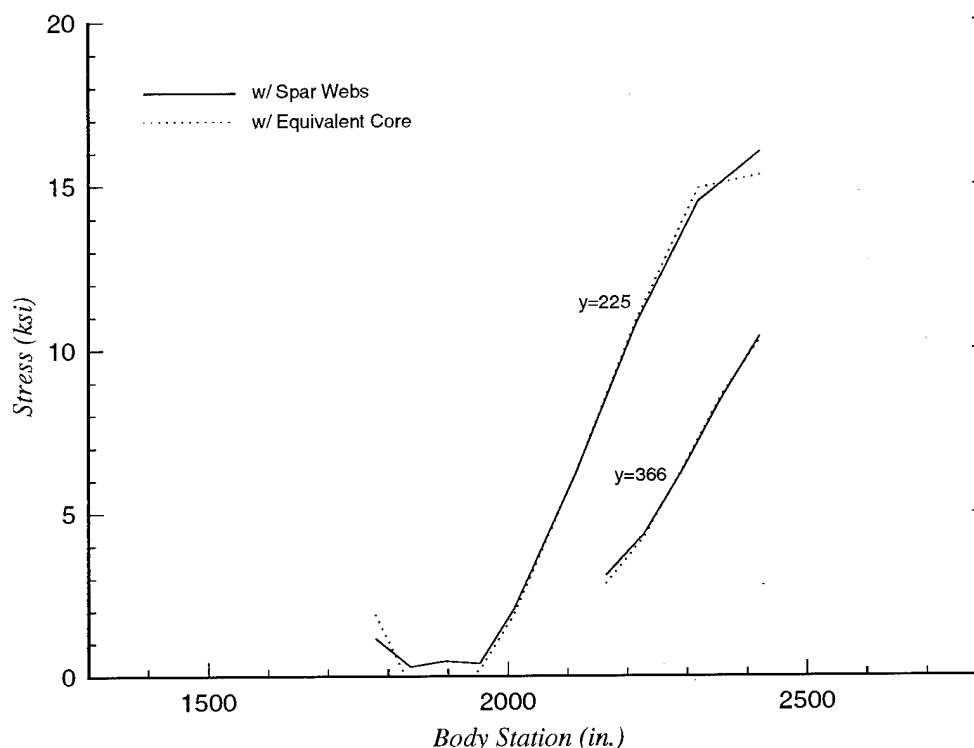


Figure 6.7: HSCT Wing Vertical Displacements

Table 6.4: HSCT Natural Frequencies (in Hz)

Frequency #	ELFINI	FSDPT Reference	FSDPT Equiv. Core
#1	9.50	9.50	9.37
#2	23.9	24.2	24.0
#3	26.9	24.8	24.7
#4	33.7	32.3	32.2
#5	36.1	38.8	38.8
#6	42.7	43.8	43.0
#7	45.2	50.0	48.8
#8	49.6	55.5	55.5



*Figure 6.8: Normal Stress in Layer Oriented at 0°
to Inboard Wing Spar Direction*

Table 6.4 shows a comparison of natural frequencies for ELFINI, FSDPT with normal spar webs, and FSDPT with the equivalent shear core. The frequencies are dependent upon the stiffness of the springs used to constrain displacements at the wing root. Using the spring stiffness coefficients listed in Appendix D, the FSDPT capability using spar webs matches the ELFINI capability reasonably. The equivalent core results correlate

Table 6.5: Stiffness Matrix Assembly Time (CPU seconds)

# of terms for Displacements	42 Spar Webs	Equivalent Core
10	2893.5	14.1
15	1861.5	10.8
21	765.7	3.3

well with both of these. Both tests with the Turner-Martin-Weikel wing and HSCT wing demonstrate the accuracy of modeling when an array of spar webs is replaced by an equivalent core.

The effectiveness of using an equivalent core is shown in a comparison of the computer resources required to assemble the stiffness matrix contributions for an array of spar webs and an equivalent core. Computations were performed on an HP Apollo 700 workstation. Table 6.5 compares the CPU time used in assembling the stiffness matrix for 42 spar webs vs. the time used in assembling the stiffness matrix for an equivalent core. As hoped for, the computational savings are significant.

Chapter 7: Conclusion

7.1 Summary

This work has presented recent improvements in equivalent plate modeling of aircraft wings for use in multi-disciplinary design optimization. A mathematical wing model was outlined using energy principles and the Ritz solution method. Formulations of mass, stiffness, and load contributions were given using both Classical Plate Theory and First Order Shear Deformation Plate Theory. These formulations allow each displacement field in the model to be independently approximated by a polynomial Ritz series of a chosen order. Additionally, a formulation for determining the spring stiffness contributions from the connection of a CPT zone to a FSDPT zone was derived. A method for approximating the stiffness of an array of spar webs using an equivalent core was also developed.

Results are presented from numerical tests performed on two different wings. Tests of the Turner-Martin-Weikel wing showed that low order polynomials may be used for linear in-plane displacements at the mid-surface, resulting in retained accuracy from a model of significantly reduced order. This wing was also used to show that an equivalent core can be used in place of an array of spar webs with acceptable accuracy. Tests of a simplified HSCT wing validated the accuracy and demonstrated the computational efficiency of the equivalent core approximation applied to a wing with many spar webs.

The findings here serve to advance the capabilities of equivalent plate wing modeling. These new developments allow wings of increasing complexity to be modeled with a better combination of accuracy and efficiency than could be achieved previously. Ultimately, this builds support for the use of equivalent plate modeling as the primary wing structural analysis tool in preliminary design optimization.

7.2 Future Work

Future extension of this work should include thorough numerical testing of the formulation for spring connection of FSDPT and CPT zones. This new capability should be tested on several wing configurations with available data for comparison. Also, for this capability to be used in design optimization, analytic sensitivities with respect to the design variables must be obtained and implemented for any new parameters introduced into the model. The developed code must also be modified to allow it to be linked with optimizing routines.

References

1. (AL69) Allen, Howard G., *Analysis and Design of Structural Sandwich Panels*, Pergamon, Oxford, England, UK, 1969.
2. (CHGK91) Chang, K.J., Haftka, R.T., Giles, G.L., and Kao, P.J., "Sensitivity Based Scaling for Correlating Structural Response from Different Analytical Models", *Proceedings of the AIAA/ASME/ASCE/AHS/ASC 32nd Structures, Structural Dynamics, and Materials Conference*, Pt. 1, AIAA, Washington, DC, pp. 238-246, (AIAA Paper 91-0925), 1991.
3. (FE75) Felippa, C.A., "Solution of Linear Equations with Skyline-Stored Symmetric Matrix", *Computers and Structures*, Vol. 5, pp. 13-29, 1975.
4. (GI86) Giles, G.L., "Equivalent Plate Analysis of Aircraft Wing Box Structure with General Planform Geometry", *Journal of Aircraft*, Vol. 23, No. 11, pp. 859-864, 1986.
5. (GI89) Giles, G.L. "Further Generalization of an Equivalent Plate Representation for Aircraft Structural Analysis", *Journal of Aircraft*, Vol. 26, No. 1, pp. 67-74, 1989.
6. (GR61) Gallagher, R.H., and Rattinger, I., "The Deformational Behavior of Low Aspect Ratio Multi Web Wings", *The Aeronautical Quarterly*, pp. 361-371, Nov. 1961, pp. 71-87, Feb. 1962, pp. 143-166, May 1962; also in *A Correlation Study of Methods of Matrix Structural Analysis*, MacMillan, 1964.
7. (GVL89) Golub, G.H. and Van Loan, C.F., *Matrix Computations*, 2nd ed., Johns Hopkins University Press, pp. 394-406, 1989.
8. (HA93) Harvey, M.S., "Automated Finite Element Modeling of Wing Structures for Shape Optimization", Master of Science Thesis, Department of Aeronautics and Astronautics, University of Washington, 1993.
9. (HG92) Haftka, R.T. and Gurdal, Z., *Elements of Structural Optimization*, 3rd ed., Kluwer, Dordrecht, The Netherlands, pp. 256-263, 1992.
10. (JH92) Jeon, J.S. and Hong, C.S., "Bending of Tapered Anisotropic Plates with Arbitrary Edge Conditions", *AIAA Journal*, Vol. 30, No. 7, pp. 1762-1769, 1992.
11. (JO75) Jones, Robert M., *Mechanics of Composite Materials*, McGraw-Hill, New York, 1975.
12. (KA92) Kao, P.J., "Coupled Raleigh-Ritz/Finite Element Structural Analysis using Penalty Function Method", *Proceedings of the AIAA/ASME/ASCE/AHS/ASC 33rd Structures, Structural Dynamics, and Materials Conference*, Pt. 1, AIAA, Washington, DC, pp. 135-141, (AIAA Paper 92-2238), 1992.

13. (LAN94) Langelaan, Jacob W., "Design Oriented Structural Analysis for Shape Optimization of Isotropic and Composite Fuselage Structures", Master of Science Thesis, Department of Aeronautics and Astronautics, University of Washington, 1994.
14. (LIV90) Livne, E., "Integrated Multidisciplinary Optimization of Actively Controlled Fiber Composite Wings", Ph.D. Dissertation, Dept. of Mechanical, Aerospace, and Nuclear Engineering, Univ. of California Los Angeles, Los Angeles, CA, 1990.
15. (LIV94) Livne, E., "Equivalent Plate Structural Modeling for Wing Shape Optimization Including Transverse Shear", *AIAA Journal*, Vol. 32, No. 6, pp. 1278-1288, June 1994.
16. (LIV294) Livne, E., "Analytical Sensitivities for Shape Optimization in Equivalent Plate Structural Wing Models", *Journal of Aircraft*, Vol. 31, No. 4, pp. 961-969, July-August 1994.
17. (LOT85) Lottati, I., "Flutter and Divergence Aeroelastic Characteristics for Composite Forward Swept Cantilevered Wing", *Journal of Aircraft*, Vol. 22, No. 11, pp.1001-1007, 1985.
18. (LP87) Lecina, G. and Petiau, C., "Advances in Optimal Design with Composite Materials", *Computer Aided Optimal Design: Structural and Mechanical Systems*, edited by C.A. Mota-Soares, Springer-Verlag, Berlin, 1987.
19. (LS88) Librescu, L. and Simovich, J., "A General Formulation for the Aeroelastic Divergence of Composite Sweptforward Wing Structures", *Journal of Aircraft*, Vol. 25, No. 4, pp.364-371, 1988.
20. (LSB93) Livne, E., Sels, R.A., and Bhatia, K.G., "Lessons Learned from Application of Equivalent Plate Structural Modeling to an HSCT Wing", *Proceedings of the AIAA/ASME/ASCE/AHS/ASC 34th Structures, Structural Dynamics, and Materials Conference*, Pt. 2, AIAA, Washington, DC, pp. 959-969, (AIAA Paper 93-1413), 1993.
21. (LSF88) Livne, E., Schmit, L.A., and Friedmann, P.P., "Design Oriented Structural Analysis for Fiber Composite Wings", Dept. of Mechanical, Aerospace, and Nuclear Engineering, Univ. of California Los Angeles, UCLA-ENG-88-36, Los Angeles, CA, November 1988.
22. (LRB77) Lynch, R.W., Rogers, W.A., and Brayman, W.W., "Aeroelastic Tailoring of Advanced Composite Structures for Military Aircraft", U.S. Air Force Flight Dynamics Lab, AFFDL-TR-76-100, Dayton, OH, April 1977.
23. (MC83) McCullers, L.A., "Automated Design of Advanced Composite Structures", *Mechanics of Composite Materials*, edited by Z. Hashin, Pergamon Press, Oxford, England, UK, 1983.
24. (MIL94) Milosavljevic, R., "Buckling Analysis and Analytic Sensitivities for Trapezoidal Panels in Wing Preliminary Design", Master of Science Thesis, Department of Aeronautics and Astronautics, University of Washington, 1994.
25. (MIU72) Miura, H., "An Optimal Configuration Design of Lifting Surface Type

- Structures under Dynamic Constraints", Ph.D. Dissertation, Case Western Reserve Univ., Cleveland, OH, January 1972.
26. (RE84) Reddy, J.N., *Energy and Variational Methods in Applied Mechanics*, Wiley, New York, 1984.
 27. (SCH81) Schmit, L.A., "Structural Synthesis - It's Genesis and Development", *AIAA Journal*, Vol. 19, No. 10, pp. 1249-1236, October 1981.
 28. (SB59) Schmit, L.A. and Balmer, H.A., "Procedures for Including Temperature Effects in Structural Analysis of Elastic Wings", Wright Air Development Center, WADC TR 57-754, NTIS AD 230 981, Dayton, OH, May 1959.
 29. (SP68) Spiegel, M.R., *Mathematical Handbook*, Schaum's Outline Series, McGraw-Hill, p. 61, 1968.
 30. (SV90) Stritz, A.G. and Venkayya, V.B., "Influence of Structural and Aerodynamic Modeling on Flutter Analysis", *Proceedings of the AIAA/ASME/ASCE/AHS/ASC 31st Structures, Structural Dynamics, and Materials Conference*, Pt. 1, AIAA, Washington, DC, pp. 110-118, 1990.
 31. (TMW64) Turner, M.J., Martin, H.C., and Weikel, R.C., "Further Development and Application of the Stiffness Method", *Matrix Methods of Structural Analysis*, edited by F.B. de Veubeker, Pergamon Press, Oxford, England, UK, pp. 203-266, 1964.
 32. (TR80) Triplett, W.E., "Aeroelastic Tailoring Studies in Fighter Aircraft Design", *Journal of Aircraft*, Vol. 17, No. 7, pp. 508-513, 1980.

Appendix A: Analytical Foundations of an Equivalent Plate Model Using CPT

A.1 Overview

In this appendix are derived the equations necessary to construct mass and stiffness matrices for wing structural components based on Classical Plate Theory. This appendix starts with a discussion of the assumptions of Classical Plate Theory and the ensuing strain-displacement relationships. Following this foundation are the derivations of the mass and stiffness matrix equations for a single skin layer. Next are the derivations of the mass and stiffness matrix equations for a single spar. Presented last are the derivations of the mass and stiffness matrix equations for a single rib.

A.2 Assumptions

Classical Plate Theory (CPT) is the name given to the small-deflection theory of bending of elastic thin plates (RE84). The first assumption of CPT for a plate in the x - y reference plane is that the displacements of the mid-surface are small compared to the thickness of the plate, thus meaning the slope of the deflected surface is very small. The second assumption is that the plate mid-surface remains unstrained after bending. The third assumption, known as the Kirchhoff-Love assumption, is that planes normal to the plate's mid-surface will remain plane and normal to the plate's mid-surface after the plate is deformed (RE84,JO75). This assumption is equivalent to ignoring the shear strains γ_{xz} and γ_{yz} . The fourth assumption is that the transverse normal strain ϵ_{zz} is negligible since the transverse loads are transferred primarily to bending strains. In other words, the transverse deflection does not vary across the plate thickness. The final assumption is that the transverse normal stress σ_z may be neglected since it is small compared to the other stresses.

Certain assumptions must be made about the wing being modeled as well. The first of these assumptions is that no spar webs or rib webs will be included. Only skins, spar caps, and rib caps, will be accounted for. See Figure 1.1. The second assumption is that the

wing is thin and symmetric with respect to the x - y plane. The final assumption is that the wing skins are thin with respect to the wing depth allowing all skin layers in each of the upper and lower skins to have the same depth distribution (LIV90).

A.3 Strain-Displacement Relationships

The established assumptions allow the plate problem to be considered under plane stress conditions where the in-plane strains ϵ_{xx} , ϵ_{yy} , and γ_{xy} are the only strains of concern. It may also be concluded that the normal displacement in the z direction is a function of only x and y ; therefore

$$w = w(x, y) \quad (\text{A.1})$$

Because of the Kirchhoff-Love assumption and the symmetry of the wing, the inplane displacements u and v are given as

$$u = -z \frac{\partial w}{\partial x} = -zw_{,x} \quad (\text{A.2})$$

$$v = -z \frac{\partial w}{\partial y} = -zw_{,y} \quad (\text{A.3})$$

The strains are then given as

$$\epsilon_{xx} = \frac{\partial u}{\partial x} = -zw_{,xx} \quad (\text{A.4})$$

$$\epsilon_{yy} = \frac{\partial v}{\partial y} = -zw_{,yy} \quad (\text{A.5})$$

$$\gamma_{xy} = \frac{\partial u}{\partial y} + \frac{\partial v}{\partial x} = -2zw_{,xy} \quad (\text{A.6})$$

It is evident that all the displacements and strains are functions of the independent transverse displacement $w(x,y)$. These relationships form the basis for the stiffness and mass matrix formulations (LIV90).

A.4 Displacement Function

To use the Ritz method described in Chapter 1, it is necessary to define the displacement function $w(x,y,t)$ as a polynomial series having Nq_w terms using Eq. 1.9. Thus,

$$w(x, y, t) = \sum_{i=1}^{Nq_w} q_w(t)_i \cdot x^{mq_i} y^{nq_i} \quad (\text{A.7})$$

where the time dependent coefficients $q_w(t)_i$ become the generalized displacements solved for in the Ritz formulation, and the powers mq_i and nq_i are predetermined (LIV90). This may be expressed more simply in vector form as

$$w(x, y, t) = \{a_w(x, y)\}^T \{q_w(t)\} \quad (\text{A.8})$$

where

$$\{a_w(x, y)\}^T = \{\dots, x^{mq_i} y^{nq_i}, \dots\} \quad (\text{A.9})$$

and $\{q_w(t)\}$ is a column vector. Both vectors contain Nq_w terms. This vector form for $w(x,y,t)$ will be used in the mass and stiffness matrix formulations.

A.5 Mass Matrix Contributions of a Skin Layer

Neglecting rotary inertia the contribution to the kinetic energy T of an infinitesimal skin element dx by dy of the j th skin layer is

$$dT_{jl} = \frac{1}{2} \rho_{jl} t_{jl}(x, y) \dot{w}^2(x, y, t) dx dy \quad (\text{A.10})$$

where ρ_{jl} is the constant material density of the skin layer, and $t_{jl}(x,y)$ is the thickness of the skin layer given in Eq. 1.2 as

$$t_{jl}(x, y) = \sum_{k=1}^{Nt_{jl}} \hat{T}_{jl_k} \cdot x^{mt_k} y^{nt_k} \quad (\text{A.11})$$

(LIV90). Substituting Eq. A.8 into Eq. A.10 gives

$$dT_{jl} = \frac{1}{2} \rho_{jl} t_{jl}(x, y) \{\dot{q}_w\}^T \{a_w\} \{a_w\}^T \{\dot{q}_w\} dx dy \quad (\text{A.12})$$

Integrating this over the whole trapezoidal panel area yields

$$T_{jl} = \frac{1}{2} \rho_{jl} \iint_{yx} t_{jl}(x, y) \{\dot{q}_w\}^T \{a_w\} \{a_w\}^T \{\dot{q}_w\} dx dy \quad (\text{A.13})$$

Equivalently,

$$T_{jl} = \frac{1}{2} \omega^2 \rho_{jl} \iint_{yx} t_{jl}(x, y) \{q_w\}^T \{a_w\} \{a_w\}^T \{q_w\} dx dy \quad (\text{A.14})$$

where ω is the natural vibrational frequency of the skin layer. The variational extremum condition from Eq. 1.10 applied here becomes

$$\frac{\partial T_{jl}}{\partial q_{w_i}} = 0 \quad (\text{A.15})$$

yielding the mass matrix for the j th skin layer given as

$$[M_{sk}]_{jl} = \rho_{jl} \iint_{yx} t_{jl}(x, y) \{a_w\} \{a_w\}^T dx dy \quad (\text{A.16})$$

Substitution of Eq. A.11 for $t_{jl}(x, y)$ gives

$$[M_{sk}]_{jl} = \rho_{jl} \sum_{k=1}^{N_{t_{jl}}} \hat{T}_{jl_k} \iint_{yx} x^{m_{t_k}} y^{n_{t_k}} \{a_w\} \{a_w\}^T dx dy \quad (\text{A.17})$$

The mass matrix term in the i th row and j th column for the j th skin layer may be expressed as

$$[M_{sk}(i, j)]_{jl} = \rho_{jl} \sum_{k=1}^{N_{t_{jl}}} \hat{T}_{jl_k} \iint_{yx} x^m y^n dx dy \quad (\text{A.18})$$

where

$$m = m_{q_i} + m_{q_j} + m_{t_k} \quad (\text{A.19})$$

$$n = nq_i + nq_j + nt_k \quad (\text{A.20})$$

Let us define a family of integrals over the area of the trapezoidal panel where

$$I_{TR}(m, n) = \int \int_{y \ x} x^m y^n dx dy \quad (\text{A.21})$$

Then the final expression for the i, j th term of $[M_{sk}]_{jl}$ is

$$[M_{sk}(i, j)]_{jl} = \rho_{jl} \sum_{k=1}^{Nt_{jl}} \hat{T}_{jl_k} I_{TR}(m, n) \quad (\text{A.22})$$

Appendix C discusses how the family of integrals $I_{TR}(m, n)$ is analytically derived. The mass matrix for all the skin layers combined $[M_{sk}]_{tot}$ is obtained by summing the contributions of all the layers given by Eq. A.22. Because the wing is assumed to be symmetric with respect to the x - y plane, the total skin contribution can be found by summing the contributions from the layers of the upper skin and then multiplying by 2. This matrix is then appropriately merged into the global mass matrix $[M_{glob}]$.

A.6 Stiffness Matrix Contributions of a Skin Layer

The contribution to the potential or strain energy U of an infinitesimal skin element dx by dy of the jl th skin layer is

$$dU_{jl} = \frac{1}{2} \{\kappa\}^T [D]_{jl} \{\kappa\} dx dy \quad (\text{A.23})$$

where

$$\{\kappa\} = - \begin{Bmatrix} w_{,xx} \\ w_{,yy} \\ 2w_{,xy} \end{Bmatrix} \quad (\text{A.24})$$

using Eqs. A.4, A.5, and A.6, and $[D]_{jl}$ is the plate bending stiffness matrix defined by

$$[D]_{jl} = \int_z [Q]_{jl} z^2 dz \quad (\text{A.25})$$

(JO75, LIV90). The j th layer's constitutive matrix $[Q]_{jl}$, as discussed in Section 1.5, has the form

$$[Q]_{jl} = \begin{bmatrix} Q_{11} & Q_{12} & Q_{16} \\ Q_{12} & Q_{22} & Q_{26} \\ Q_{16} & Q_{26} & Q_{66} \end{bmatrix}_{jl} \quad (\text{A.26})$$

where its components are determined for the x - y axis system from $[\tilde{Q}]_{jl}$, the j th layer's constitutive matrix referenced to its own principal material axes. Assuming the j th layer to be an orthotropic lamina, its invariant properties may be used to find $[Q]_{jl}$ when the principal material axes are oriented at some angle β to the x - y axes as shown in Figure A.1 (JO75). The components of $[Q]_{jl}$ may be written as

$$Q_{11} = C_1 + C_2 \cos 2\beta + C_3 \cos 4\beta \quad (\text{A.27})$$

$$Q_{12} = C_4 - C_3 \cos 4\beta \quad (\text{A.28})$$

$$Q_{22} = C_1 - C_2 \cos 2\beta + C_3 \cos 4\beta \quad (\text{A.29})$$

$$Q_{16} = -\frac{1}{2}C_2 \sin 2\beta - C_3 \sin 4\beta \quad (\text{A.30})$$

$$Q_{26} = -\frac{1}{2}C_2 \sin 2\beta + C_3 \sin 4\beta \quad (\text{A.31})$$

$$Q_{66} = C_5 - C_3 \cos 4\beta \quad (\text{A.32})$$

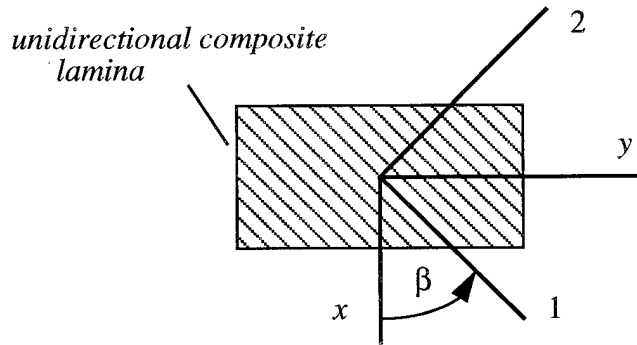


Figure A.1: Positive Rotation of Principal Material Axes from x - y Axes

for which the invariants are given as

$$C_1 = \frac{3\tilde{Q}_{11} + 3\tilde{Q}_{22} + 2\tilde{Q}_{12} + 4\tilde{Q}_{66}}{8} \quad (\text{A.33})$$

$$C_2 = \frac{\tilde{Q}_{11} - \tilde{Q}_{22}}{2} \quad (\text{A.34})$$

$$C_3 = \frac{\tilde{Q}_{11} + \tilde{Q}_{22} - 2\tilde{Q}_{12} - 4\tilde{Q}_{66}}{8} \quad (\text{A.35})$$

$$C_4 = \frac{\tilde{Q}_{11} + \tilde{Q}_{22} + 6\tilde{Q}_{12} - 4\tilde{Q}_{66}}{8} \quad (\text{A.36})$$

$$C_5 = \frac{\tilde{Q}_{11} + \tilde{Q}_{22} - 2\tilde{Q}_{12} + 4\tilde{Q}_{66}}{8} \quad (\text{A.37})$$

Referring to Figure A.2, the j th skin layer lies between the coordinates $z=h/2-t_{jl}/2$ and $z=h/2+t_{jl}/2$ such that the z integral from Eq. A.25 is given by

$$\int_{(h-t_{jl})/2}^{(h+t_{jl})/2} z^2 dz = \frac{h^2}{4} t_{jl} \left[1 + \frac{1}{3} \left(\frac{t_{jl}}{h} \right)^2 \right] \quad (\text{A.38})$$

Since it is assumed that the wing thickness is much smaller than the wing depth ($t_{jl}/h \ll 1$), the right hand side of Eq. A.38 can be simplified to $h^2 t_{jl}/4$ (LIV90). Substituting Eqs. A.24 and A.25, and the simplified Eq. A.38 into Eq. A.23 then gives

$$dU_{jl} = \frac{1}{2} \left(\frac{h(x,y)^2}{4} \right) t_{jl}(x,y) \begin{Bmatrix} w_{,xx} \\ w_{,yy} \\ 2w_{,xy} \end{Bmatrix}^T [Q]_{jl} \begin{Bmatrix} w_{,xx} \\ w_{,yy} \\ 2w_{,xy} \end{Bmatrix} dx dy \quad (\text{A.39})$$

Substituting Eq. A.8 results in

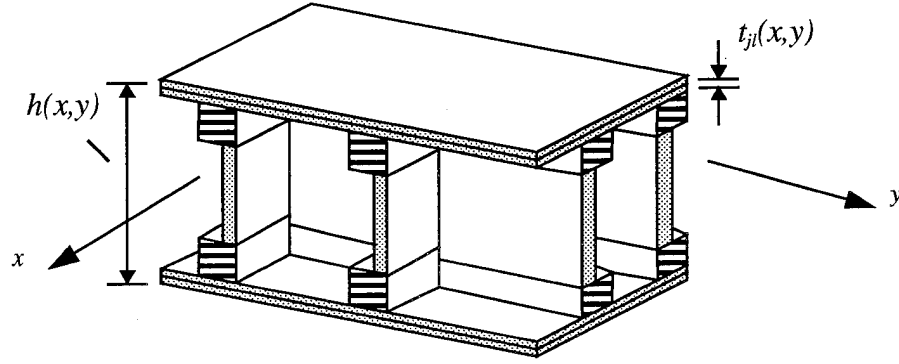


Figure A.2: Skin Layer Thickness and Depth

$$dU_{jl} = \frac{1}{2} \left(\frac{h(x,y)^2}{4} \right) t_{jl}(x,y) \{q_w\}^T [W]_{jl}^T [Q]_{jl} [W]_{jl} \{q_w\} dx dy \quad (\text{A.40})$$

where

$$[W] = \begin{bmatrix} \{a_{w,xx}\}^T \\ \{a_{w,yy}\}^T \\ 2\{a_{w,xy}\}^T \end{bmatrix} = \begin{bmatrix} \dots, m q_i (m q_i - 1) x^{m q_i - 2} y^{n q_i}, \dots \\ \dots, n q_i (n q_i - 1) x^{m q_i} y^{n q_i - 2}, \dots \\ \dots, 2 m q_i n q_i x^{m q_i - 1} y^{n q_i - 1}, \dots \end{bmatrix} \quad (\text{A.41})$$

Integration of Eq. A.40 over the whole trapezoidal panel area gives

$$U_{jl} = \frac{1}{2} \iint_{yx} \left(\frac{h(x,y)^2}{4} \right) t_{jl}(x,y) \{q_w\}^T [W]_{jl}^T [Q]_{jl} [W]_{jl} \{q_w\} dx dy \quad (\text{A.42})$$

The variational extremum condition from Eq. 1.10 applied here becomes

$$\frac{\partial U_{jl}}{\partial q_{w_i}} = 0 \quad (\text{A.43})$$

yielding the stiffness matrix for the j th skin layer given as

$$[K_{sk}]_{jl} = \iint_{yx} \left(\frac{h(x,y)^2}{4} \right) t_{jl}(x,y) [W]^T [Q]_{jl} [W] dx dy \quad (A.44)$$

Substitution of Eq. A.11 for $t_{jl}(x,y)$ and the following

$$h(x,y) = \sum_{ik=1}^{Nh} H_{ik} \cdot x^{mh_{ik}} y^{nh_{ik}} \quad (A.45)$$

for $h(x,y)$ (See Eq. 1.1) into Eq. A.43 yields

$$[K_{sk}]_{jl} = \frac{1}{4} \sum_{ik=1}^{Nh} \sum_{jk=1}^{Nh} \sum_{k=1}^{Nt_{jl}} H_{ik} H_{jk} \hat{T}_{jl_k} \cdot \iint_{yx} x^{mh_{ik}+mh_{jk}+mt_k} y^{nh_{ik}+nh_{jk}+nt_k} [W]^T [Q]_{jl} [W] dx dy \quad (A.46)$$

Let the r , i th term of the matrix $[W]$ ($3 \times Nq_w$ in dimension) be

$$[W(r,i)] = \tilde{W}(r,i) x^{mW(r,i)} y^{nW(r,i)} \quad (A.47)$$

Then the i , j th term of the triple matrix product $[W]^T [Q]_{jl} [W]$ is

$$term(i,j) = \sum_{r=1}^3 \sum_{s=1}^3 \tilde{W}(r,i) \tilde{W}(s,j) Q_{jl}(r,s) x^{mW(r,i)+mW(s,j)} y^{nW(r,i)+nW(s,j)} \quad (A.48)$$

Upon substitution of Eq. A.48 into Eq. A.46, the stiffness matrix term in the i th row and j th column for the j th skin layer may be expressed as

$$[K_{sk}(i,j)]_{jl} = \frac{1}{4} \sum_{ik=1}^{Nh} \sum_{jk=1}^{Nh} \sum_{k=1}^{Nt_{jl}} \sum_{r=1}^3 \sum_{s=1}^3 H_{ik} H_{jk} \hat{T}_{jl_k} \cdot \tilde{W}(r,i) \tilde{W}(s,j) Q_{jl}(r,s) \iint_{yx} x^m y^n dx dy \quad (A.49)$$

where

$$m = mW(r, i) + mW(s, j) + mh_{ik} + mh_{jk} + mt_k \quad (\text{A.50})$$

$$n = nW(r, i) + nW(s, j) + nh_{ik} + nh_{jk} + nt_k \quad (\text{A.51})$$

Noting that Eq. A.49 contains an integral from the family $I_{TR}(m, n)$ defined in Eq. A.21, the final expression for the i, j th term of $[K_{sk}]_{jl}$ is

$$[K_{sk}(i, j)]_{jl} = \frac{1}{4} \sum_{ik=1}^{Nh} \sum_{jk=1}^{Nh} \sum_{k=1}^{Nt_{jl}} \sum_{r=1}^3 \sum_{s=1}^3 H_{ik} H_{jk} \hat{T}_{jl_k} \cdot \tilde{W}(r, i) \tilde{W}(s, j) Q_{jl}(r, s) I_{TR}(m, n) \quad (\text{A.52})$$

The stiffness matrix for all the skin layers combined $[K_{sk}]_{tot}$ is obtained by summing the contributions of all the layers given by Eq. A.52. Because the wing is assumed to be symmetric with respect to the x - y plane, the total skin contribution can be found by summing the contributions from the layers of the upper skin and then multiplying by 2. This matrix is then appropriately merged into the global mass matrix $[K_{glob}]$.

A.7 Mass Matrix Contributions of a Spar

Neglecting rotary inertia the contribution to the kinetic energy T of an element of length $d\eta$ of the j stth spar is

$$dT_{js} = \frac{1}{2} \rho_{js} A(\eta)_{sp_{js}} \dot{w}^2 d\eta \quad (\text{A.53})$$

where η is the coordinate along the spar axis rotated from the y axis by an angle Λ , ρ_{js} is the constant material density of the spar, and the cap area $A_{sp_{js}}$ is expressed as a function of η (LIV90). Referring to Figure A.3, all η dependence of this equation may be changed to y dependence using

$$\frac{\eta}{L} = \frac{y - sy_L}{sy_R - sy_L} \quad (\text{A.54})$$

from which

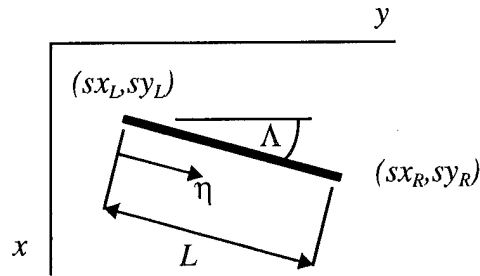


Figure A.3: Spar Geometry

$$d\eta = dy \cdot \frac{L}{sy_R - sy_L} = \frac{dy}{\cos \Lambda} \quad (\text{A.55})$$

The spar cap area may be expressed as a linear function of y by

$$A_{sp_{js}}(y) = A_{sp0_{js}} + A_{sp1_{js}} y \quad (\text{A.56})$$

as shown in Eq. 1.3. The variable x may also be expressed as a function of y in the form

$$x(y) = S1y + S2 \quad (\text{A.57})$$

where

$$S1 = \frac{sx_R - sx_L}{sy_R - sy_L} \quad (\text{A.58})$$

$$S2 = \frac{sx_L sy_R - sx_R sy_L}{sy_R - sy_L} \quad (\text{A.59})$$

Combining Eq. A.57 with Eq. A.7 allows the displacement $w(x,y,t)$ to be written as

$$w(x, y, t) = \sum_{i=1}^{Nq_i} q_w(t)_i \cdot (S1y + S2)^{mq_i} y^{nq_i} \quad (\text{A.60})$$

from which Eq. A.9 becomes

$$\{a_w(x, y, t)\}^T = \{\dots, (S1y + S2)^{mq_i} y^{nq_i}, \dots\} \quad (\text{A.61})$$

Using Eqs. A.8, A.55, and A.61, the expression from Eq. A.53 now becomes

$$dT_{js} = \frac{1}{2} \rho_{js} \left(\frac{L}{sy_R - sy_L} \right) A(y)_{sp_{js}} \{\dot{q}_w\}^T \{a_w\} \{a_w\}^T \{\dot{q}_w\} dy \quad (\text{A.62})$$

in terms of y . Integrating over the length of the spar gives

$$T_{js} = \frac{1}{2} \rho_{js} \left(\frac{L}{sy_R - sy_L} \right) \int_{y=sy_L}^{y=sy_R} A(y)_{sp_{js}} \{\dot{q}_w\}^T \{a_w\} \{a_w\}^T \{\dot{q}_w\} dy \quad (\text{A.63})$$

Equivalently,

$$T_{js} = \frac{1}{2} \omega^2 \rho_{js} \left(\frac{L}{sy_R - sy_L} \right) \int_{y=sy_L}^{y=sy_R} A(y)_{sp_{js}} \{q_w\}^T \{a_w\} \{a_w\}^T \{q_w\} dy \quad (\text{A.64})$$

where ω is the natural vibrational frequency of the spar. Application here of the variational extremum condition from Eq. 1.10 yields the mass matrix for the j th spar given as

$$[M_{sp}]_{js} = \rho_{js} \left(\frac{L}{sy_R - sy_L} \right) \int_{y=sy_L}^{y=sy_R} A(y)_{sp_{js}} \{a_w\} \{a_w\}^T dy \quad (\text{A.65})$$

Substituting Eq. A.56 gives

$$[M_{sp}]_{js} = \rho_{js} \left(\frac{L}{sy_R - sy_L} \right) \int_{y=sy_L}^{y=sy_R} (A_{sp0_{js}} + A_{sp1_{js}} y) \{a_w\} \{a_w\}^T dy \quad (\text{A.66})$$

The mass matrix term in the i th row and j th column for the j th spar may be expressed as

$$[M_{sp}(i, j)]_{js} = \rho_{js} \left[A_{sp0_{js}} \left(\frac{L}{sy_R - sy_L} \right) \int_{y=sy_L}^{y=sy_R} (S1y + S2)^m y^n dy \right. \\ \left. + A_{sp1_{js}} \left(\frac{L}{sy_R - sy_L} \right) \int_{y=sy_L}^{y=sy_R} (S1y + S2)^m y^{n+1} dy \right] \quad (\text{A.67})$$

where

$$m = mq_i + mq_j \quad (\text{A.68})$$

$$n = nq_i + nq_j \quad (\text{A.69})$$

Let us define a family of integrals where

$$I_{SP}(m, n) = \frac{L}{sy_R - sy_L} \int_{y=sy_L}^{y=sy_R} (S1y + S2)^m y^n dy \quad (A.70)$$

Then the final expression for the i, j th term of $[M_{sp}]_{js}$ is

$$[M_{sp}(i, j)]_{js} = \rho_{js} [A_{sp0_{js}} I_{SP}(m, n) + A_{sp1_{js}} I_{SP}(m, n + 1)] \quad (A.71)$$

(LIV90). Appendix C discusses how the family of integrals $I_{SP}(m, n)$ is analytically derived. The mass matrix for all the spars combined $[M_{sp}]_{tot}$ is obtained by summing the contributions of all the spars given by Eq. A.71. Because the wing is assumed to be symmetric with respect to the x - y plane, the total spar contribution can be found by summing the contributions from the spars on the upper wing surface and then multiplying by 2. This matrix is then appropriately merged into the global mass matrix $[M_{glob}]$.

A.8 Stiffness Matrix Contributions of a Spar

The contribution to the potential or strain energy U of an element of length $d\eta$ of the j stth spar is

$$dU_{js} = \frac{1}{2} E_{js} A(\eta)_{sp_{js}} \frac{h(\eta)^2}{4} w_{,\eta\eta}^2 d\eta \quad (A.72)$$

where E_{js} is the longitudinal modulus of elasticity, the cap area $A_{sp_{js}}$ is a linear function of η , and $h(\eta)$ is the wing depth distribution along the spar line (LIV90). It is necessary to replace η dependence with y dependence in this expression. Referring to Figure A.3 and Eq. A.55 the transformation for the bending strain is given by

$$w_{,\eta\eta} = \cos^2 \Lambda \cdot w_{,yy} = \left(\frac{sy_R - sy_L}{L} \right)^2 w_{,yy} \quad (A.73)$$

The depth distribution may be written as a function of y by substituting the spar line equation from Eq. A.57 into Eq. A.45 giving

$$h(y) = \sum_{ik=1}^{Nh} H_{ik} \cdot (S1y + S2)^{mh_{ik}} y^{nh_{ik}} \quad (A.74)$$

The cap area is also easily expressed as a linear function of y as shown in Eq. A.56. Substituting Eqs. A.55 and A.73 into Eq. A.72 gives

$$dU_{js} = \frac{1}{2} E_{js} \left(\frac{sy_R - sy_L}{L} \right)^3 A(y)_{sp_{js}} \frac{h(y)^2}{4} w_{,yy}^2 dy \quad (A.75)$$

Using Eqs. A.8 and A.61 to define $w(x,y,t)$, Eq. A.75 becomes

$$dU_{js} = \frac{1}{2} E_{js} \left(\frac{sy_R - sy_L}{L} \right)^3 A(y)_{sp_{js}} \frac{h(y)^2}{4} \{q_w\}^T \{a_{w,yy}\} \{a_{w,yy}\}^T \{q_w\} dy \quad (A.76)$$

Integrating this over the length of the spar gives

$$U_{js} = \frac{1}{2} E_{js} \left(\frac{sy_R - sy_L}{L} \right)^3 \int_{y=sy_L}^{y=sy_R} A(y)_{sp_{js}} \frac{h(y)^2}{4} \{q_w\}^T \{a_{w,yy}\} \{a_{w,yy}\}^T \{q_w\} dy \quad (A.77)$$

Application here of the variational extremum condition from Eq. 1.10 yields the stiffness matrix for the j th spar given as

$$[K_{sp}]_{js} = E_{js} \left(\frac{sy_R - sy_L}{L} \right)^3 \int_{y=sy_L}^{y=sy_R} A(y)_{sp_{js}} \frac{h(y)^2}{4} \{a_{w,yy}\} \{a_{w,yy}\}^T dy \quad (A.78)$$

Substituting Eq. A.56 for $A_{sp_{js}}$ and Eq. A.74 for $h(y)$ here gives

$$[K_{sp}]_{js} = \frac{E_{js}}{4} \sum_{ik=1}^{Nh} \sum_{jk=1}^{Nh} H_{ik} H_{jk} \left(\frac{sy_R - sy_L}{L} \right)^3 \int_{y=sy_L}^{y=sy_R} (A_{sp0_{js}} + A_{sp1_{js}} y) \cdot (S1y + S2)^{mh_{ik} + mh_{jk}} y^{nh_{ik} + nh_{jk}} \{a_{w,yy}\} \{a_{w,yy}\}^T dy \quad (A.79)$$

Now differentiating Eq. A.61 twice with respect to y gives

$$\begin{aligned}
\{a_{w,yy}\}^T = \{ & \dots, mq_i(mq_i-1)S1^2(S1y+S2)^{mq_i-2}y^{nq_i} \\
& + 2mq_inq_iS1(S1y+S2)^{mq_i-1}y^{nq_i-1} \\
& + nq_i(nq_i-1)(S1y+S2)^{mq_i}y^{nq_i-2}, \dots \}
\end{aligned}
\tag{A.80}$$

It follows that the i,j th term of $\{a_{w,yy}\}\{a_{w,yy}\}^T$ can be given by

$$term(i,j) = \sum_{r=1}^5 AY(i,j)_r (S1y+S2)^{mY(i,j)_r} y^{nY(i,j)_r}
\tag{A.81}$$

where $AY(i,j)_r$, $mY(i,j)_r$ and $nY(i,j)_r$ are given in Table A.1 (LIV90). Upon substitution of Eq. A.81 into Eq. A.79, the stiffness matrix term in the i th row and j th column for the j st spar may be expressed as

$$\begin{aligned}
[K_{sp}(i,j)]_{js} = & \frac{E_{js}}{4} \left(\frac{sy_R - sy_L}{L} \right)^4 \sum_{ik=1}^{Nh} \sum_{jk=1}^{Nh} H_{ik} H_{jk} \sum_{r=1}^5 AY(i,j)_r \\
& \cdot \left[A_{sp0js} \left(\frac{L}{sy_R - sy_L} \right) \int_{y=sy_L}^{y=sy_R} (S1y+S2)^m y^n dy \right. \\
& \left. + A_{sp1js} \left(\frac{L}{sy_R - sy_L} \right) \int_{y=sy_L}^{y=sy_R} (S1y+S2)^m y^{n+1} dy \right]
\end{aligned}
\tag{A.82}$$

Table A.1: Coefficients and Powers for Curvature Along a Spar Line

r	$AY(i,j)_r$	$mY(i,j)_r$	$nY(i,j)_r$
1	$(mq_i)(mq_j)(mq_i-1)(mq_j-1)S1^4$	$mq_i-4 + mq_j$	$nq_i + nq_j$
2	$2(mq_i)(mq_j)(mq_i-1)(nq_j)S1^3$ $+ 2(mq_i)(mq_j)(mq_j-1)(nq_i)S1^3$	$mq_i + mq_j-3$	nq_i+nq_j-1
3	$(mq_i)(nq_j)(mq_i-1)(nq_j-1)S1^2$ $+ 4(mq_i)(mq_j)(nq_i)(nq_j)S1^2$ $+ (nq_i)(mq_j)(nq_i-1)(mq_j-1)S1^2$	$mq_i-2 + mq_j$	$nq_i + nq_j-2$
4	$2(mq_i)(nq_j)(nq_j-1)(nq_j)S1$ $+ 2(nq_i)(mq_j)(nq_i-1)(nq_j)S1$	mq_i+mq_j-1	$nq_i + nq_j-3$
5	$(nq_i)(nq_j)(nq_i-1)(nq_j-1)$	$mq_i + mq_j$	$nq_i + nq_j-4$

where

$$m = mY(i, j)_r + mh_{ik} + mh_{jk} \quad (\text{A.83})$$

$$n = nY(i, j)_r + nh_{ik} + nh_{jk} \quad (\text{A.84})$$

Noting that Eq. A.82 is composed of linear combinations of the integral family $I_{SP}(m, n)$ defined in Eq. A.70, the final expression for the i, j th term of $[K_{sp}]_{js}$ is

$$[K_{sp}(i, j)]_{js} = \frac{E_{js}}{4} \left(\frac{sy_R - sy_L}{L} \right)^4 \sum_{ik=1}^{Nh} \sum_{jk=1}^{Nh} H_{ik} H_{jk} \sum_{r=1}^5 AY(i, j)_r \cdot [A_{sp0_{js}} I_{SP}(m, n) + A_{sp1_{js}} I_{SP}(m, n+1)] \quad (\text{A.85})$$

(LIV90). The stiffness matrix for all the spars combined $[K_{sp}]_{tot}$ is obtained by summing the contributions of all the spars given by Eq. A.85. Because the wing is assumed to be symmetric with respect to the x - y plane, the total spar contribution can be found by summing the contributions from the spars on the upper wing surface and then multiplying by 2. This matrix is then appropriately merged into the global stiffness matrix $[K_{glob}]$.

A.9 Mass Matrix Contributions of a Rib

Neglecting rotary inertia the contribution to the kinetic energy T of an element of length dx of the j th rib is

$$dT_{jr} = \frac{1}{2} \rho_{jr} A(x)_{rb_{jr}} \dot{w}^2 dx \quad (\text{A.86})$$

where ρ_{jr} is the constant material density of the rib, and the cap area $A_{rb_{jr}}$ is a linear function of x (LIV90). The rib cap area defined in Eq. 1.4 is given by

$$A_{rb_{jr}}(x) = A_{rb0_{jr}} + A_{rb1_{jr}} x \quad (\text{A.87})$$

Using Eq. A.8 for $w(x, y, t)$, Eq. A.86 becomes

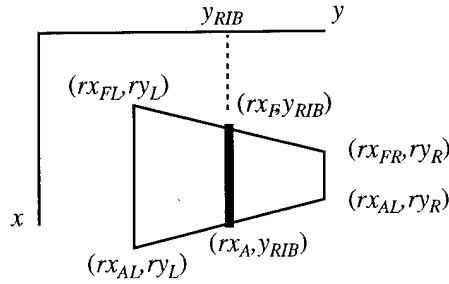


Figure A.4: Rib Geometry

$$dT_{jr} = \frac{1}{2} \rho_{jr} A(x) {}_{rb_{jr}} \{ \dot{q}_w \}^T \{ a_w \} \{ a_w \}^T \{ \dot{q}_w \} dx \quad (\text{A.88})$$

Integrating Eq. A.88 over the length of the rib gives

$$T_{jr} = \frac{1}{2} \rho_{jr} \int_{x=rx_F}^{x=rx_A} A(x) {}_{rb_{jr}} \{ \dot{q}_w \}^T \{ a_w \} \{ a_w \}^T \{ \dot{q}_w \} dx \quad (\text{A.89})$$

where the limits of integration rx_F and rx_A , as shown in Figure A.4, are given by

$$rx_F = F1 y_{RIB} + F2 \quad (\text{A.90})$$

$$rx_A = A1 y_{RIB} + A2 \quad (\text{A.91})$$

where

$$F1 = \frac{rx_{FR} - rx_{FL}}{ry_R - ry_L} \quad (\text{A.92})$$

$$F2 = \frac{rx_{FL} ry_R - rx_{FR} ry_L}{ry_R - ry_L} \quad (\text{A.93})$$

$$A1 = \frac{rx_{AR} - rx_{AL}}{ry_R - ry_L} \quad (\text{A.94})$$

$$A2 = \frac{rx_{AL}ry_R - rx_{AR}ry_L}{ry_R - ry_L} \quad (A.95)$$

Equivalent to Eq. A.89 is the expression

$$T_{jr} = \frac{1}{2} \omega^2 \rho_{jr} \int_{x=rx_F}^{x=rx_A} A(x) {}_{rb_{jr}} \{q_w\}^T \{a_w\} \{a_w\}^T \{q_w\} dx \quad (A.96)$$

where ω is the natural vibrational frequency of the rib. Application here of the variational extremum condition from Eq. 1.10 yields the mass matrix for the j th rib given as

$$[M_{rb}]_{jr} = \rho_{jr} \int_{x=rx_F}^{x=rx_A} A(x) {}_{rb_{jr}} \{a_w\} \{a_w\}^T dx \quad (A.97)$$

Substituting Eq. A.87 for $A_{rb_{jr}}$ gives

$$[M_{rb}]_{jr} = \rho_{jr} \int_{x=rx_F}^{x=rx_A} (A_{rb0_{jr}} + A_{rb1_{jr}} x) \{a_w\} \{a_w\}^T dx \quad (A.98)$$

Since y is fixed at a constant value y_{RIB} along the rib, the mass matrix term in the i th row and j th column for the j th rib may be expressed as

$$[M_{rb}(i, j)]_{jr} = \rho_{jr} \left[A_{rb0_{jr}} y_{RIB}^n \int_{x=rx_F}^{x=rx_A} x^m dx + A_{rb1_{jr}} y_{RIB}^n \int_{x=rx_F}^{x=rx_A} x^{m+1} dx \right] \quad (A.99)$$

where

$$m = mq_i + mq_j \quad (A.100)$$

$$n = nq_i + nq_j \quad (A.101)$$

Let us define a family of integrals where

$$I_{RB}(m, n) = y_{RIB}^n \int_{x=rx_F}^{x=rx_A} x^m dx \quad (A.102)$$

Then the final expression for the i, j th term of $[M_{rb}]_{jr}$ is

$$[M_{rb}(i, j)]_{jr} = \rho_{jr} [A_{rb0_{jr}} I_{RB}(m, n) + A_{rb1_{jr}} I_{RB}(m+1, n)] \quad (A.103)$$

(LIV90). Appendix C discusses how the family of integrals $I_{RB}(m, n)$ is analytically

derived. The mass matrix for all the ribs combined $[M_{rb}]_{tot}$ is obtained by summing the contributions of all the ribs given by Eq. A.103. Because the wing is assumed to be symmetric with respect to the x - y plane, the total rib contribution can be found by summing the contributions from the ribs on the upper wing surface and then multiplying by 2. This matrix is then appropriately merged into the global mass matrix $[M_{glob}]$.

A.10 Stiffness Matrix Contributions of a Rib

The contribution to the potential or strain energy U of an element of length dx of the j th rib is

$$dU_{jr} = \frac{1}{2} E_{jr} A(x)_{rb_{jr}} \frac{h(x)^2}{4} w_{,xx}^2 dx \quad (A.104)$$

where E_{jr} is the longitudinal modulus of elasticity, the cap area $A_{rb_{jr}}$ is a linear function of x , and $h(x)$ is the wing depth distribution along the rib line (LIV90). The depth distribution may be expressed as

$$h(x) = \sum_{ik=1}^{Nh} H_{ik} \cdot x^{mh_{ik}} y_{RIB}^{nh_{ik}} \quad (A.105)$$

since y is equal to a constant y_{RIB} along the length of the rib. Using Eq. A.8 for $w(x,y,t)$, Eq. A.104 becomes

$$dU_{jr} = \frac{1}{2} E_{jr} A(x)_{rb_{jr}} \frac{h(x)^2}{4} \{q_w\}^T \{a_{w,xx}\} \{a_{w,xx}\}^T \{q_w\} dx \quad (A.106)$$

Integrating this over the length of the rib gives

$$U_{jr} = \frac{1}{2} E_{jr} \int_{x=r_{x_F}}^{x=r_{x_A}} A(x)_{rb_{jr}} \frac{h(x)^2}{4} \{q_w\}^T \{a_{w,xx}\} \{a_{w,xx}\}^T \{q_w\} dx \quad (A.107)$$

where the limits of integration have been defined in Eqs. A.90 and A.91. Application here of the variational extremum condition from Eq. 1.10 yields the stiffness matrix for the j th rib given as

$$[K_{rb}]_{jr} = E_{jr} \int_{x=r_{x_F}}^{x=r_{x_A}} A(x)_{rb_{jr}} \frac{h(x)^2}{4} \{a_{w,xx}\} \{a_{w,xx}\}^T dx \quad (A.108)$$

Substituting Eq. A.87 for A_{rbjr} and Eq. A.105 for $h(x)$ here gives

$$[K_{rb}]_{jr} = \frac{E_{jr}}{4} \sum_{ik=1}^{Nh} \sum_{jk=1}^{Nh} H_{ik} H_{jk} \int_{x=r x_F}^{x=r x_A} x^{mh_{ik} + mh_{jk}} y_{RIB}^{nh_{ik} + nh_{jk}} \cdot (A_{rb0jr} + A_{rb1jr} x) \{a_{w,xx}\} \{a_{w,xx}\}^T dx \quad (A.109)$$

Now differentiating Eq. A.9 twice with respect to x and setting y equal to a constant y_{RIB} gives

$$\{a_{w,xx}\}^T = \{ \dots, mq_i(mq_i - 1) x^{mq_i - 2} y_{RIB}^{nq_i}, \dots \} \quad (A.110)$$

Upon substitution of Eq. A.110 into Eq. A.109 the stiffness matrix term in the i th row and j th column for the j th rib may be expressed as

$$[K_{rb}(i, j)]_{jr} = \frac{E_{jr}}{4} \sum_{ik=1}^{Nh} \sum_{jk=1}^{Nh} H_{ik} H_{jk} AX(i, j) \cdot \left[A_{rb0jr} y_{RIB}^n \int_{x=r x_F}^{x=r x_A} x^m dx + A_{rb1jr} y_{RIB}^n \int_{x=r x_F}^{x=r x_A} x^{m+1} dx \right] \quad (A.111)$$

where

$$AX(i, j) = mq_i(mq_i - 1) mq_j(mq_j - 1) \quad (A.112)$$

$$m = mq_i + mq_j - 4 + mh_{ik} + mh_{jk} \quad (A.113)$$

$$n = nq_i + nq_j + nh_{ik} + nh_{jk} \quad (A.114)$$

Noting that Eq. A.111 is composed of linear combinations of the integral family $I_{RB}(m, n)$ defined in Eq. A.102, the final expression for the i, j th term of $[K_{rb}]_{jr}$ is

$$[K_{rb}(i, j)]_{jr} = \frac{E_{jr}}{4} \sum_{ik=1}^{Nh} \sum_{jk=1}^{Nh} H_{ik} H_{jk} AX(i, j) \cdot [A_{rb0jr} I_{RB}(m, n) + A_{rb1jr} I_{RB}(m + 1, n)] \quad (A.115)$$

(LIV90). The stiffness matrix for all the ribs combined $[K_{rb}]_{tot}$ is obtained by summing the contributions of all the ribs given by Eq. A.111. Because the wing is assumed to be symmetric with respect to the x - y plane, the total rib contribution can be found by summing the contribution from the ribs on the upper surface and then multiplying by 2. This matrix is then appropriately merged into the global stiffness matrix $[K_{glob}]$.

Appendix B: Analytical Foundations of an Equivalent Plate Model Using FSDPT

B.1 Overview

In this appendix are derived the equations necessary to construct mass and stiffness matrices for wing structural components based on First Order Shear Deformation Plate Theory. This appendix starts with a discussion of the assumptions of the theory and the ensuing strain-displacement relationships. Displacement functions are then defined. Following this foundation are the derivations of the mass and stiffness matrix equations for a single skin layer. These are followed by the derivations of the mass and stiffness matrix equations for a single spar and a single rib. Last are the derivations of the mass and stiffness matrix equations for a single spar web and a single rib web.

B.2 Assumptions

First Order Shear Deformation Plate Theory (FSDPT) differs from Classical Plate Theory in that the Kirchhoff-Love assumption is not employed. Rather, it is assumed that plane sections normal to the plate's midsurface remain plane but not necessarily normal to that surface after deformation. This is analogous to Timoshenko beam theory (RE84). Hence, the shear strains γ_{xz} and γ_{yz} may not be ignored. It is assumed that the out of plane displacements are small, and there may be in-plane displacement of points at the plate's mid-surface. It is assumed that the transverse normal strain ϵ_{zz} is negligible since the transverse deflection does not vary through the thickness of the plate. This requires that the transverse normal displacement w be a function of x and y only.

There is no requirement that the wing structure must be symmetric. Spar webs and rib webs are included in the model along with the skins, spars caps, and rib caps. It is not assumed in the general case that skin thickness is small compared to the wing depth. When this is assumed then it may also be assumed that all the skin layers in each of the upper and lower skins have the same depth distribution (LIV194).

B.3 Strain-Displacement Relationships

The established assumptions allow the displacements in the x , y , and z directions respectively to be approximated by

$$u(x, y, z) = u_0(x, y) + z\psi_x(x, y) \quad (\text{B.1})$$

$$v(x, y, z) = v_0(x, y) + z\psi_y(x, y) \quad (\text{B.2})$$

$$w(x, y, z) = w_0(x, y) \quad (\text{B.3})$$

where u_0 , v_0 , w_0 are the x, y, z displacement components of a point along the reference mid-surface, and ψ_x and ψ_y are rotations of a line element, originally perpendicular to the mid-surface plane, about the y and x axes respectively (RE84, LIV194). The associated strains are given by

$$\epsilon_{xx} = \frac{\partial u}{\partial x} = \frac{\partial u_0}{\partial x} + z \frac{\partial \psi_x}{\partial x} \quad (\text{B.4})$$

$$\epsilon_{yy} = \frac{\partial v}{\partial y} = \frac{\partial v_0}{\partial y} + z \frac{\partial \psi_y}{\partial y} \quad (\text{B.5})$$

$$\gamma_{xy} = \frac{\partial u}{\partial y} + \frac{\partial v}{\partial x} = \frac{\partial u_0}{\partial y} + \frac{\partial v_0}{\partial x} + z \left(\frac{\partial \psi_x}{\partial y} + \frac{\partial \psi_y}{\partial x} \right) \quad (\text{B.6})$$

$$\gamma_{xz} = \psi_x + \frac{\partial w_0}{\partial x} \quad (\text{B.7})$$

$$\gamma_{yz} = \psi_y + \frac{\partial w_0}{\partial y} \quad (\text{B.8})$$

(LIV194, RE84). These displacement and strain relationships form the basis for the mass and stiffness matrix formulations.

B.4 Displacement Functions

To use the Ritz method described in Chapter 1, it is necessary to approximate each of the 5 x, y, t dependent deformation fields by a polynomial series given in vector form by

$$u_0(x, y, t) = \{a_1(x, y)\}^T \{q_1(t)\} \quad (\text{B.9})$$

$$v_0(x, y, t) = \{a_2(x, y)\}^T \{q_2(t)\} \quad (\text{B.10})$$

$$\psi_x(x, y, t) = \{a_3(x, y)\}^T \{q_3(t)\} \quad (\text{B.11})$$

$$\psi_y(x, y, t) = \{a_4(x, y)\}^T \{q_4(t)\} \quad (\text{B.12})$$

$$w_0(x, y, t) = \{a_5(x, y)\}^T \{q_5(t)\} \quad (\text{B.13})$$

where

$$\{a_1(x, y)\}^T = \{\dots, x^{mq_1} y^{nq_1}, \dots\} \quad (\text{B.14})$$

and similar expressions are used for $\{a_2\}^T$, $\{a_3\}^T$, $\{a_4\}^T$, and $\{a_5\}^T$ (LIV194). The column vectors $\{q_1\}$, $\{q_2\}$, $\{q_3\}$, $\{q_4\}$, and $\{q_5\}$ contain the polynomial coefficients which are the generalized displacements solved for in the Ritz formulation. These polynomials have Nq_1 , Nq_2 , Nq_3 , Nq_4 , and Nq_5 terms respectively, and the x and y powers are predetermined.

B.5 Mass Matrix Contributions of a Skin Layer

Let the vectors $\{q_1\}$, $\{q_2\}$, $\{q_3\}$, $\{q_4\}$, and $\{q_5\}$ be combined into one column vector of generalized displacements $\{q\}$ where

$$\{q\}^T = \{q_1^T, q_2^T, q_3^T, q_4^T, q_5^T\} \quad (\text{B.15})$$

Substituting Eqs. B.9-B.13 into Eqs. B.1-B.3 allows the u, v, w components of deformation to be written in terms of $\{q\}$. This is given by

$$\begin{Bmatrix} u \\ \bar{v} \\ \bar{w} \end{Bmatrix} = \{ [S_0(x, y)] + z[S_1(x, y)] \} \{q(t)\} \quad (\text{B.16})$$

where S_0 and S_1 are matrices containing polynomial terms of the form $x^{mS_0(r, i)} y^{nS_0(r, i)}$ and $x^{mS_1(r, i)} y^{nS_1(r, i)}$ respectively. Partitioned into subvectors of dimension $1 \times Nq_s$ ($s=1,2,\dots,5$), the matrices are given as

$$[S_0(x, y)] = \begin{bmatrix} a_1^T & 0 & 0 & 0 & 0 \\ 0 & a_2^T & 0 & 0 & 0 \\ 0 & 0 & 0 & 0 & a_5^T \end{bmatrix} \quad (\text{B.17})$$

$$[S_1(x, y)] = \begin{bmatrix} 0 & 0 & a_3^T & 0 & 0 \\ 0 & 0 & 0 & a_4^T & 0 \\ 0 & 0 & 0 & 0 & 0 \end{bmatrix} \quad (\text{B.18})$$

where both are $3 \times Nq_{tot}$ in dimension with

$$Nq_{tot} = Nq_1 + Nq_2 + Nq_3 + Nq_4 + Nq_5 \quad (\text{B.19})$$

based on the length of the subvectors.

Now the contribution to the kinetic energy T of an infinitesimal skin element dx by dy of the j th skin layer is

$$dT_{jl} = \frac{1}{2} \rho_{jl} t_{jl}(x, y) \left\{ \begin{Bmatrix} \dot{u} \\ \bar{\dot{v}} \\ \bar{\dot{w}} \end{Bmatrix} \right\}^T \left\{ \begin{Bmatrix} \dot{u} \\ \bar{\dot{v}} \\ \bar{\dot{w}} \end{Bmatrix} \right\} dx dy \quad (\text{B.20})$$

where ρ_{jl} is the constant material density of the skin layer, and $t_{jl}(x, y)$ is the thickness of the skin layer given in Eq. 1.2 as

$$t_{jl}(x, y) = \sum_{k=1}^{Nt_{jl}} \hat{T}_{jl_k} \cdot x^{mt_k} y^{mt_k} \quad (\text{B.21})$$

(LIV194). Substituting Eq. B.16 into Eq. B.20 gives

$$dT_{jl} = \frac{1}{2} \rho_{jl} t_{jl}(x, y) \{ \dot{q} \}^T \left[S_0^T S_0 + z \left(S_0^T S_1 \right) + z \left(S_1^T S_0 \right) + z^2 \left(S_1^T S_1 \right) \right] \{ \dot{q} \} dx dy \quad (B.22)$$

Integrating this over the whole trapezoidal panel area yields

$$T_{jl} = \frac{1}{2} \rho_{jl} \iint_{yx} t_{jl}(x, y) \{ \dot{q} \}^T \left[S_0^T S_0 + z \left(S_0^T S_1 \right) + z \left(S_1^T S_0 \right) + z^2 \left(S_1^T S_1 \right) \right] \{ \dot{q} \} dx dy \quad (B.23)$$

Equivalently,

$$T_{jl} = \frac{1}{2} \omega^2 \rho_{jl} \iint_{yx} t_{jl}(x, y) \{ q \}^T \left[S_0^T S_0 + z \left(S_0^T S_1 \right) + z \left(S_1^T S_0 \right) + z^2 \left(S_1^T S_1 \right) \right] \{ q \} dx dy \quad (B.24)$$

where ω is the natural vibrational frequency of the skin layer. The variational extremum condition from Eq. 1.10 applied here becomes

$$\frac{\partial T_{jl}}{\partial q_i} = 0 \quad (B.25)$$

yielding the mass matrix for the j th skin layer given as

$$[M_{sk}]_{jl} = \rho_{jl} \iint_{yx} t_{jl}(x, y) \left[S_0^T S_0 + z \left(S_0^T S_1 \right) + z \left(S_1^T S_0 \right) + z^2 \left(S_1^T S_1 \right) \right] dx dy \quad (B.26)$$

(LIV194). Substitution of Eq. B.21 for $t_{jl}(x, y)$ gives

$$[M_{sk}]_{jl} = \rho_{jl} \sum_{k=1}^{Nt_{jl}} \hat{T}_{jl_k} \iint_{yx} x^{mt_k} y^{nt_k} \left[S_0^T S_0 + z \left(S_0^T S_1 \right) + z \left(S_1^T S_0 \right) + z^2 \left(S_1^T S_1 \right) \right] dx dy \quad (B.27)$$

The variable z is assigned the value of the depth distribution of the j th skin layer given in Eq. 1.1 by

$$h_{jl}(x, y) = \sum_{ik=1}^{Nh_{jl}} H_{jl_{ik}} \cdot x^{mh_{ik}} y^{nh_{ik}} \quad (B.28)$$

Substituting this into Eq. B.27 gives

$$\begin{aligned}
 [M_{sk}]_{jl} = & \rho_{jl} \sum_{k=1}^{Nt_{jl}} \hat{T}_{jl_k} \left[\iint_{yx} x^{mt_k} y^{nt_k} (S_0^T S_0) dx dy \right. \\
 & + \sum_{ik=1}^{Nh_{jl}} H_{jl_{ik}} \iint_{yx} x^{mt_k + mh_{ik}} y^{nt_k + nh_{ik}} \left[(S_0^T S_1) + (S_1^T S_0) \right] dx dy \\
 & \left. + \sum_{ik=1}^{Nh_{jl}} \sum_{jk=1}^{Nh_{jl}} H_{jl_{ik}} H_{jl_{jk}} \iint_{yx} x^{mt_k + mh_{ik} + mh_{jk}} y^{nt_k + nh_{ik} + nh_{jk}} (S_1^T S_1) dx dy \right]
 \end{aligned} \quad (B.29)$$

The mass matrix term in the i th row and j th column for the jl th skin layer may be expressed as

$$\begin{aligned}
 [M_{sk}(i, j)]_{jl} = & \rho_{jl} \sum_{k=1}^{Nt_{jl}} \sum_{r=1}^3 \hat{T}_{jl_k} \left[\iint_{yx} x^{m1} y^{n1} dx dy \right. \\
 & + \sum_{ik=1}^{Nh_{jl}} H_{jl_{ik}} \left(\iint_{yx} x^{m2} y^{n2} dx dy + \iint_{yx} x^{m3} y^{n3} dx dy \right) \\
 & \left. + \sum_{ik=1}^{Nh_{jl}} \sum_{jk=1}^{Nh_{jl}} H_{jl_{ik}} H_{jl_{jk}} \iint_{yx} x^{m4} y^{n4} dx dy \right]
 \end{aligned} \quad (B.30)$$

where

$$m1 = mt_k + mS0(r, i) + mS0(r, j) \quad (B.31)$$

$$n1 = nt_k + nS0(r, i) + nS0(r, j) \quad (B.32)$$

$$m2 = mt_k + mh_{ik} + mS0(r, i) + mS1(r, j) \quad (B.33)$$

$$n2 = nt_k + nh_{ik} + nS0(r, i) + nS1(r, j) \quad (B.34)$$

$$m3 = mt_k + mh_{ik} + mS1(r, i) + mS0(r, j) \quad (B.35)$$

$$n3 = nt_k + nh_{ik} + nS1(r, i) + nS0(r, j) \quad (B.36)$$

$$m4 = mt_k + mh_{ik} + mh_{jk} + mS1(r, i) + mS1(r, j) \quad (B.37)$$

$$n4 = nt_k + nh_{ik} + nh_{jk} + nS1(r, i) + nS1(r, j) \quad (B.38)$$

Noting that Eq. B.30 is composed of linear combinations of the integral family $I_{TR}(m, n)$ defined in Eq. A.21 and discussed in Appendix C, the final expression for the i, j th term of $[M_{sk}]_{jl}$ is

$$\begin{aligned} [M_{sk}(i, j)]_{jl} = & \rho_{jl} \sum_{k=1}^{Nt_{jl}} \sum_{r=1}^3 \hat{T}_{jl_k} [I_{TR}(m1, n2) \\ & + \sum_{ik=1}^{Nh_{jl}} H_{jl_{ik}} (I_{TR}(m2, n2) + I(m3, n3)) \\ & + \sum_{ik=1}^{Nh_{jl}} \sum_{jk=1}^{Nh_{jl}} H_{jl_{ik}} H_{jl_{jk}} I_{TR}(m4, n4)] \end{aligned} \quad (B.39)$$

The mass matrix for all the skin layers combined $[M_{sk}]_{tot}$ is obtained by summing the contributions of all the layers given by Eq. B.39. This matrix is then appropriately merged into the global mass matrix $[M_{glob}]$.

B.6 Stiffness Matrix Contributions of a Skin Layer

Each skin layer is treated as a plane stress panel for which the only strains of concern are ϵ_{xx} , ϵ_{yy} , and γ_{xy} . Substituting Eqs. B.9-B.13 into Eqs. B.4-B.6 allows these strains to be written in terms of the generalized displacements $\{q\}$ defined in Eq. B.15. This is given by

$$\begin{Bmatrix} \epsilon_{xx} \\ \epsilon_{yy} \\ \gamma_{xy} \end{Bmatrix} = \{ [R_0(x, y)] + z [R_1(x, y)] \} \{ q(t) \} \quad (B.40)$$

where R_0 and R_1 are matrices containing polynomial terms of the form $C(r, i) x^{mR0(r, i)} y^{nR0(r, i)}$ and $C(r, i) x^{mR1(r, i)} y^{nR1(r, i)}$ respectively. Partitioned into subvectors of dimension $1 \times Nq_s$ ($s=1, 2, \dots, 5$), these matrices are given by

$$[R_0(x, y)] = \begin{bmatrix} a_{1,x}^T & 0 & 0 & 0 & 0 \\ 0 & a_{2,y}^T & 0 & 0 & 0 \\ a_{1,y}^T & a_{2,x}^T & 0 & 0 & 0 \end{bmatrix} \quad (\text{B.41})$$

$$[R_1(x, y)] = \begin{bmatrix} 0 & 0 & a_{3,x}^T & 0 & 0 \\ 0 & 0 & 0 & a_{4,y}^T & 0 \\ 0 & 0 & a_{3,y}^T & a_{4,x}^T & 0 \end{bmatrix} \quad (\text{B.42})$$

where the notation for the partial derivatives is defined by the examples

$$a_{1,x}^T = \frac{\partial}{\partial x} \{a_1\}^T = \{..., m q 1_i \cdot x^{m q 1_i - 1} y^{n q 1_i}, ...\} \quad (\text{B.43})$$

and

$$a_{1,y}^T = \frac{\partial}{\partial y} \{a_1\}^T = \{..., n q 1_i \cdot x^{m q 1_i} y^{n q 1_i - 1}, ...\} \quad (\text{B.44})$$

Both matrices are $3 \times N_{q_{tot}}$ in dimension with $N_{q_{tot}}$ having been defined in Eq. B.19.

Now the contribution to the potential or strain energy U of a infinitesimal skin element dx by dy of the j th skin layer is

$$dU_{jl} = \frac{1}{2} t_{jl}(x, y) \begin{Bmatrix} \epsilon_{xx} \\ \epsilon_{yy} \\ \gamma_{xy} \end{Bmatrix}^T [Q]_{jl} \begin{Bmatrix} \epsilon_{xx} \\ \epsilon_{yy} \\ \gamma_{xy} \end{Bmatrix} dx dy \quad (\text{B.45})$$

where $[Q]_{jl}$ is the material constitutive matrix of the skin layer, 3×3 in dimension, as defined in Eqs. A.26-A.37, and $t_{jl}(x, y)$ is the thickness of the skin layer given by Eq. B.21 (LIV194). Substituting Eq. B.40 into Eq. B.45 gives

$$dU_{jl} = \frac{1}{2} t_{jl}(x, y) \{q\}^T \left[R_0^T [Q]_{jl} R_0 + z \left(R_0^T [Q]_{jl} R_1 \right) \right. \\ \left. + z \left(R_1^T [Q]_{jl} R_0 \right) + z^2 \left(R_1^T [Q]_{jl} R_1 \right) \right] \{q\} dx dy \quad (\text{B.46})$$

Integrating this over the whole trapezoidal panel area yields

$$U_{jl} = \frac{1}{2} \iint_{yx} t_{jl}(x, y) \{q\}^T \left[R_0^T [Q]_{jl} R_0 + z \left(R_0^T [Q]_{jl} R_1 \right) + z \left(R_1^T [Q]_{jl} R_0 \right) + z^2 \left(R_1^T [Q]_{jl} R_1 \right) \right] \{q\} dx dy \quad (B.47)$$

The variational extremum condition of Eq. 1.10 applied here becomes

$$\frac{\partial U_{jl}}{\partial q_i} = 0 \quad (B.48)$$

yielding the stiffness matrix for the j th skin layer given as

$$[K_{sk}]_{jl} = \iint_{yx} t_{jl}(x, y) \left[R_0^T [Q]_{jl} R_0 + z \left(R_0^T [Q]_{jl} R_1 \right) + z \left(R_1^T [Q]_{jl} R_0 \right) + z^2 \left(R_1^T [Q]_{jl} R_1 \right) \right] dx dy \quad (B.49)$$

Substitution of Eq. B.21 for $t_{jl}(x, y)$ and Eq. B.28 for the variable z gives

$$\begin{aligned} [K_{sk}]_{jl} = & \sum_{k=1}^{Nt_{jl}} \hat{T}_{jl_k} \left[\iint_{yx} x^{mt_k} y^{nt_k} \left(R_0^T [Q]_{jl} R_0 \right) dx dy \right. \\ & + \sum_{ik=1}^{Nh_{jl}} H_{jl_{ik}} \iint_{yx} x^{mt_k + mh_{ik}} y^{nt_k + nh_{ik}} \left[\left(R_0^T [Q]_{jl} R_1 \right) + \left(R_1^T [Q]_{jl} R_0 \right) \right] dx dy \\ & \left. + \sum_{ik=1}^{Nh_{jl}} \sum_{jk=1}^{Nh_{jl}} H_{jl_{ik}} H_{jl_{jk}} \iint_{yx} x^{mt_k + mh_{ik} + mh_{jk}} y^{nt_k + nh_{ik} + nh_{jk}} \left(R_1^T [Q]_{jl} R_1 \right) dx dy \right] \end{aligned} \quad (B.50)$$

Let the r , i th term of the matrices R_0 and R_1 be

$$R_0(r, i) = \tilde{R}_0(r, i) x^{mR_0(r, i)} y^{nR_0(r, i)} \quad (B.51)$$

$$R_1(r, i) = \tilde{R}_1(r, i) x^{mR1(r, i)} y^{nR1(r, i)} \quad (\text{B.52})$$

respectively. Upon substitution of Eqs. B.51 and B.52 into Eq. B.50, the stiffness matrix term in the i th row and the j th column for the j th skin layer may be expressed as

$$\begin{aligned} [K_{sk}(i, j)]_{jl} = & \sum_{k=1}^{Nt_{jl}} \sum_{r=1}^3 \sum_{s=1}^3 \hat{T}_{jl_k} \left[\tilde{R}_0(r, i) \tilde{R}_0(s, j) \iint_{yx} x^{m1} y^{n1} dx dy \right. \\ & + \sum_{ik=1}^{Nh_{jl}} H_{jl_{ik}} \tilde{R}_0(r, i) \tilde{R}_1(s, j) \iint_{yx} x^{m2} y^{n2} dx dy \\ & + \sum_{ik=1}^{Nh_{jl}} H_{jl_{ik}} \tilde{R}_1(r, i) \tilde{R}_0(s, j) \iint_{yx} x^{m3} y^{n3} dx dy \\ & \left. + \sum_{ik=1}^{Nh_{jl}} \sum_{jk=1}^{Nh_{jl}} H_{jl_{ik}} H_{jl_{jk}} \tilde{R}_1(r, i) \tilde{R}_1(s, j) \iint_{yx} x^{m4} y^{n4} dx dy \right] \end{aligned} \quad (\text{B.53})$$

where

$$m1 = mt_k + mR0(r, i) + mR0(s, j) \quad (\text{B.54})$$

$$n1 = nt_k + nR0(r, i) + nR0(s, j) \quad (\text{B.55})$$

$$m2 = mt_k + mh_{ik} + mR0(r, i) + mR1(s, j) \quad (\text{B.56})$$

$$n2 = nt_k + nh_{ik} + nR0(r, i) + nR1(s, j) \quad (\text{B.57})$$

$$m3 = mt_k + mh_{ik} + mR1(r, i) + mR0(s, j) \quad (\text{B.58})$$

$$n3 = nt_k + nh_{ik} + nR1(r, i) + nR0(s, j) \quad (\text{B.59})$$

$$m4 = mt_k + mh_{ik} + mh_{jk} + mR1(r, i) + mR1(s, j) \quad (\text{B.60})$$

$$n4 = nt_k + nh_{ik} + nh_{jk} + nR1(r, i) + nR1(s, j) \quad (\text{B.61})$$

Noting that Eq. B.53 is composed of linear combinations of the integral family $I_{TR}(m,n)$ defined in Eq. A.21, the final expression for the i,j th term of $[K_{sk}]_{jl}$ is

$$\begin{aligned}
 [K_{sk}(i,j)]_{jl} = & \sum_{k=1}^{Nt_{jl}} \sum_{r=1}^3 \sum_{s=1}^3 \hat{T}_{jl_k} [\tilde{R}_0(r,i) \tilde{R}_0(s,j) I_{TR}(m1,n1) \\
 & + \sum_{ik=1}^{Nh_{jl}} H_{jl_{ik}} \tilde{R}_0(r,i) \tilde{R}_1(s,j) I_{TR}(m2,n2) \\
 & + \sum_{ik=1}^{Nh_{jl}} H_{jl_{ik}} \tilde{R}_1(r,i) \tilde{R}_0(s,j) I_{TR}(m3,n3) \\
 & + \sum_{ik=1}^{Nh_{jl}} \sum_{jk=1}^{Nh_{jl}} H_{jl_{ik}} H_{jl_{jk}} \tilde{R}_1(r,i) \tilde{R}_1(s,j) I_{TR}(m4,n4)] \quad (B.62)
 \end{aligned}$$

The stiffness matrix for all the skin layers combined $[K_{sk}]_{tot}$ is obtained by summing the contributions of all the layers given by Eq. B.62. This matrix is then appropriately merged into the global stiffness matrix $[K_{glob}]$.

B.7 Mass Matrix Contributions of a Spar

The contribution to the kinetic energy T of an element of length $d\eta$ of the j st spar is

$$dT_{js} = \frac{1}{2} \rho_{js} A(\eta)_{sp_{js}} \left\{ \begin{array}{c} \dot{u} \\ \bar{\dot{v}} \\ \bar{\dot{w}} \end{array} \right\}^T \left\{ \begin{array}{c} \dot{u} \\ \bar{\dot{v}} \\ \bar{\dot{w}} \end{array} \right\} d\eta \quad (B.63)$$

where η is the coordinate along the spar axis rotated from the y axis by an angle Λ , ρ_{js} is the constant material density of the spar, the cap area $A_{sp_{js}}$ is a linear function of η , and the velocity vector is the time derivative of the displacement vector defined in Eq. B.16. Referring to Figure A.3, all η dependence of Eq. B.63 may be changed to y dependence. Substituting Eq. A.55 for $d\eta$ into Eq. B.63 and allowing the cap area to be expressed as a linear function of y gives

$$dT_{js} = \frac{1}{2} \rho_{js} \left(\frac{L}{sy_R - sy_L} \right) A(y)_{sp_{js}} \left\{ \begin{array}{c} \dot{u} \\ \bar{\dot{v}} \\ \bar{\dot{w}} \end{array} \right\}^T \left\{ \begin{array}{c} \dot{u} \\ \bar{\dot{v}} \\ \bar{\dot{w}} \end{array} \right\} dy \quad (B.64)$$

Substituting Eq. B.16 into this gives

$$dT_{js} = \frac{1}{2} \rho_{js} \left(\frac{L}{sy_R - sy_L} \right) A(y)_{sp_{js}} \{ \dot{q} \}^T \left[S_0^T S_0 + z \left(S_0^T S_1 \right) \right. \\ \left. + z \left(S_1^T S_0 \right) + z^2 \left(S_1^T S_1 \right) \right] \{ \dot{q} \} dy \quad (\text{B.65})$$

Here the spar line equation from Eq. A.57 may be employed to express x within the matrices S_0 and S_1 as a function of y . Therefore the polynomial terms contained in S_0 and S_1 take the form $(S_1 y + S_2)^{mS_0(r,i)} y^{nS_0(r,i)}$ and $(S_1 y + S_2)^{mS_1(r,i)} y^{nS_1(r,i)}$ respectively.

Integrating Eq. B.65 over the length of the spar now gives

$$T_{js} = \frac{1}{2} \rho_{js} \left(\frac{L}{sy_R - sy_L} \right) \int_{y=sy_L}^{y=sy_R} A(y)_{sp_{js}} \{ \dot{q} \}^T \left[S_0^T S_0 + z \left(S_0^T S_1 \right) \right. \\ \left. + z \left(S_1^T S_0 \right) + z^2 \left(S_1^T S_1 \right) \right] \{ \dot{q} \} dy \quad (\text{B.66})$$

Equivalently,

$$T_{js} = \frac{1}{2} \omega^2 \rho_{js} \left(\frac{L}{sy_R - sy_L} \right) \int_{y=sy_L}^{y=sy_R} A(y)_{sp_{js}} \{ q \}^T \left[S_0^T S_0 + z \left(S_0^T S_1 \right) \right. \\ \left. + z \left(S_1^T S_0 \right) + z^2 \left(S_1^T S_1 \right) \right] \{ q \} dy \quad (\text{B.67})$$

where ω is the natural vibrational frequency of the spar. Application here of the variational extremum condition from Eq. 1.10 yields the mass matrix for the j st spar given by

$$[M_{sp}]_{js} = \rho_{js} \left(\frac{L}{sy_R - sy_L} \right) \int_{y=sy_L}^{y=sy_R} A(y)_{sp_{js}} \left[S_0^T S_0 + z \left(S_0^T S_1 \right) \right. \\ \left. + z \left(S_1^T S_0 \right) + z^2 \left(S_1^T S_1 \right) \right] dy \quad (\text{B.68})$$

Substituting Eq. A.56 for the cap area and Eq. A.74, the spar depth distribution in terms of y , for the variable z gives

$$\begin{aligned}
[M_{sp}]_{js} &= \rho_{js} \left(\frac{L}{sy_R - sy_L} \right) \left[\int_{y=sy_L}^{y=sy_R} (A_{sp0_{js}} + A_{sp1_{js}} y) \left(S_0^T S_0 \right) dy \right. \\
&+ \sum_{ik=1}^{Nh_{js}} H_{js_{ik}} \int_{y=sy_L}^{y=sy_R} (S1y + S2)^{mh_{ik}} y^{nh_{ik}} (A_{sp0_{js}} + A_{sp1_{js}} y) \left[\left(S_0^T S_1 \right) + \left(S_1^T S_0 \right) \right] dy \\
&\left. + \sum_{ik=1}^{Nh_{js}} \sum_{jk=1}^{Nh_{js}} H_{js_{ik}} H_{js_{jk}} \int_{y=sy_L}^{y=sy_R} (S1y + S2)^{mh_{ik} + mh_{jk}} y^{nh_{ik} + nh_{jk}} (A_{sp0_{js}} + A_{sp1_{js}} y) \left(S_1^T S_1 \right) dy \right] \quad (B.69)
\end{aligned}$$

The mass matrix term in the i th row and j th column for the j stth spar may be expressed as

$$\begin{aligned}
[M_{sp}(i, j)]_{js} &= \rho_{js} \left(\frac{L}{sy_R - sy_L} \right) \sum_{r=1}^3 \left[\int_{y=sy_L}^{y=sy_R} (A_{sp0_{js}} + A_{sp1_{js}} y) (S1y + S2)^{m1} y^{n1} dy \right. \\
&+ \sum_{ik=1}^{Nh_{js}} H_{js_{ik}} \int_{y=sy_L}^{y=sy_R} (A_{sp0_{js}} + A_{sp1_{js}} y) \left[(S1y + S2)^{m2} y^{n2} + (S1y + S2)^{m3} y^{n3} \right] dy \\
&\left. + \sum_{ik=1}^{Nh_{js}} \sum_{jk=1}^{Nh_{js}} H_{js_{ik}} H_{js_{jk}} \int_{y=sy_L}^{y=sy_R} (A_{sp0_{js}} + A_{sp1_{js}} y) (S1y + S2)^{m4} y^{n4} dy \right] \quad (B.70)
\end{aligned}$$

where

$$m1 = mS0(r, i) + mS0(r, j) \quad (B.71)$$

$$n1 = nS0(r, i) + nS0(r, j) \quad (B.72)$$

$$m2 = mh_{ik} + mS0(r, i) + mS1(r, j) \quad (B.73)$$

$$n2 = nh_{ik} + nS0(r, i) + nS1(r, j) \quad (B.74)$$

$$m3 = mh_{ik} + mS1(r, i) + mS0(r, j) \quad (B.75)$$

$$n3 = nh_{ik} + nS1(r, i) + nS0(r, j) \quad (B.76)$$

$$m4 = mh_{ik} + mh_{jk} + mS1(r, i) + mS1(r, j) \quad (B.77)$$

$$n4 = nh_{ik} + nh_{jk} + nS1(r, i) + nS1(r, j) \quad (\text{B.78})$$

Noting that Eq. B.70 is composed of linear combinations of the integral family $I_{SP}(m, n)$ defined in Eq. A.70 and discussed in Appendix C, the final expression for the i, j th term of $[M_{sp}]_{jl}$ is

$$\begin{aligned} [M_{sk}(i, j)]_{js} = & \rho_{js} \sum_{r=1}^3 [A_{sp0_{js}} I_{SP}(m1, n1) + A_{sp1_{js}} I_{SP}(m1, n1 + 1) \\ & + \sum_{ik=1}^{Nh_{js}} H_{js_{ik}} A_{sp0_{js}} (I_{SP}(m2, n2) + I_{SP}(m3, n3)) \\ & + \sum_{ik=1}^{Nh_{js}} H_{js_{ik}} A_{sp1_{js}} (I_{SP}(m2, n2 + 1) + I_{SP}(m3, n3 + 1)) \\ & + \sum_{ik=1}^{Nh_{js}} \sum_{jk=1}^{Nh_{js}} H_{js_{ik}} H_{js_{jk}} (A_{sp0_{js}} I_{SP}(m4, n4) + A_{sp1_{js}} I_{SP}(m4, n4 + 1))] \end{aligned} \quad (\text{B.79})$$

The mass matrix for all the spars combined $[M_{sp}]_{tot}$ is obtained by summing the contributions of all the spars given by Eq. B.79. This matrix is then appropriately merged into the global mass matrix $[M_{glob}]$.

B.8 Stiffness Matrix Contributions of a Spar

The contribution to the potential or strain energy U of an element of length $d\eta$ of the j st spar is

$$dU_{js} = \frac{1}{2} E_{js} A(\eta)_{sp_{js}} \epsilon_{\eta\eta}^2 d\eta \quad (\text{B.80})$$

where E_{js} is the longitudinal modulus of elasticity, the cap area $A_{sp_{js}}$ is a linear function of the spar line coordinate η , and $\epsilon_{\eta\eta}$ is the normal strain along the spar axis. Referring to Figure A.3 and using standard tensor transformation rules, the normal strain in the η direction may be written in terms of strains in the x and y directions by

$$\epsilon_{\eta\eta} = \{TR\}^T \begin{Bmatrix} \epsilon_{xx} \\ \epsilon_{yy} \\ \gamma_{xy} \end{Bmatrix} \quad (\text{B.81})$$

where

$$\{TR\}^T = \{\sin^2\Lambda, \cos^2\Lambda, \sin\Lambda\cos\Lambda\} = \{s^2\Lambda, c^2\Lambda, s\Lambda c\Lambda\} \quad (\text{B.82})$$

The spar cap area may easily be expressed as a linear function of y as shown in Eq. A.56. Substituting Eq. A.55 for $d\eta$ and Eq. B.81 for $\epsilon_{\eta\eta}$ into Eq. B.80 gives

$$dU_{js} = \frac{1}{2}E_{js}\left(\frac{L}{sy_R - sy_L}\right)A(y)_{sp_{js}} \begin{Bmatrix} \epsilon_{xx} \\ \epsilon_{yy} \\ \gamma_{xy} \end{Bmatrix}^T \{TR\} \{TR\}^T \begin{Bmatrix} \epsilon_{xx} \\ \epsilon_{yy} \\ \gamma_{xy} \end{Bmatrix} dy \quad (\text{B.83})$$

Define

$$[Q_{sp}] = \{TR\} \{TR\}^T = \begin{bmatrix} (s^4\Lambda) & (s^2\Lambda c^2\Lambda) & (s^3\Lambda c\Lambda) \\ (s^2\Lambda c^2\Lambda) & (c^4\Lambda) & (s\Lambda c^3\Lambda) \\ (s^3\Lambda c\Lambda) & (s\Lambda c^3\Lambda) & (s^2\Lambda c^2\Lambda) \end{bmatrix} \quad (\text{B.84})$$

Substituting Eqs. B.40 and B.84 into Eq. B.83 gives

$$dU_{js} = \frac{1}{2}E_{js}\left(\frac{L}{sy_R - sy_L}\right)A(y)_{sp_{js}} \{q\}^T \left[R_0^T [Q_{sp}] R_0 + z \left(R_0^T [Q_{sp}] R_1 \right) \right. \\ \left. + z \left(R_1^T [Q_{sp}] R_0 \right) + z^2 \left(R_1^T [Q_{sp}] R_1 \right) \right] \{q\} dy \quad (\text{B.85})$$

Here the spar line equation from Eq. A.57 may be employed to express x within the matrices R_0 and R_1 as a function of y . Then the polynomial terms contained in R_0 and R_1 take the form $C(r, i) (S1y + S2)^{mR0(r, i)} y^{nR0(r, i)}$ and $C(r, i) (S1y + S2)^{mR1(r, i)} y^{nR1(r, i)}$ respectively. Integrating Eq. B.85 over the length of the spar yields

$$U_{js} = \frac{1}{2} E_{js} \left(\frac{L}{sy_R - sy_L} \right) \int_{y=sy_L}^{y=sy_R} A(y)_{sp_{js}} \{q\}^T \left[R_0^T [Q_{sp}] R_0 + z \left(R_0^T [Q_{sp}] R_1 \right) \right. \\ \left. + z \left(R_1^T [Q_{sp}] R_0 \right) + z^2 \left(R_1^T [Q_{sp}] R_1 \right) \right] \{q\} dy \quad (B.86)$$

Application here of the variational extremum condition from Eq. 1.10 yields the stiffness matrix for the j stth spar given as

$$[K_{sp}]_{js} = E_{js} \left(\frac{L}{sy_R - sy_L} \right) \int_{y=sy_L}^{y=sy_R} A(y)_{sp_{js}} \left[R_0^T [Q_{sp}] R_0 + z \left(R_0^T [Q_{sp}] R_1 \right) \right. \\ \left. + z \left(R_1^T [Q_{sp}] R_0 \right) + z^2 \left(R_1^T [Q_{sp}] R_1 \right) \right] dy \quad (B.87)$$

Substitution of Eq. A.56 for the cap area and Eq. A.74 for the variable z gives

$$[K_{sp}]_{jl} = E_{js} \left(\frac{L}{sy_R - sy_L} \right) \left[\int_{y=sy_L}^{y=sy_R} (A_{sp0_{js}} + A_{sp1_{js}} y) R_0^T [Q_{sp}] R_0 dy \right. \\ + \sum_{ik=1}^{Nh_{js}} H_{js_{ik}} \int_{y=sy_L}^{y=sy_R} (S1y + S2)^{mh_{ik}} y^{nh_{ik}} (A_{sp0_{js}} + A_{sp1_{js}} y) R_0^T [Q_{sp}] R_1 dy \\ + \sum_{ik=1}^{Nh_{js}} H_{js_{ik}} \int_{y=sy_L}^{y=sy_R} (S1y + S2)^{mh_{ik}} y^{nh_{ik}} (A_{sp0_{js}} + A_{sp1_{js}} y) R_1^T [Q_{sp}] R_0 dy \\ \left. + \sum_{ik=1}^{Nh_{js}} \sum_{jk=1}^{Nh_{js}} H_{js_{ik}} H_{js_{jk}} \int_{y=sy_L}^{y=sy_R} (S1y + S2)^{mh_{ik} + mh_{jk}} y^{nh_{ik} + nh_{jk}} (A_{sp0_{js}} + A_{sp1_{js}} y) R_1^T [Q_{sp}] R_1 dy \right] \quad (B.88)$$

Eqs. B.51 and B.52 are used to define the r, i th term of the matrices R_0 and R_1 respectively with x replaced by Eq. A.57. Upon substitution of Eqs. B.51 and B.52 into Eq. B.88, the stiffness matrix term in the i th row and the j th column for the j stth spar may be expressed as

$$[K_{sp}(i, j)]_{js} = E_{js} \left(\frac{L}{sy_R - sy_L} \right) \sum_{r=1}^3 \sum_{s=1}^3 Q_{sp}(r, s) \\ \left[\tilde{R}_0(r, i) \tilde{R}_0(s, j) \int_{y=sy_L}^{y=sy_R} (A_{sp0_{js}} + A_{sp1_{js}} y) (S1y + S2)^{m1} y^{n1} dy \right]$$

(B.89)

$$\begin{aligned}
& + \sum_{ik=1}^{Nh_{js}} H_{js_{ik}} \tilde{R}_0(r, i) \tilde{R}_1(s, j) \int_{y=sy_L}^{y=sy_R} (A_{sp0_{js}} + A_{sp1_{js}} y) (S1y + S2)^{m2} y^{n2} dy \\
& + \sum_{ik=1}^{Nh_{js}} H_{js_{ik}} \tilde{R}_1(r, i) \tilde{R}_0(s, j) \int_{y=sy_L}^{y=sy_R} (A_{sp0_{js}} + A_{sp1_{js}} y) (S1y + S2)^{m3} y^{n3} dy \\
& + \sum_{ik=1}^{Nh_{js}} \sum_{jk=1}^{Nh_{js}} H_{js_{ik}} H_{js_{jk}} \tilde{R}_1(r, i) \tilde{R}_1(s, j) \int_{y=sy_L}^{y=sy_R} (A_{sp0_{js}} + A_{sp1_{js}} y) (S1y + S2)^{m4} y^{n4} dy \Big]
\end{aligned}$$

where

$$m1 = mR0(r, i) + mR0(s, j) \quad (B.90)$$

$$n1 = nR0(r, i) + nR0(s, j) \quad (B.91)$$

$$m2 = mh_{ik} + mR0(r, i) + mR1(s, j) \quad (B.92)$$

$$n2 = nh_{ik} + nR0(r, i) + nR1(s, j) \quad (B.93)$$

$$m3 = mh_{ik} + mR1(r, i) + mR0(s, j) \quad (B.94)$$

$$n3 = nh_{ik} + nR1(r, i) + nR0(s, j) \quad (B.95)$$

$$m4 = mh_{ik} + mh_{jk} + mR1(r, i) + mR1(s, j) \quad (B.96)$$

$$n4 = nh_{ik} + nh_{jk} + nR1(r, i) + nR1(s, j) \quad (B.97)$$

Noting that Eq. B.89 is composed of linear combinations of the integral family $I_{sp}(m, n)$ defined in Eq. A.70, the final expression for the ij th term of $[K_{sp}]_{js}$ is

$$[K_{sp}(i, j)]_{js} = E_{js} \sum_{r=1}^3 \sum_{s=1}^3 Q_{sp}(r, s)$$

$$[\tilde{R}_0(r, i) \tilde{R}_0(s, j) (A_{sp0_{js}} I_{SP}(m1, n1) + A_{sp1_{js}} I_{SP}(m1, n1 + 1))$$

$$\begin{aligned}
& + \sum_{ik=1}^{Nh_{js}} H_{js_{ik}} \tilde{R}_0(r, i) \tilde{R}_1(s, j) (A_{sp0_{js}} I_{SP}(m2, n2) + A_{sp1_{js}} I_{SP}(m2, n2 + 1)) \\
& + \sum_{ik=1}^{Nh_{js}} H_{js_{ik}} \tilde{R}_1(r, i) \tilde{R}_0(s, j) (A_{sp0_{js}} I_{SP}(m3, n3) + A_{sp1_{js}} I_{SP}(m3, n3 + 1)) \\
& + \sum_{ik=1}^{Nh_{js}} \sum_{jk=1}^{Nh_{js}} H_{js_{ik}} H_{js_{jk}} \tilde{R}_1(r, i) \tilde{R}_1(s, j) (A_{sp0_{js}} I_{SP}(m4, n4) + A_{sp1_{js}} I_{SP}(m4, n4 + 1))]
\end{aligned} \tag{B.98}$$

The stiffness matrix for all the spars combined $[K_{sp}]_{tot}$ is obtained by summing the contributions of all the spars given by Eq. B.98. This matrix is then appropriately merged into the global stiffness matrix $[K_{glob}]$.

B.9 Mass Matrix Contributions of a Rib

The contribution to the kinetic energy T of an element of length dx of the j th rib is

$$dT_{jr} = \frac{1}{2} \rho_{jr} A(x)_{rb_{jr}} \left\{ \begin{matrix} \dot{u} \\ \dot{v} \\ \dot{w} \end{matrix} \right\}^T \left\{ \begin{matrix} u \\ v \\ w \end{matrix} \right\} dx \tag{B.99}$$

where ρ_{jr} is the constant material density of the rib, the cap area $A_{rb_{jr}}$ is a linear function of x , and the velocity vector is the time derivative of the displacement vector defined in Eq. B.16. Substituting Eq. B.16 into Eq. B.99 gives

$$dT_{jr} = \frac{1}{2} \rho_{jr} A(x)_{rb_{jr}} \{\dot{q}\}^T \left[S_0^T S_0 + z \left(S_0^T S_1 \right) + z \left(S_1^T S_0 \right) + z^2 \left(S_1^T S_1 \right) \right] \{\dot{q}\} dx \tag{B.100}$$

Since y is equal to a constant y_{RIB} over the length of the rib, the polynomial terms contained in S_0 and S_1 take the form $x^{mS0(r, i)} y_{RIB}^{nS0(r, i)}$ and $x^{mS1(r, i)} y_{RIB}^{nS1(r, i)}$ respectively. Integrating Eq. B.100 over the length of the rib now gives

$$T_{jr} = \frac{1}{2} \rho_{jr} \int_{x=r_{x_F}}^{x=r_{x_A}} A(x)_{rb_{jr}} \{\dot{q}\}^T \left[S_0^T S_0 + z \left(S_0^T S_1 \right) + z \left(S_1^T S_0 \right) + z^2 \left(S_1^T S_1 \right) \right] \{\dot{q}\} dx \tag{B.101}$$

where the limits of integration rx_F and rx_A are defined in Eqs. A.90 and A.91 referencing Figure A.4. Equivalent to Eq. B.101 is the expression

$$T_{jr} = \frac{1}{2} \omega^2 \rho_{jr} \int_{x=rx_F}^{x=rx_A} A(x)_{rb_{jr}} \{q\}^T \left[S_0^T S_0 + z \left(S_0^T S_1 \right) + z \left(S_1^T S_0 \right) + z^2 \left(S_1^T S_1 \right) \right] \{q\} dx \quad (\text{B.102})$$

where ω is the natural vibrational frequency of the rib. Application here of the variational extremum condition from Eq. 1.10 yields the mass matrix for the j th rib given as

$$[M_{rb}]_{jr} = \rho_{jr} \int_{x=rx_F}^{x=rx_A} A(x)_{rb_{jr}} \left[S_0^T S_0 + z \left(S_0^T S_1 \right) + z \left(S_1^T S_0 \right) + z^2 \left(S_1^T S_1 \right) \right] dx \quad (\text{B.103})$$

Substituting Eq. A.87 for the rib cap area and Eq. A.105 for the variable z gives

$$\begin{aligned} [M_{rb}]_{jr} = & \rho_{jr} \left[\int_{x=rx_F}^{x=rx_A} (A_{rb0_{jr}} + A_{rb1_{jr}} x) \left(S_0^T S_0 \right) dx \right. \\ & + \sum_{ik=1}^{Nh_{jr}} H_{jr_{ik}} \int_{x=rx_F}^{x=rx_A} x^{mh_{ik}} y_{RIB}^{nh_{ik}} (A_{rb0_{jr}} + A_{rb1_{jr}} x) \left[\left(S_0^T S_1 \right) + \left(S_1^T S_0 \right) \right] dx \\ & \left. + \sum_{ik=1}^{Nh_{jr}} \sum_{jk=1}^{Nh_{jr}} H_{jr_{ik}} H_{jr_{jk}} \int_{x=rx_F}^{x=rx_A} x^{mh_{ik} + mh_{jk}} y_{RIB}^{nh_{ik} + nh_{jk}} (A_{rb0_{jr}} + A_{rb1_{jr}} x) \left(S_1^T S_1 \right) dx \right] \end{aligned} \quad (\text{B.104})$$

The mass matrix term in the i th row and j th column for the j th rib may be expressed as

$$\begin{aligned} [M_{rb}(i, j)]_{jr} = & \rho_{jr} \sum_{r=1}^3 \left[y_{RIB}^{n1} \int_{x=rx_F}^{x=rx_A} (A_{rb0_{jr}} + A_{rb1_{jr}} x) x^{m1} dx \right. \\ & + \sum_{ik=1}^{Nh_{jr}} H_{jr_{ik}} y_{RIB}^{n2} \int_{x=rx_F}^{x=rx_A} (A_{rb0_{jr}} + A_{rb1_{jr}} x) x^{m2} dx \\ & + \sum_{ik=1}^{Nh_{jr}} H_{jr_{ik}} y_{RIB}^{n3} \int_{x=rx_F}^{x=rx_A} (A_{rb0_{jr}} + A_{rb1_{jr}} x) x^{m3} dx \\ & \left. + \sum_{ik=1}^{Nh_{jr}} \sum_{jk=1}^{Nh_{jr}} H_{jr_{ik}} H_{jr_{jk}} y_{RIB}^{n4} \int_{x=rx_F}^{x=rx_A} (A_{rb0_{jr}} + A_{rb1_{jr}} x) x^{m4} dx \right] \end{aligned} \quad (\text{B.105})$$

where the x and y powers are defined in Eqs. B.71-B.78. Noting that Eq. B.105 is composed of linear combinations of the integral family $I_{RB}(m,n)$ defined in Eq. A.102 and discussed in Appendix C, the final expression for the i,j th term of $[M_{rb}]_{jr}$ is

$$\begin{aligned}
 [M_{rb}(i,j)]_{jr} = & \rho_{jr} \sum_{r=1}^3 [A_{rb0_{jr}} I_{RB}(m1, n1) + A_{rb1_{jr}} I_{RB}(m1 + 1, n1) \\
 & + \sum_{ik=1}^{Nh_{jr}} H_{jr_{ik}} A_{rb0_{jr}} (I_{RB}(m2, n2) + I_{RB}(m3, n3)) \\
 & + \sum_{ik=1}^{Nh_{jr}} H_{jr_{ik}} A_{rb1_{jr}} (I_{RB}(m2 + 1, n2) + I_{RB}(m3 + 1, n3)) \\
 & + \sum_{ik=1}^{Nh_{jr}} \sum_{jk=1}^{Nh_{jr}} H_{jr_{ik}} H_{jr_{jk}} (A_{rb0_{jr}} I_{RB}(m4, n4) + A_{rb1_{jr}} I_{RB}(m4 + 1, n4))]
 \end{aligned} \tag{B.106}$$

The mass matrix for all the ribs combined $[M_{rb}]_{tot}$ is obtained by summing the contributions of all the ribs given by Eq. B.106. This matrix is then appropriately merged into the global mass matrix $[M_{glob}]$.

B.10 Stiffness Matrix Contributions of a Rib

The contribution to the potential or strain energy U of an element of length dx of the j th rib is

$$dU_{jr} = \frac{1}{2} E_{jr} A_{rb_{jr}}(x) \epsilon_{xx}^2 dx \tag{B.107}$$

where E_{jr} is the longitudinal modulus of elasticity, and the cap area $A_{rb_{jr}}$ is a linear function of x . Using Eqs. B.4, B.9, and B.11 let us define

$$\epsilon_{xx} = \{ [Y_0(x, y)] + z [Y_1(x, y)] \} \{ \hat{q}(t) \} \tag{B.108}$$

where

$$\{\hat{q}\}^T = \{q_1^T, q_3^T\} \quad (\text{B.109})$$

$$[Y_0(x, y)] = \begin{bmatrix} a_{1,x}^T & 0 \end{bmatrix} \quad (\text{B.110})$$

$$[Y_1(x, y)] = \begin{bmatrix} 0 & a_{3,x}^T \end{bmatrix} \quad (\text{B.111})$$

Both matrices Y_0 and Y_1 are partitioned into 2 subvectors, $1 \times Nq_1$ and $1 \times Nq_3$ in dimension respectively. Since y is equal to a constant y_{RIB} along the length of the rib, Y_0 and Y_1 contain polynomial terms of the form $C_i x^{mY0_i} y_{RIB}^{nY0_i}$ and $C_i x^{mY1_i} y_{RIB}^{nY1_i}$. Substituting Eq. B.108 into B.107 gives

$$dU_{jr} = \frac{1}{2} E_{jr} A(x)_{rb_{jr}} \{\hat{q}\}^T \left[Y_0^T Y_0 + z \left(Y_0^T Y_1 \right) + z \left(Y_1^T Y_0 \right) + z^2 \left(Y_1^T Y_1 \right) \right] \{\hat{q}\} dx \quad (\text{B.112})$$

Integrating this over the length of the rib gives

$$U_{jr} = \frac{1}{2} E_{jr} \int_{x=r_{x_F}}^{x=r_{x_A}} A(x)_{rb_{jr}} \{\hat{q}\}^T \left[Y_0^T Y_0 + z \left(Y_0^T Y_1 \right) + z \left(Y_1^T Y_0 \right) + z^2 \left(Y_1^T Y_1 \right) \right] \{\hat{q}\} dx \quad (\text{B.113})$$

where the limits of integration have been defined in Eqs. A.90 and A.91. Application here of the variational extremum condition from Eq. 1.10 yields the stiffness matrix for the j th rib given as

$$[K_{rb}]_{jr} = E_{jr} \int_{x=r_{x_F}}^{x=r_{x_A}} A(x)_{rb_{jr}} \left[Y_0^T Y_0 + z \left(Y_0^T Y_1 \right) + z \left(Y_1^T Y_0 \right) + z^2 \left(Y_1^T Y_1 \right) \right] dx \quad (\text{B.114})$$

Substituting Eq. A.87 for the rib cap area and Eq. A.105, the rib depth distribution, for the variable z gives

$$\begin{aligned} [K_{rb}]_{jr} = & E_{jr} \left[\int_{x=r_{x_F}}^{x=r_{x_A}} (A_{rb0_{jr}} + A_{rb1_{jr}} x) \left(Y_0^T Y_0 \right) dx \right. \\ & + \sum_{ik=1}^{Nh_{jr}} H_{jr_{ik}} \int_{x=r_{x_F}}^{x=r_{x_A}} x^{mh_{ik}} y_{RIB}^{nh_{ik}} (A_{rb0_{jr}} + A_{rb1_{jr}} x) \left[\left(Y_0^T Y_1 \right) + \left(Y_1^T Y_0 \right) \right] dx \\ & \left. + \sum_{ik=1}^{Nh_{jr}} \sum_{jk=1}^{Nh_{jr}} H_{jr_{ik}} H_{jr_{jk}} \int_{x=r_{x_F}}^{x=r_{x_A}} x^{mh_{ik} + mh_{jk}} y_{RIB}^{nh_{ik} + nh_{jk}} (A_{rb0_{jr}} + A_{rb1_{jr}} x) \left(Y_1^T Y_1 \right) dx \right] \end{aligned} \quad (\text{B.115})$$

Let the i th term of the single row matrices Y_0 and Y_1 be

$$Y_{0_i} = \tilde{Y}_{0_i} x^{mY0_i} y^{nY0_i} \quad (\text{B.116})$$

$$Y_{1_i} = \tilde{Y}_{1_i} x^{mY1_i} y^{nY1_i} \quad (\text{B.117})$$

Upon substitution of Eqs. B.116 and B.117 into Eq. B.115, the stiffness matrix term in the i th row and j th column for the j th rib may be expressed as

$$\begin{aligned} [K_{rb}(i, j)]_{jr} = E_{jr} & \left[\tilde{Y}_{0_i} \tilde{Y}_{0_j} y^{n1} \int_{x=r x_F}^{x=r x_A} (A_{rb0_{jr}} + A_{rb1_{jr}} x) x^{m1} dx \right. \\ & + \sum_{ik=1}^{Nh_{jr}} H_{jr_{ik}} \tilde{Y}_{0_i} \tilde{Y}_{1_j} y^{n2} \int_{x=r x_F}^{x=r x_A} (A_{rb0_{jr}} + A_{rb1_{jr}} x) x^{m2} dx \\ & + \sum_{ik=1}^{Nh_{jr}} H_{jr_{ik}} \tilde{Y}_{1_i} \tilde{Y}_{0_j} y^{n3} \int_{x=r x_F}^{x=r x_A} (A_{rb0_{jr}} + A_{rb1_{jr}} x) x^{m3} dx \\ & \left. + \sum_{ik=1}^{Nh_{jr}} \sum_{jk=1}^{Nh_{jr}} H_{jr_{ik}} H_{jr_{jk}} \tilde{Y}_{1_i} \tilde{Y}_{1_j} y^{n4} \int_{x=r x_F}^{x=r x_A} (A_{rb0_{jr}} + A_{rb1_{jr}} x) x^{m4} dx \right] \end{aligned} \quad (\text{B.118})$$

where

$$m1 = mY0_i + mY0_j \quad (\text{B.119})$$

$$n1 = nY0_i + nY0_j \quad (\text{B.120})$$

$$m2 = mh_{ik} + mY0_i + mY1_j \quad (\text{B.121})$$

$$n2 = nh_{ik} + nY0_i + nY1_j \quad (\text{B.122})$$

$$m3 = mh_{ik} + mY1_i + mY0_j \quad (\text{B.123})$$

$$n3 = nh_{ik} + nY1_i + nY0_j \quad (\text{B.124})$$

$$m4 = mh_{ik} + mh_{jk} + mY1_i + mY1_j \quad (B.125)$$

$$n4 = nh_{ik} + nh_{jk} + nY1_i + nY1_j \quad (B.126)$$

Noting that Eq. B.118 is composed of linear combinations of the integral family $I_{RB}(m,n)$ defined in Eq. A.102 and discussed in Appendix C, the final expression for the i,j th term of $[K_{rb}]_{jr}$ is

$$\begin{aligned} [K_{rb}(i,j)]_{jr} = & E_{jr} [\bar{Y}_{0i} \bar{Y}_{0j} (A_{rb0_{jr}} I_{RB}(m1, n1) + A_{rb1_{jr}} I_{RB}(m1 + 1, n1)) \\ & + \sum_{ik=1}^{Nh_{jr}} H_{jr_{ik}} \bar{Y}_{0i} \bar{Y}_{1j} (A_{rb0_{jr}} I_{RB}(m2, n2) + A_{rb0_{jr}} I_{RB}(m2 + 1, n2)) \\ & + \sum_{ik=1}^{Nh_{jr}} H_{jr_{ik}} \bar{Y}_{1i} \bar{Y}_{0j} (A_{rb1_{jr}} I_{RB}(m3, n3) + A_{rb1_{jr}} I_{RB}(m3 + 1, n3)) \\ & + \sum_{ik=1}^{Nh_{jr}} \sum_{jk=1}^{Nh_{jr}} H_{jr_{ik}} H_{jr_{jk}} \bar{Y}_{1i} \bar{Y}_{1j} (A_{rb0_{jr}} I_{RB}(m4, n4) + A_{rb1_{jr}} I_{RB}(m4 + 1, n4))] \end{aligned} \quad (B.127)$$

The stiffness matrix for all the ribs combined $[K_{rb}]_{tot}$ is obtained by summing the contributions of all the ribs given by Eq. B.127. This matrix is then appropriately merged into the global stiffness matrix $[K_{glob}]$.

B.11 Mass Matrix Contributions of a Spar Web Layer

A spar web is positioned in the vertical plane between parallel spar caps on the upper and lower wing surfaces. This plane is defined to be the η - z plane where η is the coordinate along the corresponding parallel upper and lower spar axes rotated from the y axis by an angle Λ . See Figure A.3 for spar line geometry. The contribution to the kinetic energy T of an infinitesimal element $d\eta$ by dz of the jl th spar web layer is

$$dT_{jl} = \frac{1}{2} \rho_{jl} t_{jl}(\eta, z) \left\{ \begin{array}{c} \dot{u} \\ \bar{\dot{v}} \\ \bar{\dot{w}} \end{array} \right\}^T \left\{ \begin{array}{c} \dot{u} \\ \bar{\dot{v}} \\ \bar{\dot{w}} \end{array} \right\} d\eta dz \quad (B.128)$$

where ρ_{jl} is the constant material density of the web layer, the velocity vector is the time derivative of the displacement vector defined in Eq. B.16, and $t_{jl}(\eta, z)$ is the thickness of the layer. The layer thickness may be expressed as a linear function y only. Referring to Figure A.3, all η dependence may be changed to y dependence by substituting Eq. A.55 for $d\eta$. This gives

$$dT_{jl} = \frac{1}{2}\rho_{jl}\left(\frac{L}{sy_R - sy_L}\right)t_{jl}(y) \left\{ \begin{matrix} \dot{u} \\ \dot{v} \\ \dot{w} \end{matrix} \right\}^T \left\{ \begin{matrix} \dot{u} \\ \dot{v} \\ \dot{w} \end{matrix} \right\} dydz \quad (\text{B.129})$$

where the parameters L , sy_R , and sy_L may be defined from either the upper spar cap or the lower spar cap, and the layer thickness is given by

$$t_{jl}(y) = \hat{T}_{0_{jl}} + \hat{T}_{1_{jl}}y \quad (\text{B.130})$$

Substituting Eq. B.16 into Eq. B.129 gives

$$dT_{jl} = \frac{1}{2}\rho_{jl}\left(\frac{L}{sy_R - sy_L}\right)t_{jl}(y) \{\dot{q}\}^T [S_0^T S_0 + z(S_0^T S_1) + z(S_1^T S_0) + z^2(S_1^T S_1)] \{\dot{q}\} dydz \quad (\text{B.131})$$

Here the spar line equation from Eq. A.57 may be employed to express x within the matrices S_0 and S_1 as a function of y . Therefore the polynomial terms contained in S_0 and S_1 take the form $(S_1y + S_2)^{mS_0(r, i)} y^{nS_0(r, i)}$ and $(S_1y + S_2)^{mS_1(r, i)} y^{nS_1(r, i)}$ respectively. Integrating Eq. B.130 over the area of the web layer now gives

$$T_{jl} = \frac{1}{2}\rho_{jl}\left(\frac{L}{sy_R - sy_L}\right) \int_{h_L(x, y)}^{h_U(x, y)} \int_{y=sy_L}^{y=sy_R} t_{jl}(y) \{\dot{q}\}^T [S_0^T S_0 + z(S_0^T S_1) + z(S_1^T S_0) + z^2(S_1^T S_1)] \{\dot{q}\} dydz \quad (\text{B.132})$$

where the limits of z integration are the depth distributions of the lower and upper spar caps given respectively by

$$h_U(x, y) = \sum_{ik=1}^{Nh_U} H_{ik}^U \cdot x^{mhU_{ik}} y^{nhU_{ik}} \quad (\text{B.133})$$

$$h_L(x, y) = \sum_{ik=1}^{Nh_L} H_{ik}^L \cdot x^{mhL_{ik}} y^{nhL_{ik}} \quad (\text{B.134})$$

Equivalent to Eq. B.131 is the expression

$$T_{jl} = \frac{1}{2} \omega^2 \rho_{jl} \left(\frac{L}{sy_R - sy_L} \right) \int_{y=sy_L}^{y=sy_R} \int_{h_L(x,y)}^{h_U(x,y)} t_{jl}(y) \{q\}^T \left[S_0^T S_0 + z \left(S_0^T S_1 \right) \right. \\ \left. + z \left(S_1^T S_0 \right) + z^2 \left(S_1^T S_1 \right) \right] \{q\} dz dy \quad (\text{B.135})$$

where ω is the natural vibrational frequency of the web layer. Application here of the variational extremum condition from Eq. 1.10 yields the mass matrix for the j th spar web layer given as

$$[M_{swb}]_{jl} = \rho_{jl} \left(\frac{L}{sy_R - sy_L} \right) \int_{y=sy_L}^{y=sy_R} \int_{h_L(x,y)}^{h_U(x,y)} t_{jl}(y) \left[S_0^T S_0 + z \left(S_0^T S_1 \right) \right. \\ \left. + z \left(S_1^T S_0 \right) + z^2 \left(S_1^T S_1 \right) \right] dz dy \quad (\text{B.136})$$

The z integration is performed first analytically using

$$\int_{h_L(x,y)}^{h_U(x,y)} z^s = \frac{1}{s+1} \left[h_U^{s+1}(x, y) - h_L^{s+1}(x, y) \right] \quad (\text{B.137})$$

Eq. B.136 thus becomes

$$[M_{swb}]_{jl} = \rho_{jl} \left(\frac{L}{sy_R - sy_L} \right) \int_{y=sy_L}^{y=sy_R} t_{jl}(y) \left[(h_U(x, y) - h_L(x, y)) \left(S_0^T S_0 \right) \right. \\ \left. + \frac{1}{2} \left(h_U^2(x, y) - h_L^2(x, y) \right) \left(\left(S_0^T S_1 \right) + \left(S_1^T S_0 \right) \right) \right. \\ \left. + \frac{1}{3} \left(h_U^3(x, y) - h_L^3(x, y) \right) \left(S_1^T S_1 \right) \right] dy \quad (\text{B.138})$$

Substituting Eq. B.130 for the layer thickness and Eqs. B.133 and B.134 for the spar cap depth distributions gives

$$\begin{aligned}
 [M_{swb}]_{jl} = & \rho_{jl} \left(\frac{L}{sy_R - sy_L} \right) \left[\sum_{ik=1}^{Nh_U} H_{ik}^U \int_{y=sy_L}^{y=sy_R} x^{mhU_{ik}} y^{nhU_{ik}} \left(\hat{T}_{0_{jl}} + \hat{T}_{1_{jl}} y \right) \left(S_0^T S_0 \right) dy \right. \\
 & - \sum_{ik=1}^{Nh_L} H_{ik}^L \int_{y=sy_L}^{y=sy_R} x^{mhL_{ik}} y^{nhL_{ik}} \left(\hat{T}_{0_{jl}} + \hat{T}_{1_{jl}} y \right) \left(S_0^T S_0 \right) dy \\
 & + \frac{1}{2} \sum_{ik=1}^{Nh_U} \sum_{jk=1}^{Nh_U} H_{ik}^U H_{jk}^U \int_{y=sy_L}^{y=sy_R} x^{mhU_{ik} + mhU_{jk}} y^{nhU_{ik} + nhU_{jk}} \left(\hat{T}_{0_{jl}} + \hat{T}_{1_{jl}} y \right) \left(\left(S_0^T S_1 \right) + \left(S_1^T S_0 \right) \right) dy \\
 & - \frac{1}{2} \sum_{ik=1}^{Nh_L} \sum_{jk=1}^{Nh_L} H_{ik}^L H_{jk}^L \int_{y=sy_L}^{y=sy_R} x^{mhL_{ik} + mhL_{jk}} y^{nhL_{ik} + nhL_{jk}} \left(\hat{T}_{0_{jl}} + \hat{T}_{1_{jl}} y \right) \left(\left(S_0^T S_1 \right) + \left(S_1^T S_0 \right) \right) dy \\
 & + \frac{1}{3} \sum_{ik=1}^{Nh_U} \sum_{jk=1}^{Nh_U} \sum_{lk=1}^{Nh_U} H_{ik}^U H_{jk}^U H_{lk}^U \int_{y=sy_L}^{y=sy_R} x^{mhU_{ik} + mhU_{jk} + mhU_{lk}} y^{nhU_{ik} + nhU_{jk} + nhU_{lk}} \\
 & \quad \cdot \left(\hat{T}_{0_{jl}} + \hat{T}_{1_{jl}} y \right) \left(S_1^T S_1 \right) dy \\
 & - \frac{1}{3} \sum_{ik=1}^{Nh_L} \sum_{jk=1}^{Nh_L} \sum_{lk=1}^{Nh_L} H_{ik}^L H_{jk}^L H_{lk}^L \int_{y=sy_L}^{y=sy_R} x^{mhL_{ik} + mhL_{jk} + mhL_{lk}} y^{nhL_{ik} + nhL_{jk} + nhL_{lk}} \\
 & \quad \cdot \left(\hat{T}_{0_{jl}} + \hat{T}_{1_{jl}} y \right) \left(S_1^T S_1 \right) dy \left. \right] \quad (B.139)
 \end{aligned}$$

Substituting the spar line equation from Eq. A.57 for all x , the mass matrix term in the i th row and j th column for the j th spar web layer may be expressed as

$$\begin{aligned}
 [M_{swb}(i, j)]_{jl} = & \rho_{jl} \left(\frac{L}{sy_R - sy_L} \right) \sum_{r=1}^3 \left[\sum_{ik=1}^{Nh_U} H_{ik}^U \int_{y=sy_L}^{y=sy_R} \left(\hat{T}_{0_{jl}} + \hat{T}_{1_{jl}} y \right) (S_1 y + S_2)^{mU_1} y^{nU_1} dy \right. \\
 & - \sum_{ik=1}^{Nh_L} H_{ik}^L \int_{y=sy_L}^{y=sy_R} \left(\hat{T}_{0_{jl}} + \hat{T}_{1_{jl}} y \right) (S_1 y + S_2)^{mL_1} y^{nL_1} dy
 \end{aligned}$$

$$\begin{aligned}
& + \frac{1}{2} \sum_{ik=1}^{Nh_U} \sum_{jk=1}^{Nh_U} H_{ik}^U H_{jk}^U \int_{y=sy_L}^{y=sy_R} \left(\hat{T}_{0_{ji}} + \hat{T}_{1_{jr}} y \right) \left((S1y + S2)^{mU2} y^{nU2} + (S1y + S2)^{mU3} y^{nU3} \right) dy \\
& - \frac{1}{2} \sum_{ik=1}^{Nh_L} \sum_{jk=1}^{Nh_L} H_{ik}^L H_{jk}^L \int_{y=sy_L}^{y=sy_R} \left(\hat{T}_{0_{ji}} + \hat{T}_{1_{jr}} y \right) \left((S1y + S2)^{mL2} y^{nL2} + (S1y + S2)^{mL3} y^{nL3} \right) dy \\
& + \frac{1}{3} \sum_{ik=1}^{Nh_U} \sum_{jk=1}^{Nh_U} \sum_{lk=1}^{Nh_U} H_{ik}^U H_{jk}^U H_{lk}^U \int_{y=sy_L}^{y=sy_R} \left(\hat{T}_{0_{ji}} + \hat{T}_{1_{jr}} y \right) (S1y + S2)^{mU4} y^{nU4} dy \\
& - \frac{1}{3} \sum_{ik=1}^{Nh_L} \sum_{jk=1}^{Nh_L} \sum_{lk=1}^{Nh_L} H_{ik}^L H_{jk}^L H_{lk}^L \int_{y=sy_L}^{y=sy_R} \left(\hat{T}_{0_{ji}} + \hat{T}_{1_{jr}} y \right) (S1y + S2)^{mL4} y^{nL4} dy \Big]
\end{aligned} \tag{B.140}$$

where

$$mU1 = mhU_{ik} + mS0(r, i) + mS0(r, j) \tag{B.141}$$

$$nU1 = nhU_{ik} + nS0(r, i) + nS0(r, j) \tag{B.142}$$

$$mL1 = mhL_{ik} + mS0(r, i) + mS0(r, j) \tag{B.143}$$

$$nL1 = nhL_{ik} + nS0(r, i) + nS0(r, j) \tag{B.144}$$

$$mU2 = mhU_{ik} + mhU_{jk} + mS0(r, i) + mS1(r, j) \tag{B.145}$$

$$nU2 = nhU_{ik} + nhU_{jk} + nS0(r, i) + nS1(r, j) \tag{B.146}$$

$$mL2 = mhL_{ik} + mhL_{jk} + mS0(r, i) + mS1(r, j) \tag{B.147}$$

$$nL2 = nhL_{ik} + nhL_{jk} + nS0(r, i) + nS1(r, j) \tag{B.148}$$

$$mU3 = mhU_{ik} + mhU_{jk} + mS1(r, i) + mS0(r, j) \tag{B.149}$$

$$nU3 = nhU_{ik} + nhU_{jk} + nS1(r, i) + nS0(r, j) \tag{B.150}$$

$$mL3 = mhL_{ik} + mhL_{jk} + mS1(r, i) + mS0(r, j) \quad (B.151)$$

$$nL3 = nhL_{ik} + nhL_{jk} + nS1(r, i) + nS0(r, j) \quad (B.152)$$

$$mU4 = mhU_{ik} + mhU_{jk} + mhU_{lk} + mS1(r, i) + mS1(r, j) \quad (B.153)$$

$$nU4 = nhU_{ik} + nhU_{jk} + nhU_{lk} + nS1(r, i) + nS1(r, j) \quad (B.154)$$

$$mL4 = mhL_{ik} + mhL_{jk} + mhL_{lk} + mS1(r, i) + mS1(r, j) \quad (B.155)$$

$$nL4 = nhL_{ik} + nhL_{jk} + nhL_{lk} + nS1(r, i) + nS1(r, j) \quad (B.156)$$

Noting that Eq. B.140 is composed of linear combinations of the integral family $I_{SP}(m, n)$ defined in Eq. A.70, the final expression for the i, j th term of $[M_{swb}]_{jl}$ is

$$\begin{aligned} [M_{swb}(i, j)]_{jl} = & \rho_{jl} \sum_{r=1}^3 \left[\sum_{ik=1}^{Nh_U} H_{ik}^U \left(\hat{T}_{0,jl} I_{SP}(mU1, nU1) + \hat{T}_{1,jl} I_{SP}(mU1, nU1 + 1) \right) \right. \\ & - \sum_{ik=1}^{Nh_L} H_{ik}^L \left(\hat{T}_{0,jl} I_{SP}(mL1, nL1) + \hat{T}_{1,jl} I_{SP}(mL1, nL1 + 1) \right) \\ & + \frac{1}{2} \sum_{ik=1}^{Nh_U} \sum_{jk=1}^{Nh_U} H_{ik}^U H_{jk}^U \left(\hat{T}_{0,jl} I_{SP}(mU2, nU2) + \hat{T}_{1,jl} I_{SP}(mU2, nU2 + 1) \right) \\ & + \frac{1}{2} \sum_{ik=1}^{Nh_U} \sum_{jk=1}^{Nh_U} H_{ik}^U H_{jk}^U \left(\hat{T}_{0,jl} I_{SP}(mU3, nU3) + \hat{T}_{1,jl} I_{SP}(mU3, nU3 + 1) \right) \\ & - \frac{1}{2} \sum_{ik=1}^{Nh_L} \sum_{jk=1}^{Nh_L} H_{ik}^L H_{jk}^L \left(\hat{T}_{0,jl} I_{SP}(mL2, nL2) + \hat{T}_{1,jl} I_{SP}(mL2, nL2 + 1) \right) \\ & \left. - \frac{1}{2} \sum_{ik=1}^{Nh_L} \sum_{jk=1}^{Nh_L} H_{ik}^L H_{jk}^L \left(\hat{T}_{0,jl} I_{SP}(mL3, nL3) + \hat{T}_{1,jl} I_{SP}(mL3, nL3 + 1) \right) \right] \end{aligned} \quad (B.157)$$

$$\begin{aligned}
& + \frac{1}{3} \sum_{ik=1}^{Nh_U} \sum_{jk=1}^{Nh_U} \sum_{lk=1}^{Nh_U} H_{ik}^U H_{jk}^U H_{lk}^U \left(\hat{T}_{0jl} I_{SP}(mU4, nU4) + \hat{T}_{1jl} I_{SP}(mU4, nU4 + 1) \right) \\
& - \frac{1}{3} \sum_{ik=1}^{Nh_L} \sum_{jk=1}^{Nh_L} \sum_{lk=1}^{Nh_L} H_{ik}^L H_{jk}^L H_{lk}^L \left(\hat{T}_{0jl} I_{SP}(mL4, nL4) + \hat{T}_{1jl} I_{SP}(mL4, nL4 + 1) \right) \Bigg]
\end{aligned}$$

The mass matrix $[M_{swb}]_{tot}$ for all the spar webs combined is obtained by summing the contributions of all the spar webs given by Eq. B.157. This matrix is then appropriately merged into the global mass matrix $[M_{glob}]$.

B.12 Stiffness Matrix Contributions of a Spar Web Layer

A spar web layer in the η - z plane is treated as a plane stress panel where the only strains of importance are $\epsilon_{\eta\eta}$, ϵ_{zz} , and $\gamma_{\eta z}$. From the assumptions stated in section B.2, ϵ_{zz} may be neglected. The normal strain $\epsilon_{\eta\eta}$ has been defined in terms of strains in the x - y plane in Eq. B.81. The shear strain $\gamma_{\eta z}$ may also be defined in terms of strains in the x - y plane using standard tensor transformation rules. It is given by

$$\gamma_{\eta z} = \{ \sin \Lambda, \cos \Lambda \} \begin{Bmatrix} \gamma_{xz} \\ \gamma_{yz} \end{Bmatrix} = \{ s\Lambda, c\Lambda \} \begin{Bmatrix} \gamma_{xz} \\ \gamma_{yz} \end{Bmatrix} \quad (B.158)$$

where Λ is the angle of rotation of the η axis from the y axis. Combining Eqs. B.81, B.82, and B.158 we may write

$$\begin{Bmatrix} \epsilon_{\eta\eta} \\ \gamma_{\eta z} \end{Bmatrix} = [TR_{25}] \{ \epsilon \} \quad (B.159)$$

where

$$\{ \epsilon \}^T = \{ \epsilon_{xx}, \epsilon_{yy}, \gamma_{xy}, \gamma_{xz}, \gamma_{yz} \} \quad (B.160)$$

and the transformation matrix is defined by

$$[TR_{25}] = \begin{bmatrix} (s^2\Lambda) & (c^2\Lambda) & (s\Lambda c\Lambda) & 0 & 0 \\ 0 & 0 & 0 & (s\Lambda) & (c\Lambda) \end{bmatrix} \quad (\text{B.161})$$

Using Eqs. B.4-B.13 and Eq. B.15, Eq. B.159 may be expressed in terms of the generalized displacement vector $\{q\}$ in the form

$$\{\epsilon\}^T = \{ [W_0(x, y)] + z [W_1(x, y)] \} \{q(t)\} \quad (\text{B.162})$$

where

$$[W_0(x, y)] = \begin{bmatrix} a_{1,x}^T & 0 & 0 & 0 & 0 \\ 0 & a_{2,y}^T & 0 & 0 & 0 \\ a_{1,y}^T & a_{2,x}^T & 0 & 0 & 0 \\ 0 & 0 & a_3^T & 0 & a_{5,x}^T \\ 0 & 0 & 0 & a_4^T & a_{5,y}^T \end{bmatrix} \quad (\text{B.163})$$

$$[W_1(x, y)] = \begin{bmatrix} 0 & 0 & a_{3,x}^T & 0 & 0 \\ 0 & 0 & 0 & a_{4,y}^T & 0 \\ 0 & 0 & a_{3,y}^T & a_{4,x}^T & 0 \\ 0 & 0 & 0 & 0 & 0 \\ 0 & 0 & 0 & 0 & 0 \end{bmatrix} \quad (\text{B.164})$$

The matrices W_0 and W_1 contain polynomial terms of the form $C(r, i) x^{mW_0(r, i)} y^{nW_0(r, i)}$ and $C(r, i) x^{mW_1(r, i)} y^{nW_1(r, i)}$ respectively and are partitioned into subvectors of dimension $1 \times Nq_s$ ($s=1,2,\dots,5$). Both matrices are $5 \times Nq_{tot}$ in dimension with Nq_{tot} having been defined in Eq. B.19.

Now the contribution to the potential or strain energy U of an infinitesimal element $d\eta$ by dz of the jl th spar web layer is

$$dU_{jl} = \frac{1}{2} t_{jl}(\eta, z) \left\{ \begin{matrix} \epsilon_{\eta\eta} \\ \gamma_{\eta z} \end{matrix} \right\}^T [\bar{Q}]_{jl} \left\{ \begin{matrix} \epsilon_{\eta\eta} \\ \gamma_{\eta z} \end{matrix} \right\} d\eta dz \quad (\text{B.165})$$

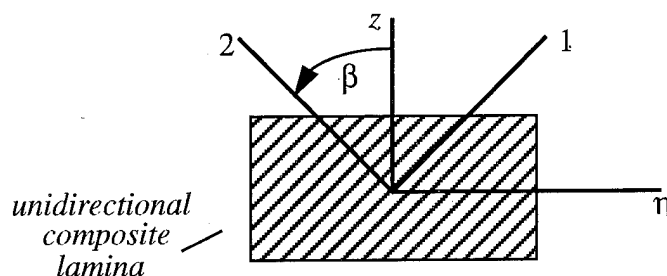


Figure B.1: Positive Rotation of Principal Material Axes from η - z Axes

where $[\bar{Q}]_{jl}$ is the j th layer's constitutive matrix, and $t_{jl}(\eta, z)$ is the thickness of the layer. The constitutive matrix, as discussed in Section 1.5, has the form

$$[\bar{Q}]_{jl} = \begin{bmatrix} \bar{Q}_{11} & \bar{Q}_{16} \\ \bar{Q}_{16} & \bar{Q}_{66} \end{bmatrix} \quad (\text{B.166})$$

where its components are determined for the η - z axis system from $[\tilde{Q}]_{jl}$, the j th layer's constitutive matrix referenced to its own principal material axes. Assuming the j th layer to be orthotropic, its invariant properties may be used to determine the components of $[\bar{Q}]_{jl}$ when the layer's principal axes are oriented at some angle β to the η - z axes as shown in Figure B.1 (JO75). The components of $[\bar{Q}]_{jl}$ may be written as

$$\bar{Q}_{11} = C_1 + C_2 \cos 2\beta + C_3 \cos 4\beta \quad (\text{B.167})$$

$$\bar{Q}_{16} = -\frac{1}{2}C_2 \sin 2\beta - C_3 \sin 4\beta \quad (\text{B.168})$$

$$\bar{Q}_{66} = C_5 - C_3 \cos 4\beta \quad (\text{B.169})$$

for which the invariants C_1 , C_2 , C_3 , and C_5 are defined in Eqs. A.33-A.37 (JO75). The layer thickness may be expressed as a linear function of y only as given in Eq. B.130. Referring to Figure A.3, all η dependence of Eq. B.165 may be changed to y dependence by substituting Eq. A.55 for $d\eta$. This gives

$$dU_{jl} = \frac{1}{2} \left(\frac{L}{sy_R - sy_L} \right) t_{jl}(y) \begin{Bmatrix} \epsilon_{\eta\eta} \\ \gamma_{\eta z} \end{Bmatrix}^T [\bar{Q}]_{jl} \begin{Bmatrix} \epsilon_{\eta\eta} \\ \gamma_{\eta z} \end{Bmatrix} dydz \quad (\text{B.170})$$

where the parameters L , sy_R , and sy_L may be defined from the geometry of either the upper spar cap or the lower spar cap. Substituting Eq. B.159 into Eq. B.170 gives

$$dU_{jl} = \frac{1}{2} \left(\frac{L}{sy_R - sy_L} \right) t_{jl}(y) \{\epsilon\}^T [TR_{25}]^T [\bar{Q}]_{jl} [TR_{25}] \{\epsilon\} dydz \quad (\text{B.171})$$

Let us define

$$[Q_s] = [TR_{25}]^T [\bar{Q}]_{jl} [TR_{25}] \quad (\text{B.172})$$

where $[Q_s]$ is 5×5 in dimension. Substituting Eqs. B.162 and B.172 into Eq. B.171 gives

$$dU_{jl} = \frac{1}{2} \left(\frac{L}{sy_R - sy_L} \right) t_{jl}(y) \{q\}^T \left[W_0^T [Q_s] W_0 + z \left(W_0^T [Q_s] W_1 \right) \right. \\ \left. + z \left(W_1^T [Q_s] W_0 \right) + z^2 \left(W_1^T [Q_s] W_1 \right) \right] \{q\} dydz \quad (\text{B.173})$$

Here the spar line equation from Eq. A.57 may be employed to express x within the matrices W_0 and W_1 as a function of y . The polynomial terms contained in W_0 and W_1 take the form $C(r, i) (S1y + S2)^{mW_0(r, i)} y^{nW_0(r, i)}$ and $C(r, i) (S1y + S2)^{mW_1(r, i)} y^{nW_1(r, i)}$ respectively. Integrating Eq. B.173 over the area of the web layer now gives

$$U_{jl} = \frac{1}{2} \left(\frac{L}{sy_R - sy_L} \right) \int_{y=sy_L}^{y=sy_R} \int_{h_L(x, y)}^{h_U(x, y)} t_{jl}(y) \{q\}^T \left[W_0^T [Q_s] W_0 + z \left(W_0^T [Q_s] W_1 \right) \right. \\ \left. + z \left(W_1^T [Q_s] W_0 \right) + z^2 \left(W_1^T [Q_s] W_1 \right) \right] \{q\} dz dy \quad (\text{B.174})$$

where the limits of z integration are the depth distributions of the lower and upper spar caps given in Eqs. B.133 and B.134. Application here of the variational extremum condition from Eq. 1.10 yields the stiffness matrix for the j th spar web layer given as

$$[K_{swb}]_{jl} = \left(\frac{L}{sy_R - sy_L} \right) \int_{y=sy_L}^{y=sy_R} \int_{h_L(x,y)}^{h_U(x,y)} t_{jl}(y) [W_0^T [Q_s] W_0 + z (W_0^T [Q_s] W_1) + z (W_1^T [Q_s] W_0) + z^2 (W_1^T [Q_s] W_1)] dz dy \quad (B.175)$$

Performing the z integration analytically using Eq. B.137 gives

$$[K_{swb}]_{jl} = \left(\frac{L}{sy_R - sy_L} \right) \int_{y=sy_L}^{y=sy_R} t_{jl}(y) \left[(h_U(x,y) - h_L(x,y)) \left(W_0^T [Q_s] W_0 \right) + \frac{1}{2} \left(h_U^2(x,y) - h_L^2(x,y) \right) \left(\left(W_0^T [Q_s] W_1 \right) + \left(W_1^T [Q_s] W_0 \right) \right) + \frac{1}{3} \left(h_U^3(x,y) - h_L^3(x,y) \right) \left(W_1^T [Q_s] W_1 \right) \right] dy \quad (B.176)$$

Substituting Eq. B.130 for the layer thickness and Eqs. B.133 and B.134 for the spar cap depth distributions gives

$$[K_{swb}]_{jl} = \left(\frac{L}{sy_R - sy_L} \right) \left[\sum_{ik=1}^{Nh_U} H_{ik}^U \int_{y=sy_L}^{y=sy_R} x^{mhU_{ik}} y^{nhU_{ik}} \left(\hat{T}_{0jl} + \hat{T}_{1jl} y \right) \left(W_0^T [Q_s] W_0 \right) dy \right. \\ - \sum_{ik=1}^{Nh_L} H_{ik}^L \int_{y=sy_L}^{y=sy_R} x^{mhL_{ik}} y^{nhL_{ik}} \left(\hat{T}_{0jl} + \hat{T}_{1jl} y \right) \left(W_0^T [Q_s] W_0 \right) dy \\ + \frac{1}{2} \sum_{ik=1}^{Nh_U} \sum_{jk=1}^{Nh_U} H_{ik}^U H_{jk}^U \int_{y=sy_L}^{y=sy_R} x^{mhU_{ik} + mhU_{jk}} y^{nhU_{ik} + nhU_{jk}} \cdot \left(\hat{T}_{0jl} + \hat{T}_{1jl} y \right) \left(\left(W_0^T [Q_s] W_1 \right) + \left(W_1^T [Q_s] W_0 \right) \right) dy \\ - \frac{1}{2} \sum_{ik=1}^{Nh_L} \sum_{jk=1}^{Nh_L} H_{ik}^L H_{jk}^L \int_{y=sy_L}^{y=sy_R} x^{mhL_{ik} + mhL_{jk}} y^{nhL_{ik} + nhL_{jk}} \cdot \left(\hat{T}_{0jl} + \hat{T}_{1jl} y \right) \left(\left(W_0^T [Q_s] W_1 \right) + \left(W_1^T [Q_s] W_0 \right) \right) dy \\ \left. + \frac{1}{3} \sum_{ik=1}^{Nh_U} \sum_{jk=1}^{Nh_U} \sum_{lk=1}^{Nh_U} H_{ik}^U H_{jk}^U H_{lk}^U \int_{y=sy_L}^{y=sy_R} x^{mhU_{ik} + mhU_{jk} + mhU_{lk}} y^{nhU_{ik} + nhU_{jk} + nhU_{lk}} \cdot \left(\hat{T}_{0jl} + \hat{T}_{1jl} y \right) \left(W_1^T [Q_s] W_1 \right) dy \right] \quad (B.177)$$

$$-\frac{1}{3} \sum_{ik=1}^{Nh_L} \sum_{jk=1}^{Nh_L} \sum_{lk=1}^{Nh_L} H_{ik}^L H_{jk}^L H_{lj}^L \int_{y=sy_L}^{y=sy_R} x^{mhL_{ik} + mhL_{jk} + mhL_{lk}} y^{nhL_{ik} + nhL_{jk} + nhL_{lk}} \cdot \left(\hat{T}_{0jl} + \hat{T}_{1jl} y \right) \left(W_1^T [Q_s] W_1 \right) dy \Big]$$

Let the r, i th term of the matrices W_0 and W_1 be

$$W_0(r, i) = \tilde{W}_0(r, i) (S1y + S2)^{mW0(r, i)} y^{nW0(r, i)} \quad (B.178)$$

$$W_1(r, i) = \tilde{W}_1(r, i) (S1y + S2)^{mW1(r, i)} y^{nW1(r, i)} \quad (B.179)$$

respectively. Substituting the spar line equation from Eq. A.57 for all x in Eq. B.177, the mass matrix term in the i th row and j th column for the jl th spar web layer may be expressed as

$$\begin{aligned} [K_{swb}(i, j)]_{jl} = & \sum_{r=1}^5 \sum_{p=1}^5 Q_s(r, p) \left(\frac{L}{sy_R - sy_L} \right) \\ & \left[\sum_{ik=1}^{Nh_U} H_{ik}^U \tilde{W}_0(r, i) \tilde{W}_0(p, j) \int_{y=sy_L}^{y=sy_R} \left(\hat{T}_{0jl} + \hat{T}_{1jl} y \right) (S1y + S2)^{mU1} y^{nU1} dy \right. \\ & - \sum_{ik=1}^{Nh_L} H_{ik}^L \tilde{W}_0(r, i) \tilde{W}_0(p, j) \int_{y=sy_L}^{y=sy_R} \left(\hat{T}_{0jl} + \hat{T}_{1jl} y \right) (S1y + S2)^{mL1} y^{nL1} dy \\ & + \frac{1}{2} \sum_{ik=1}^{Nh_U} \sum_{jk=1}^{Nh_U} H_{ik}^U H_{jk}^U \int_{y=sy_L}^{y=sy_R} \left(\hat{T}_{0jl} + \hat{T}_{1jl} y \right) \left(\tilde{W}_0(r, i) \tilde{W}_1(p, j) (S1y + S2)^{mU2} y^{nU2} \right. \\ & \quad \left. + \tilde{W}_1(r, i) \tilde{W}_0(p, j) (S1y + S2)^{mU3} y^{nU3} \right) dy \\ & \left. - \frac{1}{2} \sum_{ik=1}^{Nh_L} \sum_{jk=1}^{Nh_L} H_{ik}^L H_{jk}^L \int_{y=sy_L}^{y=sy_R} \left(\hat{T}_{0jl} + \hat{T}_{1jl} y \right) \left(\tilde{W}_0(r, i) \tilde{W}_1(p, j) (S1y + S2)^{mL2} y^{nL2} \right. \right. \\ & \quad \left. \left. + \tilde{W}_1(r, i) \tilde{W}_0(p, j) (S1y + S2)^{mL3} y^{nL3} \right) dy \right] \quad (B.180) \end{aligned}$$

$$\begin{aligned}
& + \frac{1}{3} \sum_{ik=1}^{Nh_U} \sum_{jk=1}^{Nh_U} \sum_{lk=1}^{Nh_U} H_{ik}^U H_{jk}^U H_{lk}^U \tilde{W}_1(r, i) \tilde{W}_1(p, j) \int_{y=sy_L}^{y=sy_R} \left(\hat{T}_{0jl} + \hat{T}_{1jl} y \right) (S1y + S2)^{mU4} y^{nU4} dy \\
& - \frac{1}{3} \sum_{ik=1}^{Nh_L} \sum_{jk=1}^{Nh_L} \sum_{lk=1}^{Nh_L} H_{ik}^L H_{jk}^L H_{lk}^L \tilde{W}_1(r, i) \tilde{W}_1(p, j) \int_{y=sy_L}^{y=sy_R} \left(\hat{T}_{0jl} + \hat{T}_{1jl} y \right) (S1y + S2)^{mL4} y^{nL4} dy \Big]
\end{aligned}$$

where

$$mU1 = mhU_{ik} + mW0(r, i) + mW0(p, j) \quad (B.181)$$

$$nU1 = nhU_{ik} + nW0(r, i) + nW0(p, j) \quad (B.182)$$

$$mL1 = mhL_{ik} + mW0(r, i) + mW0(p, j) \quad (B.183)$$

$$nL1 = nhL_{ik} + nW0(r, i) + nW0(p, j) \quad (B.184)$$

$$mU2 = mhU_{ik} + mhU_{jk} + mW0(r, i) + mW1(p, j) \quad (B.185)$$

$$nU2 = nhU_{ik} + nhU_{jk} + nW0(r, i) + nW1(p, j) \quad (B.186)$$

$$mL2 = mhL_{ik} + mhL_{jk} + mW0(r, i) + mW1(p, j) \quad (B.187)$$

$$nL2 = nhL_{ik} + nhL_{jk} + nW0(r, i) + nW1(p, j) \quad (B.188)$$

$$mU3 = mhU_{ik} + mhU_{jk} + mW1(r, i) + mW0(p, j) \quad (B.189)$$

$$nU3 = nhU_{ik} + nhU_{jk} + nW1(r, i) + nW0(p, j) \quad (B.190)$$

$$mL3 = mhL_{ik} + mhL_{jk} + mW1(r, i) + mW0(p, j) \quad (B.191)$$

$$nL3 = nhL_{ik} + nhL_{jk} + nW1(r, i) + nW0(p, j) \quad (B.192)$$

$$mU4 = mhU_{ik} + mhU_{jk} + mhU_{lk} + mW1(r, i) + mW1(p, j) \quad (B.193)$$

$$nU4 = nhU_{ik} + nhU_{jk} + nhU_{lk} + nW1(r, i) + nW1(p, j) \quad (B.194)$$

$$mL4 = mhL_{ik} + mhL_{jk} + mhL_{lk} + m\dot{W}1(r, i) + mW1(p, j) \quad (B.195)$$

$$nL4 = nhL_{ik} + nhL_{jk} + nhL_{lk} + nW1(r, i) + nW1(p, j) \quad (B.196)$$

Noting that Eq. B.180 is composed of linear combinations of the integral family $I_{SP}(m, n)$ defined in Eq. A.70, the final expression for the i, j th term of $[K_{swb}]_{jl}$ is

$$\begin{aligned} [K_{swb}(i, j)]_{jl} = & \sum_{r=1}^5 \sum_{p=1}^5 Q_s(r, p) \\ & \left[\sum_{ik=1}^{Nh_U} H_{ik}^U \tilde{W}_0(r, i) \tilde{W}_0(p, j) \left(\hat{T}_{0,ji} I_{SP}(mU1, nU1) + \hat{T}_{1,ji} I_{SP}(mU1, nU1 + 1) \right) \right. \\ & - \sum_{ik=1}^{Nh_L} H_{ik}^L \tilde{W}_0(r, i) \tilde{W}_0(p, j) \left(\hat{T}_{0,ji} I_{SP}(mL1, nL1) + \hat{T}_{1,ji} I_{SP}(mL1, nL1 + 1) \right) \\ & + \frac{1}{2} \sum_{ik=1}^{Nh_U} \sum_{jk=1}^{Nh_U} H_{ik}^U H_{jk}^U \left(\tilde{W}_0(r, i) \tilde{W}_1(p, j) \hat{T}_{0,ji} I_{SP}(mU2, nU2) \right. \\ & \quad \left. + \tilde{W}_0(r, i) \tilde{W}_1(p, j) \hat{T}_{1,ji} I_{SP}(mU2, nU2 + 1) \right) \\ & + \frac{1}{2} \sum_{ik=1}^{Nh_U} \sum_{jk=1}^{Nh_U} H_{ik}^U H_{jk}^U \left(\tilde{W}_1(r, i) \tilde{W}_0(p, j) \hat{T}_{0,ji} I_{SP}(mU3, nU3) \right. \\ & \quad \left. + \tilde{W}_1(r, i) \tilde{W}_0(p, j) \hat{T}_{1,ji} I_{SP}(mU3, nU3 + 1) \right) \\ & - \frac{1}{2} \sum_{ik=1}^{Nh_L} \sum_{jk=1}^{Nh_L} H_{ik}^L H_{jk}^L \left(\tilde{W}_0(r, i) \tilde{W}_1(p, j) \hat{T}_{0,ji} I_{SP}(mL2, nL2) \right. \\ & \quad \left. + \tilde{W}_0(r, i) \tilde{W}_1(p, j) \hat{T}_{1,ji} I_{SP}(mL2, nL2 + 1) \right) \\ & \left. - \frac{1}{2} \sum_{ik=1}^{Nh_L} \sum_{jk=1}^{Nh_L} H_{ik}^L H_{jk}^L \left(\tilde{W}_1(r, i) \tilde{W}_0(p, j) \hat{T}_{0,ji} I_{SP}(mL3, nL3) \right. \right. \\ & \quad \left. \left. + \tilde{W}_1(r, i) \tilde{W}_0(p, j) \hat{T}_{1,ji} I_{SP}(mL3, nL3 + 1) \right) \right] \quad (B.197) \end{aligned}$$

$$\begin{aligned}
& + \frac{1}{3} \sum_{ik=1}^{Nh_U} \sum_{jk=1}^{Nh_U} \sum_{lk=1}^{Nh_U} H_{ik}^U H_{jk}^U H_{lk}^U \tilde{W}_1(r, i) \tilde{W}_1(p, j) \left(\hat{T}_{0_{jl}} I_{SP}(mU4, nU4) \right. \\
& \qquad \qquad \qquad \left. + \hat{T}_{1_{jl}} I_{SP}(mU4, nU4 + 1) \right) \\
& - \frac{1}{3} \sum_{ik=1}^{Nh_L} \sum_{jk=1}^{Nh_L} \sum_{lk=1}^{Nh_L} H_{ik}^L H_{jk}^L H_{lk}^L \tilde{W}_1(r, i) \tilde{W}_1(p, j) \left(\hat{T}_{0_{jl}} I_{SP}(mL4, nL4) \right. \\
& \qquad \qquad \qquad \left. + \hat{T}_{1_{jl}} I_{SP}(mL4, nL4 + 1) \right)]
\end{aligned}$$

The mass matrix for all the spar webs combined $[K_{swb}]_{tot}$ is obtained by summing the contributions of all the spar webs given by Eq. B.197. This matrix is then appropriately merged into the global stiffness matrix $[K_{glob}]$.

B.13 Mass Matrix Contributions of a Rib Web Layer

A rib web is positioned in the vertical plane between parallel rib caps on the upper and lower wing surfaces. This plane is the x - z plane located at $y=y_{RIB}$. The contribution to the kinetic energy T of an infinitesimal element dx by dz of the jl th rib web layer is

$$dT_{jl} = \frac{1}{2} \rho_{jl} t_{jl}(x, z) \left\{ \begin{array}{c} \dot{u} \\ \dot{v} \\ \dot{w} \end{array} \right\}^T \left\{ \begin{array}{c} \dot{u} \\ \dot{v} \\ \dot{w} \end{array} \right\} dx dz \quad (B.198)$$

where ρ_{jl} is the constant material density of the web layer, the velocity vector is the time derivative of the displacement vector defined in Eq. B.16, and $t_{jl}(x, z)$ is the thickness of the layer. The layer thickness may be expressed as a linear function of x only given by

$$t_{jl}(x) = \hat{T}_{0_{jl}} + \hat{T}_{1_{jl}} x \quad (B.199)$$

Substituting Eq. B.16 into Eq. B.198 gives

$$dT_{jl} = \frac{1}{2} \rho_{jl} t_{jl}(x) \{ \dot{q} \}^T \left[S_0^T S_0 + z \left(S_0^T S_1 \right) + z \left(S_1^T S_0 \right) + z^2 \left(S_1^T S_1 \right) \right] \{ \dot{q} \} dx dz \quad (B.200)$$

Integrating Eq. B.200 over the area of the web layer now gives

$$T_{jl} = \frac{1}{2} \rho_{jl} \int_{h_L(x,y)}^{h_U(x,y)} \int_{x=r_{x_F}}^{x=r_{x_A}} t_{jl}(x) \{ \dot{q} \}^T \left[S_0^T S_0 + z \left(S_0^T S_1 \right) \right. \\ \left. + z \left(S_1^T S_0 \right) + z^2 \left(S_1^T S_1 \right) \right] \{ \dot{q} \} dx dz \quad (\text{B.201})$$

where the limits of z integration are the depth distributions of the upper and lower rib caps given respectively by Eqs. B.133 and B.134. Equivalent to Eq. B.200 is the expression

$$T_{jl} = \frac{1}{2} \omega^2 \rho_{jl} \int_{x=r_{x_F}}^{x=r_{x_A}} \int_{h_L(x,y)}^{h_U(x,y)} t_{jl}(x) \{ q \}^T \left[S_0^T S_0 + z \left(S_0^T S_1 \right) \right. \\ \left. + z \left(S_1^T S_0 \right) + z^2 \left(S_1^T S_1 \right) \right] \{ q \} dz dx \quad (\text{B.202})$$

where ω is the natural vibrational frequency of the web layer. Application here of the variational extremum condition from Eq. 1.10 yields the mass matrix for the j th rib web layer given as

$$[M_{rwb}]_{jl} = \rho_{jl} \int_{x=r_{x_F}}^{x=r_{x_A}} \int_{h_L(x,y)}^{h_U(x,y)} t_{jl}(x) \left[S_0^T S_0 + z \left(S_0^T S_1 \right) \right. \\ \left. + z \left(S_1^T S_0 \right) + z^2 \left(S_1^T S_1 \right) \right] dz dx \quad (\text{B.203})$$

Performing the z integration analytically using Eq. B.137 gives

$$[M_{rwb}]_{jl} = \rho_{jl} \int_{x=r_{x_F}}^{x=r_{x_A}} t_{jl}(x) \left[(h_U(x,y) - h_L(x,y)) \left(S_0^T S_0 \right) \right. \\ \left. + \frac{1}{2} (h_U^2(x,y) - h_L^2(x,y)) \left(\left(S_0^T S_1 \right) + \left(S_1^T S_0 \right) \right) \right. \\ \left. + \frac{1}{3} (h_U^3(x,y) - h_L^3(x,y)) \left(S_1^T S_1 \right) \right] dx \quad (\text{B.204})$$

Substituting Eq. B.199 for the layer thickness and Eqs. B.133 and B.134 for the spar cap depth distributions gives

$$[M_{rwb}]_{jl} = \rho_{jl} \left[\sum_{ik=1}^{Nh_U} H_{ik}^U \int_{x=r_{x_F}}^{x=r_{x_A}} x^{mhU_{ik}} y^{nhU_{ik}} \left(\hat{T}_{0jl} + \hat{T}_{1jl} x \right) \left(S_0^T S_0 \right) dx \right. \\ \left. - \sum_{ik=1}^{Nh_L} H_{ik}^L \int_{x=r_{x_F}}^{x=r_{x_A}} x^{mhL_{ik}} y^{nhL_{ik}} \left(\hat{T}_{0jl} + \hat{T}_{1jl} x \right) \left(S_0^T S_0 \right) dx \right]$$

$$\begin{aligned}
& + \frac{1}{2} \sum_{ik=1}^{Nh_U} \sum_{jk=1}^{Nh_U} H_{ik}^U H_{jk}^U \int_{x=r_{x_F}}^{x=r_{x_A}} x^{mhU_{ik} + mhU_{jk}} y^{nhU_{ik} + nhU_{jk}} \left(\hat{T}_{0_{jl}} + \hat{T}_{1_{jl}} x \right) \left(\left(S_0^T S_1 \right) + \left(S_1^T S_0 \right) \right) dx \\
& - \frac{1}{2} \sum_{ik=1}^{Nh_L} \sum_{jk=1}^{Nh_L} H_{ik}^L H_{jk}^L \int_{x=r_{x_F}}^{x=r_{x_A}} x^{mhL_{ik} + mhL_{jk}} y^{nhL_{ik} + nhL_{jk}} \left(\hat{T}_{0_{jl}} + \hat{T}_{1_{jl}} x \right) \left(\left(S_0^T S_1 \right) + \left(S_1^T S_0 \right) \right) dx \\
& + \frac{1}{3} \sum_{ik=1}^{Nh_U} \sum_{jk=1}^{Nh_U} \sum_{lk=1}^{Nh_U} H_{ik}^U H_{jk}^U H_{lk}^U \int_{x=r_{x_F}}^{x=r_{x_A}} x^{mhU_{ik} + mhU_{jk} + mhU_{lk}} y^{nhU_{ik} + nhU_{jk} + nhU_{lk}} \\
& \quad \cdot \left(\hat{T}_{0_{jl}} + \hat{T}_{1_{jl}} x \right) \left(S_1^T S_1 \right) dx \quad (B.205) \\
& - \frac{1}{3} \sum_{ik=1}^{Nh_L} \sum_{jk=1}^{Nh_L} \sum_{lk=1}^{Nh_L} H_{ik}^L H_{jk}^L H_{lk}^L \int_{x=r_{x_F}}^{x=r_{x_A}} x^{mhL_{ik} + mhL_{jk} + mhL_{lk}} y^{nhL_{ik} + nhL_{jk} + nhL_{lk}} \\
& \quad \cdot \left(\hat{T}_{0_{jl}} + \hat{T}_{1_{jl}} x \right) \left(S_1^T S_1 \right) dx \quad]
\end{aligned}$$

Since y is equal to a constant y_{RIB} for the rib line defined by the upper and lower rib caps, the mass matrix term in the i th row and j th column for the j th spar web layer may be expressed as

$$\begin{aligned}
& [M_{rwb}(i, j)]_{jl} = \\
& \rho_{jl} \sum_{r=1}^3 \left[\sum_{ik=1}^{Nh_U} H_{ik}^U \int_{x=r_{x_F}}^{x=r_{x_A}} \left(\hat{T}_{0_{jl}} + \hat{T}_{1_{jl}} x \right) x^{mU1} y_{RIB}^{nU1} dx \right. \\
& \quad - \sum_{ik=1}^{Nh_L} H_{ik}^L \int_{x=r_{x_F}}^{x=r_{x_A}} \left(\hat{T}_{0_{jl}} + \hat{T}_{1_{jl}} x \right) x^{mL1} y_{RIB}^{nL1} dx \\
& \quad + \frac{1}{2} \sum_{ik=1}^{Nh_U} \sum_{jk=1}^{Nh_U} H_{ik}^U H_{jk}^U \int_{x=r_{x_F}}^{x=r_{x_A}} \left(\hat{T}_{0_{jl}} + \hat{T}_{1_{jl}} x \right) \left(x^{mU2} y_{RIB}^{nU2} + x^{mU3} y_{RIB}^{nU3} \right) dx \\
& \quad - \frac{1}{2} \sum_{ik=1}^{Nh_L} \sum_{jk=1}^{Nh_L} H_{ik}^L H_{jk}^L \int_{x=r_{x_F}}^{x=r_{x_A}} \left(\hat{T}_{0_{jl}} + \hat{T}_{1_{jl}} x \right) \left(x^{mL2} y_{RIB}^{nL2} + x^{mL3} y_{RIB}^{nL3} \right) dx \quad (B.206) \\
& \quad + \frac{1}{3} \sum_{ik=1}^{Nh_U} \sum_{jk=1}^{Nh_U} \sum_{lk=1}^{Nh_U} H_{ik}^U H_{jk}^U H_{lk}^U \int_{x=r_{x_F}}^{x=r_{x_A}} \left(\hat{T}_{0_{jl}} + \hat{T}_{1_{jl}} x \right) x^{mU4} y_{RIB}^{nU4} dx \\
& \quad \left. - \frac{1}{3} \sum_{ik=1}^{Nh_L} \sum_{jk=1}^{Nh_L} \sum_{lk=1}^{Nh_L} H_{ik}^L H_{jk}^L H_{lk}^L \int_{x=r_{x_F}}^{x=r_{x_A}} \left(\hat{T}_{0_{jl}} + \hat{T}_{1_{jl}} x \right) x^{mL4} y_{RIB}^{nL4} dx \right]
\end{aligned}$$

where the x and y powers are defined in Eqs. B.141-B.156. Noting that Eq. B.206 is composed of linear combinations of the integral family $I_{RB}(m,n)$ defined in Eq. A.102, the final expression for the i,j th term of $[M_{rwb}]_{jl}$ is

$$\begin{aligned}
 [M_{rwb}(i,j)]_{jl} = & \rho_{jl} \sum_{r=1}^3 \left[\sum_{ik=1}^{Nh_U} H_{ik}^U \left(\hat{T}_{0_{ji}} I_{RB}(mU1, nU1) + \hat{T}_{1_{ji}} I_{RB}(mU1+1, nU1) \right) \right. \\
 & - \sum_{ik=1}^{Nh_L} H_{ik}^L \left(\hat{T}_{0_{ji}} I_{RB}(mL1, nL1) + \hat{T}_{1_{ji}} I_{RB}(mL1+1, nL1) \right) \\
 & + \frac{1}{2} \sum_{ik=1}^{Nh_U} \sum_{jk=1}^{Nh_U} H_{ik}^U H_{jk}^U \left(\hat{T}_{0_{ji}} I_{RB}(mU2, nU2) + \hat{T}_{1_{ji}} I_{RB}(mU2+1, nU2) \right) \\
 & + \frac{1}{2} \sum_{ik=1}^{Nh_U} \sum_{jk=1}^{Nh_U} H_{ik}^U H_{jk}^U \left(\hat{T}_{0_{ji}} I_{RB}(mU3, nU3) + \hat{T}_{1_{ji}} I_{RB}(mU3+1, nU3) \right) \\
 & - \frac{1}{2} \sum_{ik=1}^{Nh_L} \sum_{jk=1}^{Nh_L} H_{ik}^L H_{jk}^L \left(\hat{T}_{0_{ji}} I_{RB}(mL2, nL2) + \hat{T}_{1_{ji}} I_{RB}(mL2+1, nL2) \right) \\
 & - \frac{1}{2} \sum_{ik=1}^{Nh_L} \sum_{jk=1}^{Nh_L} H_{ik}^L H_{jk}^L \left(\hat{T}_{0_{ji}} I_{RB}(mL3, nL3) + \hat{T}_{1_{ji}} I_{RB}(mL3+1, nL3) \right) \\
 & + \frac{1}{3} \sum_{ik=1}^{Nh_U} \sum_{jk=1}^{Nh_U} \sum_{lk=1}^{Nh_U} H_{ik}^U H_{jk}^U H_{lk}^U \left(\hat{T}_{0_{ji}} I_{RB}(mU4, nU4) + \hat{T}_{1_{ji}} I_{RB}(mU4+1, nU4) \right) \\
 & \left. - \frac{1}{3} \sum_{ik=1}^{Nh_L} \sum_{jk=1}^{Nh_L} \sum_{lk=1}^{Nh_L} H_{ik}^L H_{jk}^L H_{lk}^L \left(\hat{T}_{0_{ji}} I_{RB}(mL4, nL4) + \hat{T}_{1_{ji}} I_{RB}(mL4+1, nL4) \right) \right] \quad (B.207)
 \end{aligned}$$

The mass matrix for all the rib webs combined $[M_{rwb}]_{tot}$ is obtained by summing the contributions of all the rib webs given by Eq. B.207. This matrix is then appropriately merged into the global mass matrix $[M_{glob}]$.

B.14 Stiffness Matrix Contributions of a Rib Web Layer

A rib web layer in the x - z plane is treated as a plane stress panel where the only strains of importance are ϵ_{xx} , ϵ_{zz} , and γ_{xz} . From the assumptions stated in Section B.2, ϵ_{zz} may be neglected. Using Eqs. B.4, B.7, B.9, B.11, and B.13 let us define

$$\begin{Bmatrix} \epsilon_{xx} \\ \gamma_{xz} \end{Bmatrix} = \{ [F_0(x, y)] + z[F_1(x, y)] \} \{\tilde{q}(t)\} \quad (\text{B.208})$$

where

$$\{\tilde{q}\}^T = \{q_1^T, q_3^T, q_5^T\} \quad (\text{B.209})$$

$$[F_0(x, y)] = \begin{bmatrix} a_{1,x}^T & 0 & 0 \\ 0 & a_3^T & a_{5,x}^T \end{bmatrix} \quad (\text{B.210})$$

$$[F_1(x, y)] = \begin{bmatrix} 0 & a_{3,x}^T & 0 \\ 0 & 0 & 0 \end{bmatrix} \quad (\text{B.211})$$

The matrices F_0 and F_1 are $2 \times (Nq_1 + Nq_3 + Nq_5)$ in dimension and contain polynomial terms of the form $C(r, i) x^{mF_0(r, i)} y^{nF_0(r, i)}$ and $C(r, i) x^{mF_1(r, i)} y^{nF_1(r, i)}$ respectively. They are partitioned into subvectors of dimension $1 \times Nq_s$ ($s=1,3,5$).

Now the contribution to the potential or strain energy U of an infinitesimal element dx by dz of the j th rib web layer is

$$dU_{jl} = \frac{1}{2} t_{jl}(x, z) \begin{Bmatrix} \epsilon_{xx} \\ \gamma_{xz} \end{Bmatrix}^T [\bar{Q}]_{jl} \begin{Bmatrix} \epsilon_{xx} \\ \gamma_{xz} \end{Bmatrix} dx dz \quad (\text{B.212})$$

where $[\bar{Q}]_{jl}$ is the j th layer's constitutive matrix, and $t_{jl}(x, z)$ is the thickness of the layer. The constitutive matrix is defined identically to that of the spar web in Eqs. B.166-B.169 where the η axis is defined to be the x axis. The layer thickness may be expressed as a function of x only as given in Eq. 199. Substitution of Eq. B.208 into Eq. B.212 gives

$$\begin{aligned} dU_{jl} = \frac{1}{2} t_{jl}(x) \{\tilde{q}\}^T & \left[F_0^T [\bar{Q}]_{jl} F_0 + z \left(F_0^T [\bar{Q}]_{jl} F_1 \right) \right. \\ & \left. + z \left(F_1^T [\bar{Q}]_{jl} F_0 \right) + z^2 \left(F_1^T [\bar{Q}]_{jl} F_1 \right) \right] \{\tilde{q}\} dx dz \end{aligned} \quad (\text{B.213})$$

Integrating this over the area of the web layer now gives

$$U_{jl} = \frac{1}{2} \int_{x=rx_F}^{x=rx_A} \int_{h_L(x,y)}^{h_U(x,y)} t_{jl}(x) \{ \tilde{q} \}^T \left[F_0^T [\bar{Q}]_{jl} F_0 + z \left(F_0^T [\bar{Q}]_{jl} F_1 \right) + z \left(F_1^T [\bar{Q}]_{jl} F_0 \right) + z^2 \left(F_1^T [\bar{Q}]_{jl} F_1 \right) \right] \{ \tilde{q} \} dz dx \quad (B.214)$$

where the limits of z integration are the depth distributions of the upper and lower rib caps given in Eqs. B.133 and B.134. Application here of the variational extremum condition from Eq. 1.10 yields the stiffness matrix for the jl th rib web layer given as

$$[K_{rwb}]_{jl} = \int_{x=rx_F}^{x=rx_A} \int_{h_L(x,y)}^{h_U(x,y)} t_{jl}(x) \left[F_0^T [\bar{Q}]_{jl} F_0 + z \left(F_0^T [\bar{Q}]_{jl} F_1 \right) + z \left(F_1^T [\bar{Q}]_{jl} F_0 \right) + z^2 \left(F_1^T [\bar{Q}]_{jl} F_1 \right) \right] dz dx \quad (B.215)$$

Performing the z integration analytically using Eq. B.137 gives

$$[K_{rwb}]_{jl} = \int_{x=rx_F}^{x=rx_A} t_{jl}(x) \left[(h_U(x,y) - h_L(x,y)) \left(F_0^T [\bar{Q}]_{jl} F_0 \right) + \frac{1}{2} \left(h_U^2(x,y) - h_L^2(x,y) \right) \left(\left(F_0^T [\bar{Q}]_{jl} F_1 \right) + \left(F_1^T [\bar{Q}]_{jl} F_0 \right) \right) + \frac{1}{3} \left(h_U^3(x,y) - h_L^3(x,y) \right) \left(F_1^T [\bar{Q}]_{jl} F_1 \right) \right] dx \quad (B.216)$$

Substituting Eq. B.199 for the layer thickness and Eqs. B.133 and B.134 for the rib cap depth distributions gives

$$[K_{rwb}]_{jl} = \left[\sum_{ik=1}^{Nh_U} H_{ik}^U \int_{x=rx_F}^{x=rx_A} x^{mhU_{ik}} y^{nhU_{ik}} \left(\hat{T}_{0,jl} + \hat{T}_{1,jl} x \right) \left(F_0^T [\bar{Q}]_{jl} F_0 \right) dx \right. \\ \left. - \sum_{ik=1}^{Nh_L} H_{ik}^L \int_{x=rx_F}^{x=rx_A} x^{mhL_{ik}} y^{nhL_{ik}} \left(\hat{T}_{0,jl} + \hat{T}_{1,jl} x \right) \left(F_0^T [\bar{Q}]_{jl} F_0 \right) dx \right. \\ \left. + \frac{1}{2} \sum_{ik=1}^{Nh_U} \sum_{jk=1}^{Nh_U} H_{ik}^U H_{jk}^U \int_{x=rx_F}^{x=rx_A} x^{mhU_{ik} + mhU_{jk}} y^{nhU_{ik} + nhU_{jk}} \right. \\ \left. \cdot \left(\hat{T}_{0,jl} + \hat{T}_{1,jl} x \right) \left(\left(F_0^T [\bar{Q}]_{jl} F_1 \right) + \left(F_1^T [\bar{Q}]_{jl} F_0 \right) \right) dx \right]$$

$$\begin{aligned}
& -\frac{1}{2} \sum_{ik=1}^{Nh_L} \sum_{jk=1}^{Nh_L} H_{ik}^L H_{jk}^L \int_{x=r_{x_F}}^{x=r_{x_A}} x^{mhL_{ik} + mhL_{jk}} y^{nhL_{ik} + nhL_{jk}} \\
& \cdot \left(\hat{T}_{0_{jl}} + \hat{T}_{1_{jl}} x \right) \left(F_0^T [\mathcal{Q}]_{jl} F_1 \right) + \left(F_1^T [\mathcal{Q}]_{jl} F_0 \right) dx
\end{aligned} \quad (B.217)$$

$$\begin{aligned}
& + \frac{1}{3} \sum_{ik=1}^{Nh_U} \sum_{jk=1}^{Nh_U} \sum_{lk=1}^{Nh_U} H_{ik}^U H_{jk}^U H_{lk}^U \int_{x=r_{x_F}}^{x=r_{x_A}} x^{mhU_{ik} + mhU_{jk} + mhU_{lk}} y^{nhU_{ik} + nhU_{jk} + nhU_{lk}} \\
& \cdot \left(\hat{T}_{0_{jl}} + \hat{T}_{1_{jl}} x \right) \left(F_1^T [\mathcal{Q}]_{jl} F_1 \right) dx \\
& - \frac{1}{3} \sum_{ik=1}^{Nh_L} \sum_{jk=1}^{Nh_L} \sum_{lk=1}^{Nh_L} H_{ik}^L H_{jk}^L H_{lk}^L \int_{x=r_{x_F}}^{x=r_{x_A}} x^{mhL_{ik} + mhL_{jk} + mhL_{lk}} y^{nhL_{ik} + nhL_{jk} + nhL_{lk}} \\
& \cdot \left(\hat{T}_{0_{jl}} + \hat{T}_{1_{jl}} x \right) \left(F_1^T [\mathcal{Q}]_{jl} F_1 \right) dx
\end{aligned}$$

Let the r , i th term of the matrices F_0 and F_1 be

$$F_0(r, i) = \tilde{F}_0(r, i) x^{mF_0(r, i)} y^{nF_0(r, i)} \quad (B.218)$$

$$F_1(r, i) = \tilde{F}_1(r, i) x^{mF_1(r, i)} y^{nF_1(r, i)} \quad (B.219)$$

respectively. Since y is equal to a constant y_{RIB} along the spar line defined by the upper and lower rib caps, the mass matrix term in the i th row and j th column for the jl th spar web layer may be expressed as

$$\begin{aligned}
[K_{rwb}(i, j)]_{jl} &= \sum_{r=1}^2 \sum_{p=1}^2 \mathcal{Q}_{jl}(r, p) \\
& \left[\sum_{ik=1}^{Nh_U} H_{ik}^U \tilde{F}_0(r, i) \tilde{F}_0(p, j) \int_{x=r_{x_F}}^{x=r_{x_A}} \left(\hat{T}_{0_{jl}} + \hat{T}_{1_{jl}} x \right) x^{mU1} y_{RIB}^{nU1} dx \right. \\
& \left. - \sum_{ik=1}^{Nh_L} H_{ik}^L \tilde{F}_0(r, i) \tilde{F}_0(p, j) \int_{x=r_{x_F}}^{x=r_{x_A}} \left(\hat{T}_{0_{jl}} + \hat{T}_{1_{jl}} x \right) x^{mL1} y_{RIB}^{nL1} dx \right]
\end{aligned}$$

$$\begin{aligned}
& + \frac{1}{2} \sum_{ik=1}^{Nh_U} \sum_{jk=1}^{Nh_U} H_{ik}^U H_{jk}^U \int_{x=r_{x_F}}^{x=r_{x_A}} \left(\hat{T}_{0_{jl}} + \hat{T}_{1_{jl}} x \right) \left(\tilde{F}_0(r, i) \tilde{F}_1(p, j) x^{mU2} y_{RIB}^{nU2} \right. \\
& \quad \left. + \tilde{F}_1(r, i) \tilde{F}_0(p, j) x^{mU3} y_{RIB}^{nU3} \right) dx \\
& - \frac{1}{2} \sum_{ik=1}^{Nh_L} \sum_{jk=1}^{Nh_L} H_{ik}^L H_{jk}^L \int_{x=r_{x_F}}^{x=r_{x_A}} \left(\hat{T}_{0_{jl}} + \hat{T}_{1_{jl}} x \right) \left(\tilde{F}_0(r, i) \tilde{F}_1(p, j) x^{mL2} y_{RIB}^{nL2} \right. \\
& \quad \left. + \tilde{F}_1(r, i) \tilde{F}_0(p, j) x^{mL3} y_{RIB}^{nL3} \right) dx \quad (B.220) \\
& + \frac{1}{3} \sum_{ik=1}^{Nh_U} \sum_{jk=1}^{Nh_U} \sum_{lk=1}^{Nh_U} H_{ik}^U H_{jk}^U H_{lk}^U \tilde{F}_1(r, i) \tilde{F}_1(p, j) \int_{x=r_{x_F}}^{x=r_{x_A}} \left(\hat{T}_{0_{jl}} + \hat{T}_{1_{jl}} x \right) x^{mU4} y_{RIB}^{nU4} dx \\
& - \frac{1}{3} \sum_{ik=1}^{Nh_L} \sum_{jk=1}^{Nh_L} \sum_{lk=1}^{Nh_L} H_{ik}^L H_{jk}^L H_{lk}^L \tilde{F}_1(r, i) \tilde{F}_1(p, j) \int_{x=r_{x_F}}^{x=r_{x_A}} \left(\hat{T}_{0_{jl}} + \hat{T}_{1_{jl}} x \right) x^{mL4} y_{RIB}^{nL4} dx \quad \left. \right]
\end{aligned}$$

where

$$mU1 = mhU_{ik} + mF0(r, i) + mF0(p, j) \quad (B.221)$$

$$nU1 = nhU_{ik} + nF0(r, i) + nF0(p, j) \quad (B.222)$$

$$mL1 = mhL_{ik} + mF0(r, i) + mF0(p, j) \quad (B.223)$$

$$nL1 = nhL_{ik} + nF0(r, i) + nF0(p, j) \quad (B.224)$$

$$mU2 = mhU_{ik} + mhU_{jk} + mF0(r, i) + mF1(p, j) \quad (B.225)$$

$$nU2 = nhU_{ik} + nhU_{jk} + nF0(r, i) + nF1(p, j) \quad (B.226)$$

$$mL2 = mhL_{ik} + mhL_{jk} + mF0(r, i) + mF1(p, j) \quad (B.227)$$

$$nL2 = nhL_{ik} + nhL_{jk} + nF0(r, i) + nF1(p, j) \quad (B.228)$$

$$mU3 = mhU_{ik} + mhU_{jk} + mF1(r, i) + mF0(p, j) \quad (B.229)$$

$$nU3 = nhU_{ik} + nhU_{jk} + nF1(r, i) + nF0(p, j) \quad (B.230)$$

$$mL3 = mhL_{ik} + mhL_{jk} + mF1(r, i) + mF0(p, j) \quad (B.231)$$

$$nL3 = nhL_{ik} + nhL_{jk} + nF1(r, i) + nF0(p, j) \quad (B.232)$$

$$mU4 = mhU_{ik} + mhU_{jk} + mhU_{lk} + mF1(r, i) + mF1(p, j) \quad (B.233)$$

$$nU4 = nhU_{ik} + nhU_{jk} + nhU_{lk} + nF1(r, i) + nF1(p, j) \quad (B.234)$$

$$mL4 = mhL_{ik} + mhL_{jk} + mhL_{lk} + mF1(r, i) + mF1(p, j) \quad (B.235)$$

$$nL4 = nhL_{ik} + nhL_{jk} + nhL_{lk} + nF1(r, i) + nF1(p, j) \quad (B.236)$$

Noting that Eq. B.220 is composed of linear combinations of the integral family $I_{RB}(m, n)$ defined in Eq. A.102, the final expression for the i, j th term of $[K_{rwb}]_{jl}$ is

$$\begin{aligned}
 [K_{rwb}(i, j)]_{jl} = & \sum_{r=1}^2 \sum_{p=1}^2 \bar{Q}_{jl}(r, p) \\
 & \left[\sum_{ik=1}^{Nh_U} H_{ik}^U \tilde{F}_0(r, i) \tilde{F}_0(p, j) \left(\hat{T}_{0,jl} I_{RB}(mU1, nU1) + \hat{T}_{1,jl} I_{RB}(mU1 + 1, nU1) \right) \right. \\
 & - \sum_{ik=1}^{Nh_L} H_{ik}^L \tilde{F}_0(r, i) \tilde{F}_0(p, j) \left(\hat{T}_{0,jl} I_{RB}(mL1, nL1) + \hat{T}_{1,jl} I_{RB}(mL1 + 1, nL1) \right) \\
 & + \frac{1}{2} \sum_{ik=1}^{Nh_U} \sum_{jk=1}^{Nh_U} H_{ik}^U H_{jk}^U \left(\tilde{F}_0(r, i) \tilde{F}_1(p, j) \hat{T}_{0,jl} I_{RB}(mU2, nU2) \right. \\
 & \quad \left. + \tilde{F}_0(r, i) \tilde{F}_1(p, j) \hat{T}_{1,jl} I_{RB}(mU2 + 1, nU2) \right) \\
 & + \frac{1}{2} \sum_{ik=1}^{Nh_U} \sum_{jk=1}^{Nh_U} H_{ik}^U H_{jk}^U \left(\tilde{F}_1(r, i) \tilde{F}_0(p, j) \hat{T}_{0,jl} I_{RB}(mU3, nU3) \right. \\
 & \quad \left. + \tilde{F}_1(r, i) \tilde{F}_0(p, j) \hat{T}_{1,jl} I_{RB}(mU3 + 1, nU3) \right) \left. \right]
 \end{aligned}$$

$$\begin{aligned}
& -\frac{1}{2} \sum_{ik=1}^{Nh_L} \sum_{jk=1}^{Nh_L} H_{ik}^L H_{jk}^L \left(\tilde{F}_0(r, i) \tilde{F}_1(p, j) \hat{T}_{0_{ji}} I_{RB}(mL2, nL2) \right. \\
& \quad \left. + \tilde{F}_0(r, i) \tilde{F}_1(p, j) \hat{T}_{1_{ji}} I_{RB}(mL2 + 1, nL2) \right) \\
& \quad \quad \quad (B.237) \\
& -\frac{1}{2} \sum_{ik=1}^{Nh_L} \sum_{jk=1}^{Nh_L} H_{ik}^L H_{jk}^L \left(\tilde{F}_1(r, i) \tilde{F}_0(p, j) \hat{T}_{0_{ji}} I_{RB}(mL3, nL3) \right. \\
& \quad \left. + \tilde{F}_1(r, i) \tilde{F}_0(p, j) \hat{T}_{1_{ji}} I_{RB}(mL3 + 1, nL3) \right) \\
& + \frac{1}{3} \sum_{ik=1}^{Nh_U} \sum_{jk=1}^{Nh_U} \sum_{lk=1}^{Nh_U} H_{ik}^U H_{jk}^U H_{lk}^U \tilde{F}_1(r, i) \tilde{F}_1(p, j) \left(\hat{T}_{0_{ji}} I_{RB}(mU4, nU4) \right. \\
& \quad \left. + \hat{T}_{1_{ji}} I_{RB}(mU4 + 1, nU4) \right) \\
& - \frac{1}{3} \sum_{ik=1}^{Nh_L} \sum_{jk=1}^{Nh_L} \sum_{lk=1}^{Nh_L} H_{ik}^L H_{jk}^L H_{lk}^L \tilde{F}_1(r, i) \tilde{F}_1(p, j) \left(\hat{T}_{0_{ji}} I_{RB}(mL4, nL4) \right) \\
& \quad \quad \quad + \hat{T}_{1_{ji}} I_{RB}(mL4 + 1, nL4) \left. \right]
\end{aligned}$$

The stiffness matrix for all the rib webs combined $[K_{rwb}]_{tot}$ is obtained by summing the contributions of all the layers of all the rib webs given by Eq. B.237. This matrix is then appropriately merged into the global stiffness matrix $[K_{glob}]$.

Appendix C: Fundamental Integrals and Tables

C.1 Introduction

Integrating energy contributions over the geometry of wing components has led to the definition of three integral families: $I_{TR}(m,n)$, $I_{SP}(m,n)$, and $I_{RB}(m,n)$. This appendix discusses the analytical solutions to these integrals based on the wing model's shape design variables. The discussion starts with the development of a family of solutions to integrals over the area of a trapezoidal panel. Next is the development of a family of solutions to integrals over the length of a spar. Last is the development of a family of solutions to integrals over the length of a rib. From these solutions, solution tables of each integral family may be constructed. These tables need only be calculated once for a particular wing geometry and may then be referenced multiple times in mass and stiffness matrix calculations.

C.2 Area Integrals

Derivation of mass and stiffness matrix equations for trapezoidal skin panels has resulted in the definition of a family of integrals given by

$$I_{TR}(m,n) = \iint_{yx} x^m y^n dx dy \quad (C.1)$$

where the trapezoidal area of x - y integration is defined by the vertices (x_{FL}, y_L) , (x_{FR}, y_R) , (x_{AR}, y_R) , (x_{AL}, y_L) as shown in Figure 1.3. The left and right sides of the trapezoid are parallel to the x axis and located at y coordinates y_L and y_R respectively. Equations for the front and aft lines of the trapezoid may be written as

$$x_F(y) = F_1 y + F_2 \quad (C.2)$$

$$x_A(y) = A_1 y + A_2 \quad (C.3)$$

respectively, where

$$F1 = \frac{x_{FR} - x_{FL}}{y_R - y_L} \quad (C.4)$$

$$F2 = \frac{x_{FL}y_R - x_{FR}y_L}{y_R - y_L} \quad (C.5)$$

$$A1 = \frac{x_{AR} - x_{AL}}{y_R - y_L} \quad (C.6)$$

$$A2 = \frac{x_{AL}y_R - x_{AR}y_L}{y_R - y_L} \quad (C.7)$$

The integral $I_{TR}(m, n)$ may now be written as

$$I_{TR}(m, n) = \int_{y=y_L}^{y=y_R} y^n \int_{x=x_F(y)}^{x=x_F(y)} x^m dx dy \quad (C.8)$$

Using Eqs. C.2 and C.3 gives the relationship

$$\int_{x=x_F(y)}^{x=x_F(y)} x^m dx = \frac{1}{m+1} [(A1y + A2)^{m+1} - (F1y + F2)^{m+1}] \quad (C.9)$$

Substituting Eq. C.9 into Eq. C.8 gives

$$I_{TR}(m, n) = \frac{1}{m+1} \left[\int_{y=y_L}^{y=y_R} y^n (A1y + A2)^{m+1} dy + \int_{y=y_L}^{y=y_R} y^n (F1y + F2)^{m+1} dy \right] \quad (C.10)$$

Let us define two secondary integrals I_A and I_F where

$$I_A(r, s) = \int_{y=y_L}^{y=y_R} y^r (A1y + A2)^s dy \quad (C.11)$$

and

$$I_F(r, s) = \int_{y=y_L}^{y=y_R} y^r (F1y + F2)^s dy \quad (C.12)$$

Recursion formulas may be used to obtain a closed form evaluation of these secondary integrals (SP68,LIV90). They are evaluated using the formulas

$$\int y^r (A_1 y + A_2)^s dy = \frac{y^{r+1} (A_1 y + A_2)^s}{r + s + 1} + \frac{s A_2}{r + s + 1} \int y^r (A_1 y + A_2)^{s-1} dy \quad (C.13)$$

and

$$\int y^r (F_1 y + F_2)^s dy = \frac{y^{r+1} (F_1 y + F_2)^s}{r + s + 1} + \frac{s F_2}{r + s + 1} \int y^r (F_1 y + F_2)^{s-1} dy \quad (C.14)$$

Substitution of Eqs. C.11 and C.12 into Eq. C.10 yields a final expression

$$I_{TR}(m, n) = \frac{1}{m+1} [I_A(n, m+1) - I_F(n, m+1)] \quad (C.15)$$

Tables for I_A and I_F may be constructed for ascending x and y powers using the formulas in Eqs. C.13 and C.14. From these a final table may then be constructed for the trapezoidal area integrals using Eq. C.15 (LIV90).

C.3 Spar Line Integrals

Derivation of mass and stiffness matrix equations for spars and spar webs has resulted in the definition of a family of integrals given by

$$I_{SP}(m, n) = \frac{L}{sy_R - sy_L} \int_{y=sy_L}^{y=sy_R} (S_1 y + S_2)^m y^n dy \quad (C.16)$$

where the spar line endpoints are defined by the coordinates (sx_L, sy_L) and (sx_R, sy_R) as shown in Figure 1.4, and L is the length of the spar. This integral results from substituting for x the spar line equation given by

$$x(y) = S1y + S2 \quad (C.17)$$

where

$$S1 = \frac{sx_R - sx_L}{sy_R - sy_L} \quad (C.18)$$

$$S2 = \frac{sx_L sy_R - sx_R sy_L}{sy_R - sy_L} \quad (C.19)$$

Define

$$I_S(r, s) = \int_{y=sy_L}^{y=sy_R} (S1y + S2)^r y^s dy \quad (C.20)$$

which may be evaluated in closed form using the recursion formula

$$I_S(r, s) = \frac{y^{s+1} (S1y + S2)^r}{r + s + 1} + \frac{rS2}{r + s + 1} \int (S1y + S2)^{r-1} y^s dy \quad (C.21)$$

Substitution of Eq. C.20 into Eq. C.16 yields a final expression

$$I_{SP}(m, n) = \frac{L}{sy_R - sy_L} I_S(m, n) \quad (C.22)$$

A table of spar line integrals for ascending x and y powers may be prepared using the formula from Eq. C.21 combined with Eq. C.22.

C.4 Rib Line Integrals

Derivation of mass and stiffness matrix equations for ribs and rib webs has resulted in the definition of a family of integrals given by

$$I_{RB}(m, n) = y_{RIB}^n \int_{x=rx_F}^{x=rx_A} x^m dx \quad (C.23)$$

where the rib line endpoints are defined by the coordinates (rx_F, y_{RIB}) and (rx_A, y_{RIB}) as

shown in Figure 1.4. The coordinates rx_F and rx_A are determined from the rib shape design variables using

$$rx_F = F1y_{RIB} + F2 \quad (C.24)$$

$$rx_A = A1y_{RIB} + A2 \quad (C.25)$$

where

$$F1 = \frac{rx_{FR} - rx_{FL}}{ry_R - ry_L} \quad (C.26)$$

$$F2 = \frac{rx_{FL}ry_R - rx_{FR}ry_L}{ry_R - ry_L} \quad (C.27)$$

$$A1 = \frac{rx_{AR} - rx_{AL}}{ry_R - ry_L} \quad (C.28)$$

$$A2 = \frac{rx_{AL}ry_R - rx_{AR}ry_L}{ry_R - ry_L} \quad (C.29)$$

The rib integral is easily evaluated and given by

$$I_{RB}(m, n) = \frac{y_{RIB}^n}{m+1} [rx_A^{m+1} - rx_F^{m+1}] \quad (C.30)$$

This equation may be used to construct a table of rib integrals for ascending x and y powers.

Appendix D: Test Case Data

D.1 Overview

Contained in this appendix is the structural data for the wing test cases. Data for the Turner-Martin-Weikel wing is presented first. Given next is the data for the HSCT wing.

D.2 Turner-Martin-Weikel Wing

Figure D.1 shows a finite element model of the Turner-Martin-Weikel (T-M-W) wing (LIV194). Figure D.2 illustrates details of the construction of the wing (TMW64). Depth, skin thickness, spar web thickness, and spar cap area are all constant. The wing is made totally from aluminum having the following material properties:

$$E = 10.5E6 ; \nu = 0.3 ; \rho = 0.1 \text{ lb/in}^3.$$

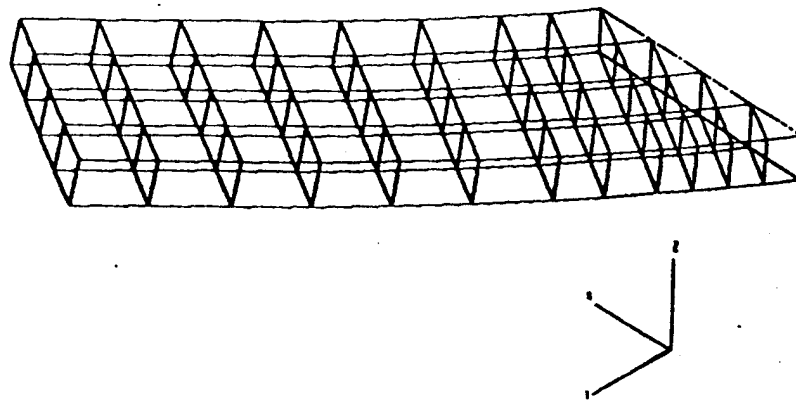
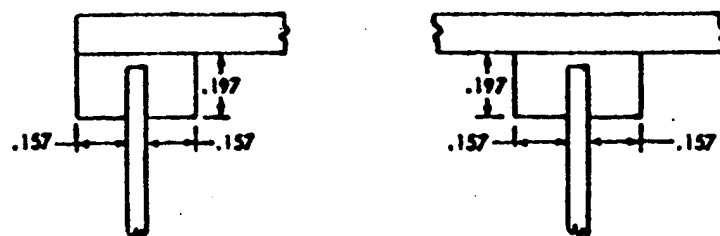
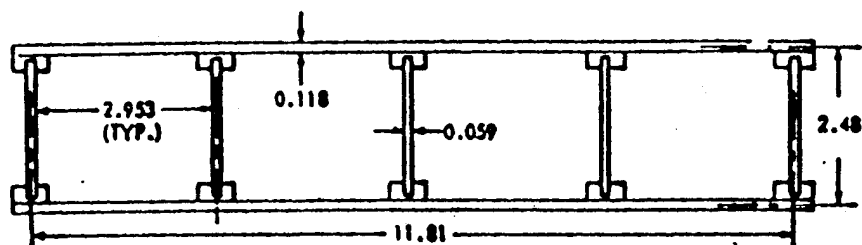
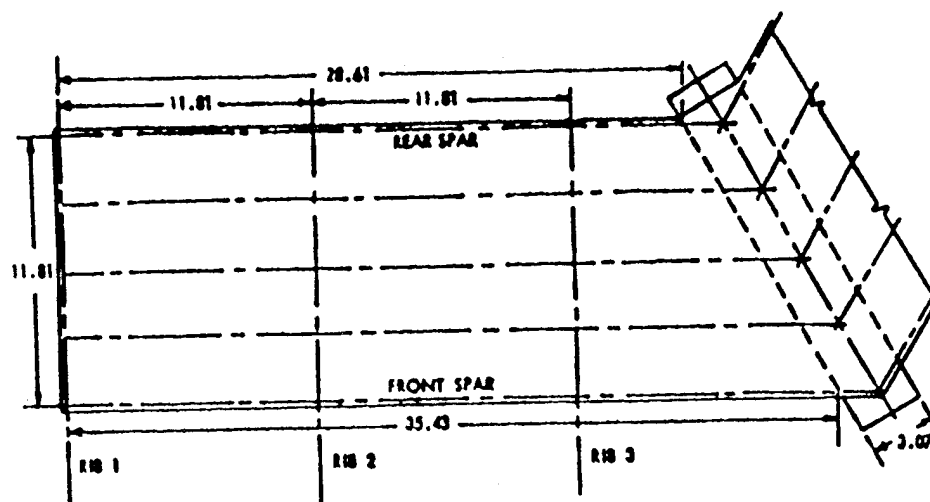


Figure D.1: FEM Model of the T-M-W Wing



DETAILS OF ATTACHMENT OF SPAR AND RIB WEBS TO COVER SKIN OF MODEL

Figure D.2: T-M-W Wing Construction

D.3 HSCT Wing

Figure D.3 shows the ELFINI finite element model of the Boeing HSCT candidate wing. The wing is symmetric about the mid-plane with the depth distribution for the upper skin given in inches by

$$h = 25.0 - 0.03097243y$$

The wing skins are composed of composite material layers with the following material properties:

$$E_{11} = 36.2\text{E}6 \text{ psi}; E_{22} = 1.4\text{E}6 \text{ psi}; \nu = 0.29; G_{12} = .666\text{E}6 \text{ psi}; \rho = 0.1 \text{ lb/in}^3$$

The inboard upper and lower wing skins are each made of 20 sets of (0/90/45/-45) laminate where ply orientation is referenced to the inboard spar lines. The same construction is used for the outer wing where the plies are oriented with respect to the outer wing spar lines. The thickness of each ply is 0.0037 in. Spar and rib webs are made of the same material using 4 sets of (0/90/45/-45) laminate where orientation is referenced from the mid-plane (LSB93).

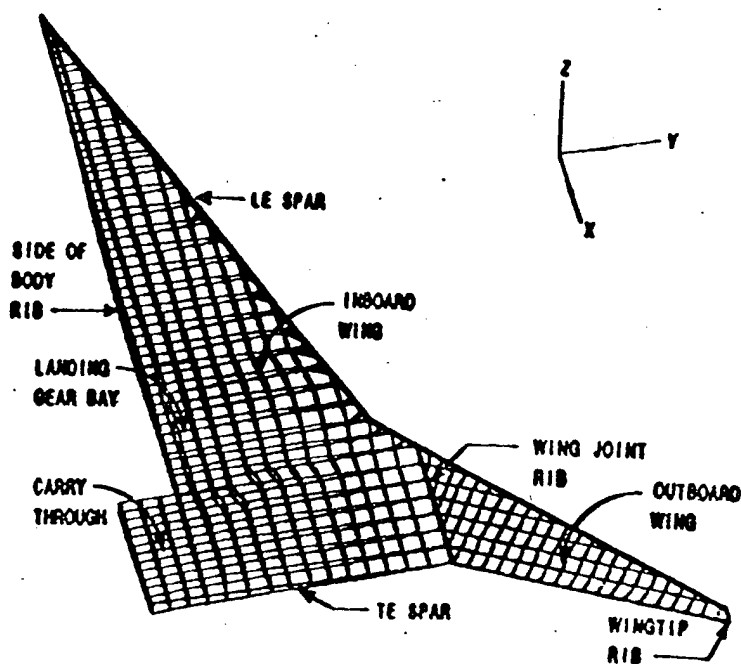


Figure D.3: ELFINI Model of HSCT Wing

Spar and rib caps have a constant area of 0.267 in^2 . They are made of composite material with the following properties:

$$E = 14.0\text{E}6 \text{ psi}; \quad \nu = 0.46; \quad \rho = 0.1 \text{ lb/in}^3$$

Table D.1 lists the vertical spring coefficients used at points along the root to represent fuselage stiffness along the side of body rib (LSB93). Linear springs with a coefficient of $2.0\text{E}10 \text{ lb/in}$ are used along the root to impose zero v_0 displacement. Rotational springs with coefficients of $1.0\text{E}16 \text{ in-lb/rad}$ along the root at $y=83 \text{ in.}$ and $1.25\text{E}16 \text{ in-lb/rad}$ along the carry through root are used to impose zero ψ_y displacement. One spring with a coefficient of $1.0\text{E}10$ is used at the rear inboard point of the wing carry through to resist u_0 displacement.

Table D.1: Root Springs Representing Fuselage Stiffness Along Side of Body Rib

Spring #	$x \text{ (in)}$	$k_5 \text{ (lb/in)}$	Spring #	$x \text{ (in)}$	$k_5 \text{ (lb/in)}$
1	1393.27	3257	17	1939.82	20127
2	1428.43	3572	18	1975.02	23397
3	1463.58	3917	19	2010.22	30295
4	1498.74	4351	20	2045.22	39460
5	1533.90	4850	21	2080.22	48539
6	1569.06	5396	22	2115.22	59351
7	1604.22	6035	23	2150.22	73546
8	1631.22	6589	24	2177.95	85157
9	1658.22	7202	25	2205.68	108019
10	1693.42	8137	26	2238.72	120000
11	1728.62	9525	27	2269.05	171571
12	1763.82	10359	28	2299.38	173602
13	1799.02	11650	29	2329.71	169070
14	1834.22	13267	30	2360.04	162117
15	1869.42	15174	31	2390.37	149298
16	1904.62	17423	32	2420.70	100000

Appendix E: CONNECT Program Information

E.1 Overview

This appendix briefly describes the code developed and used in this work. Program subroutines are listed with a description of their purpose. The program structure is outlined with a description of the main program variables.

E.2 Program Subroutines

CONNECT, the main program, is written in Fortran. Following is a list of the supporting subroutines grouped according to their purpose.

Matrix Preparation:

- MTXSKN - prepares matrices for FSDPT skin and spar stiffness calculations
- MTXRIB - prepares matrices for FSDPT rib stiffness calculations
- MTXSWB - prepares matrices for FSDPT spar web calculations
- MTXRWB - prepares matrices for FSDPT rib web calculations
- MTXMAS - prepares displacement matrices for FSDPT mass calculations
- MTXCORE - prepares matrices for FSDPT equivalent core calculations

Stiffness Matrix Evaluation:

- SKIN - evaluates stiffness matrix contributions for a single FSDPT skin layer
- SPRCAP - evaluates stiffness matrix contributions for a single FSDPT spar
- RIBCAP - evaluates stiffness matrix contributions for a single FSDPT rib
- SPRWEB - evaluates stiffness matrix contributions for a single FSDPT spar web layer
- RIBWEB - evaluates stiffness matrix contributions for a single FSDPT spar web layer
- SKIN0 - evaluates stiffness matrix contributions for a single CPT skin layer
- CORE - evaluates stiffness matrix contributions for an equivalent core

- SPNG1G - evaluates stiffness matrix contributions for a FSDPT zone attached to ground at a point via springs
- SPNG11 - evaluates stiffness matrix contributions for the spring connection of 2 FSDPT zones at a point
- SPNG10 - evaluates the stiffness matrix contributions for the spring connection of a CPT zone to a FSDPT zone at a point

Mass Matrix Evaluation:

- MSKIN - evaluates mass matrix contributions for a single FSDPT skin layer
- MSPRCAP - evaluates mass matrix contributions for a single FSDPT spar
- MRIBCAP - evaluates mass matrix contributions for a single FSDPT rib cap
- MWEB - evaluates mass matrix contributions for a single FSDPT spar or rib web layer
- MCONC - evaluates mass matrix contribution for a single FSDPT concentrated mass
- MSKIN0 - evaluates mass matrix contributions for a single CPT skin layer

Integral Table Generation:

- TABSRF - generates integral table for a single panel geometry
- GMTRY - used in TABSRF to calculate panel geometry parameters
- INTGSP - generates integral table for a single spar
- INTGRB - generates integral table for a single rib

Skyline Linear Solver:

- SKYFAC - factorizes global stiffness matrix
- SKYFAC - solves for static generalized displacements

Eigensolution:

- EIGZF - solves eigenvalue problem for natural frequencies and mode shapes

E.3 Program Structure

Phase 1: Initialization

All input parameters are set within the main code and stored in arrays. No data is read from file. To avoid numerical ill-conditioning, all geometric parameters may be shifted and scaled to fit into a unit square. All other parameters with length dimensions must also be scaled for consistency. Following is a list and description of array variables with their index descriptors.

idzone(zone#)	- identifies CPT (0) or FSDPT (1) zone
nq1(zone#)...nq5(zone#)	- # of displacement terms for u_0 , v_0 , ψ_x , ψ_y , w_0 respectively; (w from CPT zone is treated as w_0 from FSDPT zone)
mq1x(term#,zone#)...	
...mq5x(term#,zone#)	- x powers for displacement polynomials
mq1y(term#,zone#)...	
...mq5y(term#,zone#)	- y powers for displacement polynomials
scale(zone#)	- zone scaling factor
xshft(zone#)	- zone x coordinate shift value
yshft(zone#)	- zone y coordinate shift value
npnl(zone#)	- # of panels in zone
xyplan(coord#,panel#,zone#)	- panel geometry coordinates
pnlh(panel#,zone#)	- panel depth distribution (h series) tag
nlayr(panel#,zone#)	- # of skin layer in panel
ntterm(layer#,panel#,zone#)	- # of thickness distribution terms in skin layer
t(term#,layer#,panel#,zone#)	- layer thickness distribution coefficient
mtx(trm#,layr#,pnl#,zone#)	- x powers of layer thickness distribution
mtx(trm#,layr#,pnl#,zone#)	- y powers of layer thickness distribution
skbeta(layr#,pnl#,zone#)	- skin layer fiber orientation from x axis
nhterm(h series#,zone#)	- # of terms in depth distribution (h series)
h(term#,h#,zone#)	- depth distribution (h series) coefficient
mhx(term#,h#,zone#)	- x powers of depth distribution
mhy(term#,h#,zone#)	- y powers of depth distribution

spyl,spyr,spxl,
 spxr(spar#,zone#) - spar geometry coordinates
 sprh(spar#,zone#) - spar depth distribution tag
 sparea(term#,spar#,zone#) - spar cap area

rbyl,rbyr,yrib,rbxfl,rbxfr
 rbxal,rbxar(rib#,zone#) - rib geometry coordinates
 ribh(rib#,zone#) - rib depth distribution tag
 rbarea(term#,spar#,zone#) - rib cap area

npnts(zone#) - # of attach points in zone
 pntxyz(xyz#,point#,zone#) - attach point geometry
 pnth(point#,zone#) - attach point depth distribution tag

wbspr(term#,spr web#,zone#) - identifies spar caps associated with spar web
 twbspr(trm#,lyr#,spwb#,zn#) - spar web layer tickness coefficient
 bwbspr(lyr#,spwb#,zn#) - fiber orientation of spar web layer

wbrib(term#,rib web#,zone#) - identifies rib caps associated with rib web
 twbrib(trm#,lyr#,rbwb#,zn#) - rib web layer thickness coefficient
 bwbrib(lyr#,rbwb#,zn#) - fiber orientation of rib web layer

cnctn(zone#,zone#) - zone connection tag: 0-not connected, 1-connected
 (ground connection when zone number are equal)
 nspring(zone#,zone#) - # of spring used for zone connection
 xattl,xattr,yattl,
 yattr(1or2,zone#,zone#) - attach line geometry of zones being connected
 ksprng(trm#,sprng#,zn#,zn#) - spring stiffness coefficients corresponding to $k_1...k_5$

ncmass(zone#) - # of concentrated masses in zone
 cmpoint(cmass#,zone#) - concentrated mass point tag
 cmass(xyz#,cmass#,zone#) - concentrated mass coefficient

nlconc(zone#,load case#) - # of concentrated force loads

qconc(ld#,xyz#,zn#,ldcase#)	- concentrated force load coefficient
idconc(ld#,xyz#,zn#,ldcase#)	- concentrated load point tag
nlpol(panel#,zone#,ldcase#)	- # of distributed pressure loads
qppl(trm#,xyz#,ld#,pnl#, zn#,ldcase#)	- distributed load coefficient
mqpolx(term#)	- x powers of distributed loads
mqpoly(term#)	- y powers of distributes loads
noutx(panel#,zone#)	- number of panel output points in x direction
nouty(panel#,zone#)	- number of panel output points in y direction
outx(point#,panel#,zone#)	- x direction output grid coordinates
outy(point#,panel#,zone#)	- y direction output grid coordinates
yleft(panel#,zone#)	- left y coordinate of output grid on wing panel
yright(panel#,zone#)	- right y coordinate of output grid on wing panel
pnplrint(panel#,zone#)	- panel output tag: 0-no print, 1-print
noutspr(zone#)	- number of spar output points
outspr(point#,zone#)	- spar output grid coordinates
sprprnt(spar#,zone#)	- spar output tag: 0-no print, 1-print
noutrib(zone#)	- number of rib output points
outrib(point#,zone#)	- rib output grid coordinates
ribprnt(rib#,zone#)	- rib output tag: 0-no print, 1-print

In addition to these, material property variables are also assigned:

qsk11, qsk12, qsk22, qsk66	- FSDPT skin constitutive matrix values
qwb11, qwb12, qwb22, qw66	- FSDPT spar and rib web constitutive matrix values
q0sk11, q0sk12, q0sk22, q0sk66	- CPT skin constitutive matrix values
modcap	- FSDPT spar and rib cap modulus
mod0cap	- CPT spar and rib cap modulus
densk	- FSDPT skin density

denwb	- FSDPT spar and rib web density
den0sk	- CPT skin density
dencap	- FSDPT spar and rib cap density
den0cap	- CPT spar and rib cap density

Phase 2: Calculations

A) Integral Table Assembly: The following integral table arrays are assembled.

aintmn(x power,y power, panel#,zone#)	- panel integral table
spintmn(x power,y power, spar#,zone#)	- spar integral table
rbintmn(x power,y power, rib #,zone#)	- rib integral table

B) Stiffness Matrix Assembly: Here first subroutines are called to prepare the needed strain matrices. Each strain matrix from the FSDPT formulation is stored in 3 arrays: one for coefficients, one for x powers, and one for y powers. The arrays are defined as follows:

ea,eax,eay(row#,col#,zone#) - 1st FSDPT skin and spar strain matrix [R_0]
 eb,ebx,eby(row#,col#,zone#) - 2nd FSDPT skin and spar strain matrix [R_1]

e1,e1x,e1y(row#,col#,zone#) - 1st FSDPT rib strain matrix [Y_0]
 e2,e2x,e2y(row#,col#,zone#) - 2nd FSDPT rib strain matrix [Y_1]

esa,esax,esay(rw#,col#,zn#) - 1st FSDPT spar web strain matrix [W_0]
 esb,esbx,esby(rw#,col#,zn#) - 2nd FSDPT spar web strain matrix [W_1]

era,erax,eray(rw#,col#,zn#) - 1st FSDPT rib web strain matrix [F_0]
 erb,erbx,erby(rw#,col#,zn#) - 2nd FSDPT rib web strain matrix [F_1]

eec,eecx,eecy(rw#,col#,zn#) - Equivalent core strain matrix [W_s]

Next the subroutines which calculate the stiffness contributions of each wing component are called. Since the stiffness matrix is symmetric, only the upper triangular portion need be stored. Formatting of the SKYLINE solver requires that this upper triangular matrix be stored in a vector. This requires a vector of length $Nq_{glob} * (Nq_{glob} + 1) / 2$. Stiffness matrix terms are stored column by column in the vector array: `stif(term#)`. Only skin contributions are included for a CPT zone in this program.

C) Loads Assembly: Here the load vector is assembled and stored in the array:

`qload(term#,load case#)`

D) Static Solution: Here the subroutines for factorizing the stiffness matrix and solving the linear system of equations are called. The solution generalized displacements are stored in the array: `qdisp(term#,load case#)`.

E) Mass Matrix Assembly: Here first a subroutine is called to prepare the needed displacement matrices. Each displacement matrix from the FSDPT formulation is stored in 3 arrays as the strain matrices are in stiffness matrix assembly. These arrays are defined as follows:

`s0,s0x,s0y(row#,col#,zone#)` - 1st displacement matrix $[S_0]$

`s1,s1x,s1y(row#,col#,zone#)` - 2nd displacement matrix $[S_1]$

Next the subroutines which calculate the mass contributions of each wing component are called. The mass matrix is also symmetric and thus stored in the same format as the stiffness matrix in the vector array: `mass(term#)`. Only skin contributions are included for a CPT zone in this program.

F) Eigensolution: Here the eigenvalue problem involving mass and stiffness is solved. Natural frequencies are sorted by increasing size and stored in the array: `eigsort(freq#)`. Corresponding generalized modal displacements are stored in the array: `qmode(term#,mode#)`.

Phase 3: Output

Displacement, stress, and mode shape output is calculated at specified grid points and stored in the following arrays:

```

dsppnl(disp#,point#,panel#,
        zone#, load case#) - panel displacements
dspspr(disp#,point#,spar#
        zone#,load case#) - spar displacements
dsprib(disp#,point#,panel#,
        zone#,load case#) - rib displacements
strpnl(stress#,point#,layer#,
        panel#,zone#,load case#)- panel stresses (3 in x-y system, 3 in fiber axis system)
strspr(point#,spar#,zone#,
        load case#) - spar stress
strrib(point#,rib#,zone#,
        load case#) - rib stress
mddsppnl(disp#,point#,
        panel#,zone#,mode#) - panel mode shape displacements
mddspr(disp#,point#,
        spar#,zone#,mode#) - spar mode shape displacements
mddsprib(disp#,point#
        rib#.zone#,mode#) - rib mode shape displacements

```

Output is printed for each panel, spar, and rib selected.